

Investigation of pharmacological compounds to increase skeletal muscle glucose uptake *in vitro* and *in vivo*

Ph.D. Thesis

Zoltán Márton Köhler



Supervisor: *Anikó Keller-Pintér, M.D., Ph.D.*

Doctoral School of Multidisciplinary Medical Sciences

Department of Biochemistry

Albert Szent-Györgyi Medical School

UNIVERSITY OF SZEGED

SZEGED

2023

TABLE OF CONTENTS

LIST OF PUBLICATIONS	4
LIST OF ABBREVIATIONS.....	5
SUMMARY	7
1. INTRODUCTION	9
1.1. Muscle rejuvenation.....	9
1.2. Signal transduction pathways regulating skeletal muscle glucose uptake.....	9
1.3. Impairment of GLUT4 translocation and diabetes mellitus.....	11
1.4. Bone morphogenetic proteins (BMPs) and the regulation of glucose uptake	12
1.5. Tilorone dihydrochloride.....	13
1.6. The relationship between reactive oxygen species and glucose uptake.....	14
1.7. Antioxidant defense and astaxanthin	15
2. AIMS OF THE THESIS	18
3. MATERIALS AND METHODS	19
3.1. Cell culture, differentiation and treatment	19
3.2. Experimental animals.....	19
3.3. Quantitative real-time (qRT)-PCR.....	20
3.4. Gel electrophoresis and immunoblotting	21
3.5. Fluorescent staining and microscopy.....	22
3.6. <i>In vitro</i> ¹⁸ F-fluoro-2-deoxyglucose (¹⁸ FDG) uptake measurement.....	22
3.7. Assessment of mitochondrial oxygen consumption (O ₂ flux) using high-resolution respirometry.....	23
3.8. Animal treatment and <i>in vivo</i> imaging.....	24
3.9. Statistical analysis.....	24
4. RESULTS.....	25
4.1. Tilorone increases BMP signaling in myoblasts	25
4.2. Effect of tilorone on signaling molecules regulating GLUT4 translocation	26
4.3. Tilorone increases the expression of GLUTs and glucose uptake of C2C12 cells	27
4.4. Tilorone increases ¹⁸ FDG uptake of myotubes and enhances insulin effect	30
4.5. Effects of tilorone treatment on mitochondrial function in myoblasts.....	31
4.6. Tilorone administration increases ¹⁸ FDG uptake <i>in vivo</i>	33

4.7. Astaxanthin feeding influences the activation of signaling molecules affecting skeletal muscle metabolism	34
5. DISCUSSION.....	36
6. CONCLUSION	42
FUNDING.....	43
ACKNOWLEDGEMENTS.....	44
REFERENCES	45
ANNEX.....	63

LIST OF PUBLICATIONS

1. The complete list of papers directly related to the subject of the thesis:

1. **Köhler, Zoltán Márton**, György Trencsényi, László Juhász, Ágnes Zvara, Judit P. Szabo, László Dux, László G. Puskas, László Rovó and Anikó Keller-Pinter (2023). Tilorone increases glucose uptake in vivo and in skeletal muscle cells by enhancing Akt2/AS160 signaling and glucose transporter levels. *Journal of Cellular Physiology* 238(5), 1080–1094. <https://doi.org/10.1002/JCP.30998> [IF: 5.6] Q1
2. Gönczi, Mónika, Andrea Csemer, László Szabó, Mónika Sztretye, János Fodor, Krisztina Pocsai, Kálmán Szenthe, Anikó Keller-Pintér, **Zoltán Márton Köhler**, Péter Nánási, Norbert Szentandrassy, Balázs Pál, and László Csernoch (2022). Astaxanthin Exerts Anabolic Effects via Pleiotropic Modulation of the Excitable Tissue. *International Journal of Molecular Sciences* 23(2):917. <https://doi.org/10.3390/ijms23020917> [IF: 5.6] D1

Cumulative impact factors of papers directly related to the subject of the thesis: 11.2

2. Other articles:

1. Sztretye, Mónika, Zoltán Singlár, Nyamkhuu Ganbat, Dána Al-Gaadi, Kitti Szabó, **Zoltán Márton Köhler**, László Dux, Anikó Keller-Pintér, László Csernoch, and Péter Szentesi (2023). Unravelling the Effects of Syndecan-4 Knockdown on Skeletal Muscle Functions. *International Journal of Molecular Sciences*, 24(8), 6933. <https://doi.org/10.3390/ijms24086933> [IF: 5.6] D1
2. **Köhler, Zoltán Márton**, and Szepesi, Ágnes (2023). More Than a Diamine Oxidase Inhibitor: L-Aminoguanidine Modulates Polyamine-Related Abiotic Stress Responses of Plants. *Life* 2023, Vol. 13, Page 747, 13(3), 747. <https://doi.org/10.3390/LIFE13030747> [IF: 3.2] Q2
3. Szepesi, Ágnes, László Bakacsy, Henrietta Kovács, Árpád Szilágyi, and **Zoltán Márton Köhler** (2022). Inhibiting Copper Amine Oxidase Using L-Aminoguanidine Induces Cultivar and Age-Dependent Alterations of Polyamine Catabolism in Tomato Seedlings. *Agriculture (Switzerland)* 12(2):274. <https://doi.org/10.3390/agriculture12020274> [IF: 3.6] Q2
4. Becskeházi, Eszter, Marietta Margaréta Korsós, Eleonóra Gál, László Tiszlavicz, Zsófia Hoyk, Mária A. Deli, **Zoltán Márton Köhler**, Anikó Keller-Pintér, Attila Horváth, Kata Csekő, Zsuzsanna Helyes, Péter Hegyi, and Viktória Venglovecz (2021). Inhibition of NHE-1 Increases Smoke-Induced Proliferative Activity of Barrett's Esophageal Cell Line. *International Journal of Molecular Sciences* 2021, Vol. 22, Page 10581 22(19):10581. <https://doi.org/10.3390/ijms221910581> [IF: 6.208] D1

Cumulative impact factors of other full papers¹: 18.608

Total cumulative impact factors: 29.808

IF values based on Journal Citation Reports (JCR) - Clarivate

The quartile classification is based on the SCImago Journal & Country Rank (SJR)

LIST OF ABBREVIATIONS

¹⁸ FDG	¹⁸ F-fluoro-2-deoxyglucose
AMP	Adenosine monophosphate
AMPK	5' AMP-activated protein kinase
AS160	Akt substrate of 160 kDa (TBC1D4)
ATP	Adenosine triphosphate
BMP	Bone morphogenetic protein
BSA	Bovine serum albumin
CCCP	Carbonyl cyanide m-chlorophenylhydrazone
Ct	Threshold cycle
DM	Diabetes mellitus
DMEM	Dulbecco's modified Eagle medium
DTT	1,4-Dithiothreitol
ECM	Extracellular matrix
EDTA	Ethylenediaminetetraacetic acid
ETS	Electron transport system
FBS	Fetal bovine serum
GAPDH	Glyceraldehyde-3-phosphate dehydrogenase
GAP	GTPase-activating protein
GLUT	Glucose transporter
GSH	Glutathione
GSH-Px	Glutathione peroxidase
HFD	High-fat diet
HPRT	Hypoxanthine-guanine phosphoribosyltransferase
HRP	Horse-radish peroxidase
IDF	International Diabetes Federation
IRS1	Insulin receptor substrate 1
IKK β 1	Inhibitory κ B kinase β 1
JNK	c-Jun N-terminal kinase
LKB1	Liver kinase B1
NSC23766	N6-[2-(4-Diethylamino-1-methyl-butylamino)-6-methyl-pyrimidin-4-yl]-2-methyl-quinoline-4,6-diamine trihydrochloride
OGTT	Oral glucose tolerance test

Omy	Oligomycin
OXPHOS	Oxidative phosphorylation
PAK1	p21-activated kinase 1
PBS	Phosphate buffered saline
PGC-1 α	PPAR γ co-activator 1 alpha
PIP2	Phosphatidylinositol (4,5)-bisphosphate
PIP3	Phosphatidylinositol (3,4,5)-trisphosphate
PKC	Protein kinase C
PPAR γ	Peroxisome proliferator-activated receptor gamma
PRX	Peroxiredoxins
Rac1	Ras-related C3 botulinum toxin substrate 1
RNS	Reactive nitrogen species
ROS	Reactive oxygen species
ROX	Residual oxygen consumption
SDS	Sodium dodecyl sulfate
Sirt1	Sirtuin 1
SOD	Superoxide dismutases
SUV	Standardized uptake value
T2DM	Type 2 diabetes mellitus
TBS	TRIS buffer solution
TBST	Tris buffered saline with Tween
TCA	Tricarboxylic acid
TG	Triglyceride
TGF- β	Transforming growth factor beta
TNF α	Tumor necrosis factor alpha
TRX	Thioredoxin
TRXR	Thioredoxin reductase
TZD	Thiazolidinedione
UCP	Uncoupling protein

SUMMARY

Background and aims: A healthy metabolism and proper regulation of blood sugar levels are key factors to maintain the quality of our daily lives. In these, a significant role can be played by skeletal muscle, which constitutes a substantial portion of the body. Beside adipose tissue, skeletal muscle also expresses the unique type 4 glucose transporter (GLUT4) responsible for glucose uptake. The GLUT4 translocation to the plasma membrane, and consequently glucose uptake involves complex regulatory mechanisms. Initiators of this process include insulin binding to the insulin receptor, which can regulate Akt substrate of 160 kDa (AS160; also known as TBC1D4) through the phosphoinositide 3-kinase (PI3K)/ 3-phosphoinositide-dependent protein kinase 1 (PDK1)/ Akt axis. AMP-activated protein kinase (AMPK), which senses cellular energy status, is also capable of regulating GLUT4 translocation via AS160. However, in case of insulin resistance and consequently in diabetes the GLUT4 translocation becomes impaired. As a result, blood glucose levels remain consistently high, giving rise to numerous long-term complications such as cardiovascular diseases, peripheral neuropathy, retinopathy, and diabetic nephropathy. Although the dramatically increasing number of patients makes it increasingly urgent to find a solution, so far, only a few compounds have been discovered capable of improving GLUT4 translocation and normalizing blood glucose levels.

The possibility has emerged that some less explored pathways in GLUT4 translocation, such as the bone morphogenetic protein (BMP) signaling pathway, might influence blood glucose regulation. Recently, it has been discovered that BMPs can sensitize tissues to insulin, increase the amount of GLUT4, reduce blood glucose levels through the PDK1/PI3K/Akt pathway, thus enhancing GLUT4 translocation, and changes in their serum levels correlate with diabetes. Since oxidative stress is known to play a role in the development of insulin resistance and diabetes, maintaining redox balance is of paramount importance. Astaxanthin is an exceptionally potent antioxidant capable of reducing high glucose- or fatty acid-induced reactive oxygen species (ROS) formation, improving insulin sensitivity, and enhancing glucose uptake. Moreover, astaxanthin is also easily available, as it is present in numerous marine organisms and consequently in our seafoods.

Therefore, our aim was to investigate the impact of a BMP-inducing agent, tilorone, on skeletal muscle glucose uptake in vitro and in vivo. Additionally, we aimed to explore how

astaxanthin, as a potent antioxidant, can influence the regulation of proteins crucial for GLUT4 translocation.

Materials and methods: The tilorone treatment was conducted at two concentrations (20 and 35 nM) on C2C12 myoblasts for a duration of 40 hours. Additionally, after 5 days of differentiation, tilorone was applied only at the lower concentration (20 nM) on myotubes to understand its acute effects at 2 and 5 hours on myotubes. In both of our *in vivo* experiments, we used 3-month-old C57BL/6 mice. Two intraperitoneal tilorone injections (25 mg/kg body weight) were administered with a 3-day interval. For the astaxanthin feeding model, the astaxanthin-containing preparation dissolved in ethanol was added to the mice's normal food at a dosage of 4 g/kg for a duration of 4 weeks. We used qRT-PCR to determine the transcription of BMPs, as well as GLUT1 and GLUT4. Western blot technique was used to examine Smad1/5/8 activation, the levels of GLUT1 and GLUT4, and the phosphorylation changes of molecules involved in GLUT4 translocation. Immunofluorescence labeling and microscopy were also utilized to assess GLUT4 quantities. Using glucose analogue, ^{18}F -fluoro-2-deoxyglucose (^{18}FDG), we investigated cellular glucose uptake. The specific inhibitor of GLUT1 was used to specify GLUT1-associated ^{18}FDG uptake. Myoblast mitochondrial function was assessed through high-resolution respirometry. Additionally, tissue glucose uptake was measured *in vivo* using ^{18}FDG -PET/CT imaging.

Key results: Tilorone is capable of inducing multiple BMPs (BMP2, BMP4, BMP7, and BMP14) in myoblasts and activating the BMP-mediated Smad1/5/8 and Smad4. As a result of tilorone treatment, GLUT4 levels increased, and Akt2/AS160 signaling was activated. The uptake of the labeled glucose also increased, which was not accompanied by an increase in mitochondrial O_2 consumption; in fact, the basal and ATP-linked respiration decreased. AS160 phosphorylation and glucose uptake were elevated in myotubes as well. Additionally, tilorone was able to further enhance insulin-stimulated Akt2 phosphorylation and ^{18}FDG uptake. *In vivo*, tilorone increased ^{18}FDG uptake in skeletal muscle, adipose tissue, and liver. Furthermore, astaxanthin feeding elevated the activation of proteins important in glucose uptake and metabolism in an *in vivo* mouse model.

Conclusions: Our results confirm that tilorone is a suitable agent as a broad-spectrum BMP inducer. The activated BMP pathway has a beneficial effect on skeletal muscle glucose uptake by enhancing GLUT4 translocation and also acts as an insulin sensitizer. Astaxanthin, as a natural antioxidant, can also contribute to skeletal muscle glucose metabolism. In light of our findings, both BMP signaling and antioxidant protection show remarkable potential in regulating skeletal muscle glucose uptake and thus possibly in the treatment of type 2 diabetes.

1. INTRODUCTION

1.1. Muscle rejuvenation

Skeletal muscles are responsible for breathing, voluntary movement, posture and even metabolism, all of which are accompanied by a significant size, which can account for up to 40% of our total body weight (Frontera and Ochala 2015). Its unique and indispensable function for maintaining quality of life is its ability to completely restore its structure and contractile functions after every day "wear and tear" or acute damage. This self-renewal ability is due to the presence of skeletal muscle stem cells, so-called satellite cells, which are at rest in special niche microenvironments under the basal lamina and next to the plasma membrane of the myofibrils (Fuchs and Blau 2020). As a result of disease or injury, satellite cells are activated and transform into myoblasts, which differentiate into myotubes after intense proliferation (Kuang et al. 2007). However, the availability of nutrients is also an influencing factor, since the differentiation of skeletal myoblasts deteriorates in the absence of glucose (Fulco et al. 2008), such a hypoglycaemic state also negatively affects the regeneration of skeletal muscle fibers, which can eventually lead to sarcopenia (Furuichi et al. 2021). On the other hand, cell aging can also decrease cellular glucose uptake (Nehlin et al. 2011), and aging leads to complex changes where myoblasts prefer glycolytic pathways over mitochondrial oxidative phosphorylation (OXPHOS) in myoblasts (Pääsuke et al. 2016).

1.2. Signal transduction pathways regulating skeletal muscle glucose uptake

In a healthy state, the normalization of elevated blood sugar levels is predominantly attributed to skeletal muscle, approximately 90% (Baron et al. 1988; DeFronzo and Tripathy 2009). In the human body, there are 13 transporters that enable to glucose uptake, among which insulin-dependent glucose transporter type 4 (GLUT4) is the most characteristic for skeletal muscle and adipose tissue (Huang and Czech 2007), although GLUT1, GLUT5, and GLUT12 are also present in muscle cells (Stuart et al. 2000; 2006). The ratio of GLUT1 and GLUT4 is mainly determined by the level of development of the muscle, so the role of GLUT1 is also important in myoblasts (Rauch and Loughna 2005; Zorzano, Fandos, and Palacín 2000).

GLUT4 differs from other GLUTs not only by its insulin dependence, but also by the fact that it is stored in small intracellular vesicles in the absence of a stimulus (Jaldin-Fincati et al. 2017). Release of intracellularly stored GLUT4s into the plasma membrane, or by on other

name GLUT4 translocation, can be initiated by the binding of insulin to the insulin receptor (Figure 1). After insulin binding, a conformational change occurs in its receptor in the skeletal muscle, then autophosphorylates it, finally transmits the signal to the insulin receptor substrate 1 (IRS1) (Lee and Pilch 1994; Leto and Saltiel 2012). The first element of the phosphorylated IRS1-initiated cascade involves phosphoinositide 3-kinase (PI3K), this can immediately start two types of processes. On the one hand, actin remodelling via Ras-related C3 botulinum toxin substrate 1 (Rac1)/p21-activated kinase 1 (PAK1)/Cofilin pathway, since the actin skeleton is essential for GLUT4 translocation (JeBailey et al. 2007; Merz et al. 2022). On the other hand, PI3K can activate 3-phosphoinositide-dependent protein kinase 1 (PDK1) via phosphatidylinositol (3,4,5)-trisphosphate (PIP3), which in turn activates Akt (Alessi et al. 1997; Vanhaesebroeck, Stephens, and Hawkins 2012; Satoh and Takenaka 2019). Akt2, the muscle-specific isoform of the Akt family, is a protein kinase B and its many targets include Akt substrate of 160 kDa (AS160; also known as TBC1D4), which is also very important in the GLUT4-containing vesicles translocation, and consequently glucose uptake (Sakamoto and Holman 2008).

Alternatively, independent of insulin, exercise can also initiate the GLUT4 transport to the muscle cell membrane via AMP-activated protein kinase (AMPK) mediated AS160 signaling. AMPK can be activated by the tumor suppressor liver kinase B1 (LKB1) (Stahmann et al. 2006) or by the calcium calmodulin-dependent protein kinase kinase β (CAMKK β), which is activated by increases in intracellular Ca^{2+} (Racioppi and Means 2012) or by the signal of decreased energy supply, in this way, both ADP/ATP and AMP/ATP ratios can contribute (Oakhill et al. 2011). AMPK and sirtuin 1 (Sirt1) have the ability to mutually influence each other's activity, and in conjunction, they regulate the activity of peroxisome proliferator-activated receptor- γ coactivator-1 α (PGC-1 α) (Price et al. 2012). This transcriptional coactivator plays a crucial role in various biological responses, such as mitochondrial biogenesis and glucose/fatty acid metabolism (Jäer et al. 2007). The peroxisome proliferator-activated receptor- γ (PPAR γ), which is directly responsible for the transcription of GLUT4, is also under the control of PGC-1 α (Armoni, Harel, and Karnieli 2007; Yap et al. 2020). Despite having opposing effects, both AMPK and Akt are capable of influencing numerous metabolic pathways through mammalian target of rapamycin (mTOR) signaling, such as glucose/fatty acid/amino acid metabolism, thereby impacting complex processes like cell growth and survival (Saxton and Sabatini 2017).

Both Akt2 and AMPK are capable of phosphorylating and thereby inactivating the Rab-GTPase-activating protein (Rab-GAP), AS160 (Sakamoto and Holman 2008). In the absence

of phosphorylation, AS160 keeps the Rab targets (Rab8A, Rab13, Rab14) in an inactive, GDP-bound state, thereby trapping the GLUT4 intracellularly (Eguez et al. 2005; Ishikura, Bilan, and Klip 2007; Y. Sun et al. 2010). These Rabs can interact with static (MICAL-L2, α -actinin-4, actin filaments) and motile (MyoVa) effectors to facilitate the mobilization of the GLUT4 vesicle (Jaldin-Fincati et al. 2017).

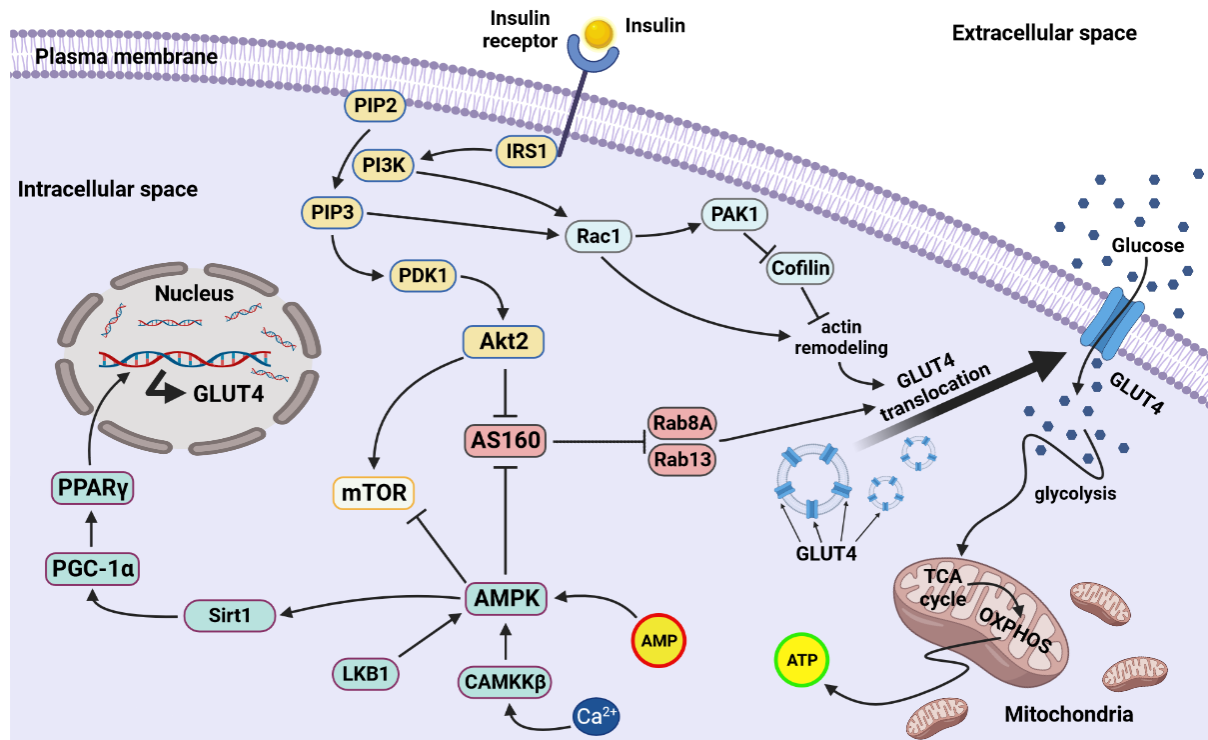


Figure 1. Regulatory mechanisms involved in GLUT4 translocation. The figure was created using BioRender.com. Akt, protein kinase B; AMP, adenosine monophosphate; AMPK, AMP-activated protein kinase; AS160, Akt substrate of 160 kDa; ATP, adenosine triphosphate; CAMKK β , calmodulin-dependent protein kinase kinase β ; GLUT4, glucose transporter type 4; IRS1, insulin receptor substrate 1; LKB1, liver kinase B1; mTOR, mammalian target of rapamycin; OXPHOS, oxidative phosphorylation; PAK1, p21-activated kinase 1; PDK1, 3-phosphoinositide-dependent protein kinase 1; PGC-1 α , peroxisome proliferator-activated receptor- γ coactivator-1 α ; PI3K, phosphoinositide-3-kinase; PIP2, phosphatidylinositol (4,5)-bisphosphate; PIP3, phosphatidylinositol (3,4,5)-trisphosphate; PPAR γ , peroxisome proliferator-activated receptor- γ ; Rac1, Ras-related C3 botulinum toxin substrate 1; Sirt1, Sirtuin 1; TCA cycle, tricarboxylic acid cycle

1.3. Impairment of GLUT4 translocation and diabetes mellitus

GLUT4 is the limiting element of skeletal muscle glucose uptake, and impaired GLUT4 translocation and reduced GLUT4 amount are the main cause of insulin resistance (Richter and Hargreaves 2013; Sanvee et al. 2019; Herman et al. 2022). Insulin resistance and inadequate insulin secretion are the underlying causes of type 2 diabetes mellitus (T2DM), also known as non-insulin-dependent diabetes mellitus (DM). T2DM accounts for 90% of all DM (Zimmet,

Alberti, and Shaw 2001; Holman, Young, and Gadsby 2015). It is well-established that the hyperglycemia in diabetic patients can lead to severe complications, as it increases oxidative stress in the heart, kidneys, and eyes (Forbes and Cooper 2013). Traditional, long-recognized complications of diabetes mellitus include stroke, coronary heart disease, heart failure, peripheral neuropathy, retinopathy, diabetic nephropathy, and peripheral vascular disease. With the advancement of diabetes mellitus treatment, new complications have been identified, such as cancer, infections, functional and cognitive impairment, liver disease, and affective disorders (Tomic, Shaw, and Magliano 2022). The number of diagnosed diabetes cases is rapidly increasing each year. In 2011, there were only 366 million people with diabetes worldwide, whereas by 2021, this number had already reached 536.6 million. This number is approaching the estimate of 552 million projected for 2030 back in 2011 (Whiting et al. 2011; H. Sun et al. 2022). The other projected numbers, based on estimations made in 2021, are also alarming: an estimated 634 million by 2030 and a staggering 783 million by 2045 (H. Sun et al. 2022). The situation is worsened by the fact that half of the diabetics (50.1%) were not diagnosed (Saeedi et al. 2019). Despite the large number of patients, only a few therapeutic agents are available. Among these, metformin (1,1-dimethylbiguanide hydrochloride), a derivative of biguanide, is the only one that specifically targets GLUT4 translocation to enhance cellular glucose uptake. Metformin is capable of downregulating mitochondrial respiration, increasing the AMP/ATP ratio, thereby activating AMPK, which senses cellular energy status and can initiate the GLUT4 translocation (Owen, Doran, and Halestrap 2000; Zhou et al. 2001). Other effective agents, thiazolidinediones (TZDs), increase the amount of GLUT4 itself via PPAR γ and thereby improve glucose uptake by cells (Kahn and McGraw 2010; Won 2021). Regrettably, they are linked to several side effects (Huan et al. 2019).

1.4. Bone morphogenetic proteins (BMPs) and the regulation of glucose uptake

Bone morphogenetic proteins (BMPs) belong to the transforming growth factor β (TGF- β) superfamily of proteins. These secreted proteins were initially described in relation to the formation of bones and cartilage (Urist 1965). However, in addition to their classical role in development, BMPs also play a role in numerous other biological processes, such as adipogenesis, obesity, and diabetes (Chen et al. 2021). BMPs can activate multiple Smad molecules through phosphorylation via their heterodimer receptor. These Smads belong to the receptor-regulatory Smads (R-Smads) (including: Smad1, 2, 3, 5, 8 and 9), one of the three groups into which the 9 Smad molecules can be classified based on their function and structure.

The second group, the co-mediating Smad (Co-Smad), consists only of Smad4. Smad1/5/8 can form a complex with Smad4 and regulate the transcription of many target genes in the nucleus (Massagué, Seoane, and Wotton 2005). The last group is the inhibitory Smads (I-Smads) with Smad6 and 7. I-Smads are able to inhibit R-Smads via BMP receptors, and their binding to Smad4 (Kim and Jin 2020). Furthermore, BMPs and Smad1/5/8 play an important role in mature skeletal muscle fibers (Sartori et al. 2013; 2021).

BMPs can be involved in the regulation of glucose uptake. BMP7 can increase glucose uptake in both muscle and adipose tissue through PDK1/PI3K/Akt pathway and GLUT4 translocation. In line with this, its amount in the serum decreased in T2DM (Chattopadhyay et al. 2017). In contrast, serum levels of BMP2 are increased in diabetic patients (Guiu-Jurado et al. 2016). However, BMP2 together with BMP6 have an insulin-sensitizing effect on adipocytes, increased the translocation of GLUT4 and, like TZDs, can increase the amount of GLUT4 via PPAR γ (Schreiber et al. 2017). BMP6 alone is capable to reduce serum lipid and glucose levels in ob/ob mice after 6 days (Pauk et al. 2019). BMP4 expression is increased in response to hyperglycemia and free fatty acids (Hong et al. 2016). Moreover, in humans, BMP4 levels correlate with adipocyte size, obesity, and insulin sensitivity (Modica et al. 2016). Unfortunately, the complex effects of BMPs are still not fully understood, and there is a lack of comprehensive studies investigating their combined actions.

1.5. Tilorone dihydrochloride

Leppäranta *et al.* demonstrated that a low molecular weight synthetic molecule, tilorone dihydrochloride (2,7-bis[2-(diethylamino)ethoxy]-9-fluorenone dihydrochloride; hereafter: tilorone) (Figure 2), can induce BMP2 and BMP7 transcription in lung epithelial cells (Leppäranta et al. 2013). Presumably through this BMP pathway, tilorone able to increase Smad1/5/8 phosphorylation, thereby inhibiting the loss of muscle mass and improve survival in mice with muscle cachexia (Sartori et al. 2021).

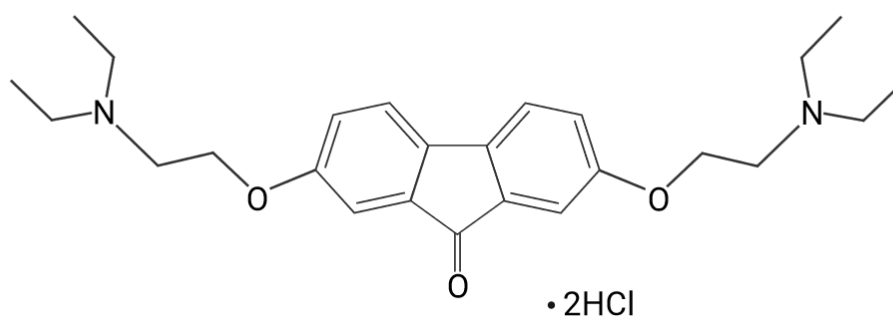


Figure 2. Chemical structure of tilorone dihydrochloride (tilorone, 2,7-bis[2-(diethylamino)ethoxy]-9-fluorenone dihydrochloride).

Tilorone has been known and used as an antiviral agent since the 1970s (Krueger and Mayer 1970). It is already used as an effective drug against many diseases, such as influenza, acute respiratory viral infection, viral hepatitis, and viral encephalitis (Ekins et al. 2018). Unfortunately, our current knowledge regarding the precise mechanism of action of tilorone is still incomplete. What we do know is that tilorone has the ability to induce transcriptional changes in numerous genes (Ratan et al. 2008), which may be attributed to its capability to intercalate to DNA (Nishimura et al. 2007). Tilorone is actively being investigated against emerging viral diseases such as herpes simplex virus, West Nile virus, Ebola virus (Katz, Margalith, and Winer 1976; Loginova et al. 2004; Ekins et al. 2018), and its effectiveness against human coronaviruses (MERS-CoV, SARS-CoV-2) has also been described (Shen et al. 2019; Puhl et al. 2021).

1.6. The relationship between reactive oxygen species and glucose uptake

The generation of reactive oxygen and nitrogen species (ROS/RNS) during metabolism is a natural process, and as long as the oxidants are in balance with the antioxidants, the functioning of the cells continues without disturbance. However, if this redox balance is disturbed, oxidants accumulate, the resulting oxidative stress can lead to many diseases, including T2DM (Abdali, Samson, and Grover 2015). ROS include superoxide anion radical ($O_2^{\cdot-}$), hydrogen peroxide (H_2O_2) and hydroxyl radical ($\cdot OH$). Among these, $\cdot OH$ is the most reactive and can be formed through the reaction of H_2O_2 with iron (or copper) ions (as the Fenton reaction). This highly reactive $\cdot OH$ can attack polyunsaturated fatty acids, leading to a loss of biomembrane integrity, damaging proteins and enzymes, impairing their functional

properties, and causing damage to nucleic acids, leading to mutations and ultimately resulting in cell senescence or death (Snezhkina et al. 2020).

The majority of ROS are formed in the mitochondria of cells during the terminal oxidation process required for ATP production (Snezhkina et al. 2020). Some metabolic factors can increase the generation of ROS, such as high environmental glucose, and this results in mitochondrial dysfunctions, inflammatory response and ultimately apoptosis (Newsholme et al. 2016; Rizwan et al. 2020). The loss of mitochondrial content and/or function and the consequent decrease in mitochondrial oxidation capacity can lead to insufficient lipid oxidation, the accumulation of excess lipids, and eventually even the development of insulin resistance (Di Meo, Iossa, and Venditti 2017). High levels of fatty acid metabolites can activate serine-threonine kinases, such as protein kinase C (PKC), c-Jun N-terminal kinase (JNK), and inhibitory κ B kinase β 1 (IKK β 1) (Hotamisligil et al. 1996; Itani et al. 2002; Arkan et al. 2005). The serine phosphorylation of IRS by these kinases inhibits the tyrosine phosphorylation of IRS by insulin, leading to a reduction in glucose uptake and insulin resistance (Hotamisligil et al. 1996). The phosphorylation of Akt and AS160, which regulates GLUT4 translocation, and the uptake of glucose also reduced due to tumor necrosis factor α - (TNF α)-induced ROS (Bouzakri and Zierath 2007). Oxidative stress impairs the binding of nuclear proteins to the insulin-responsive element of the GLUT4 promoter (Pessler, Rudich, and Bashan 2001). Moreover, ROS can also reduce the amount of GLUT4 by transporting GLUT4 to the lysosome instead of the plasma membrane. This process occurs through the disruption of the retromer complex in a casein kinase 2-dependent manner (J. Ma et al. 2014). In addition, peroxynitrite, formed by the accumulation of nitric oxide, can inhibit insulin action at multiple points. Firstly, it induces nitration of tyrosine residues and reduces IRS1 phosphorylation (Nomiyama et al. 2004). Secondly, peroxynitrite can suppress Akt activation (Zou et al. 2002). With all this knowledge in mind, it is extremely important that we preserve the redox balance and, if necessary, restore it with external help.

1.7. Antioxidant defense and astaxanthin

The human body is equipped with a number of antioxidants that are used to counteract the effects of oxidants. They can be divided into 2 categories: enzymatic and non-enzymatic. The enzymatic antioxidants include superoxide dismutases (SODs), catalase, glutathione peroxidase (GSH-Px) thioredoxins (TRXs), thioredoxin reductase (TRXRs) and

peroxiredoxins (PRXs) (Sáez and Están-Capell 2017). Nonenzymatic antioxidants include low-molecular-weight compounds, such as vitamins (vitamin C and E), carotenoids, uric acid, and glutathione (GSH) (Birben et al. 2012).

Astaxanthin (3,3'-dihydroxy- β,β' -carotene-4,4'-dione) (Figure 3) is a xanthophyll carotenoid, which first isolated from lobster (*Astacus gammarus*) in 1938 by Kuhn and Sørensen (Kuhn and Sørensen 1938). In the living world, astaxanthin can be synthesized by many species of algae, such as *Haematococcus pluvialis*, *Haematococcus lacustris*, *Chromochloris zofingiensis*, *Coelastrum sp.*, *Chlorella sorokiniana*, *Scenedesmus acutus* and *Euglena sanguinea*, as well as the yeast *Phaffia rhodozyma* (Patel et al. 2022). Crustaceans such as crabs and shrimps, which consume these over the long term, also accumulate astaxanthin, resulting in their reddish colour. Astaxanthin is transferred through the food chain to salmon as well, giving their muscles a unique pink-orange colour (Maoka 2011; Dai, Zang, and Lv 2022).

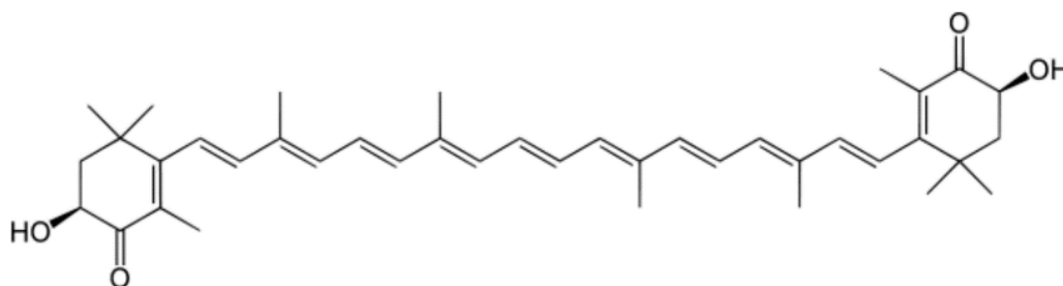


Figure 3. Chemical structure of astaxanthin (3,3'-dihydroxy- β,β' -carotene-4,4'-dione).

Astaxanthin, like other carotenoids, is lipid-soluble, and with its hydrophobic polyene carbon chain, it can fit into the interior of the lipid bilayer membrane. Additionally, its polar terminal rings enable it to appear close to both surfaces of the membrane. Thus, it is able to trap free radicals both in the membrane and on its surface (Goto et al. 2001). Astaxanthin can counteract oxidative damage through several mechanisms, including quenching singlet oxygen, scavenging radicals, inhibiting lipid peroxidation (Sztretye et al. 2019; Bjørklund et al. 2022). Astaxanthin exhibits a remarkable antioxidant activity, surpassing that of vitamin C, β -carotene, and α -tocopherol (Miki 1991; Ekpe, Inaku, and Ekpe 2018; Bjørklund et al. 2022).

Astaxanthin is capable of reducing both high glucose-, TNF α -induced ROS levels, as well as palmitic acid-induced ROS levels (Ishiki et al. 2013; Lai, Yang, and Yang 2020). As a result of astaxanthin treatment, a decrease in the phosphorylation of JNK and IRS1 serine residues can be observed. At the same time, insulin response enhancement, IRS1 tyrosine

phosphorylation, and GLUT4 translocation increase glucose uptake in mouse cell lines (Ishiki et al. 2013; W. Feng et al. 2020) and in mouse liver tissue (Bhuvaneswari and Anuradha 2012). Taking astaxanthin improved the blood sugar level after oral glucose tolerance test (OGTT) and level of HbA1c in middle-aged people, including subjects with diabetes (Urakaze et al. 2021). Moreover, astaxanthin able to reduce level of blood sugar and HbA1c, as well as the value of TG and cholesterol in T2DM patients (Chan, Chen, and Chen 2019).

2. AIMS OF THE THESIS

The effects of individual BMPs on glucose uptake and metabolism have been investigated earlier. This has allowed us to understand that certain members of BMP family influence glucose uptake through GLUT4 expression and translocation (Chattopadhyay et al. 2017; Schreiber et al. 2017). Furthermore, serum BMP levels are related to insulin sensitivity and T2DM (Guiu-Jurado et al. 2016; Modica et al. 2016). However, the combined effects of BMPs are still unknown. It has been proven that ROS reduces the amount of GLUT4 and impairs GLUT4 translocation, leading to insulin resistance in the long term (Bouzakri and Zierath 2007; J. Ma et al. 2014; Di Meo, Iossa, and Venditti 2017). However, the changes caused by the elimination of ROS with antioxidants are still incomplete in terms of regulating GLUT4 translocation. In this way, we set ourselves the goal of expanding our knowledge in relation to the following questions:

- Is tilorone really able to simultaneously increase the levels of several BMPs and activate the BMP signaling pathway in myoblasts?
- Does tilorone treatment have an effect on the proteins controlling GLUT4 translocation in myoblasts and myotubes?
- Can tilorone treatment increase the levels of GLUT1 and GLUT4, as well as glucose uptake in myoblasts?
- Is tilorone treatment able to sensitize myotubes to insulin?
- What is the effect of tilorone treatment on the amount and function of mitochondria of myoblasts?
- Does systemic tilorone treatment affect tissue glucose uptake in mice?
- Does astaxanthin feeding have an influence on the molecules that control glucose uptake in the skeletal muscle of mice?

3. MATERIALS AND METHODS

3.1. Cell culture, differentiation and treatment

Mouse C2C12 myoblast cells (ATCC, Manassas, VA, USA) were grown in high-glucose Dulbecco's modified Eagle's medium (DMEM) (4.5 g/L glucose with glutamine and pyruvate; #10-013-CV; Corning, NY, USA) supplemented with 20% fetal bovine serum (FBS) (Gibco/Thermo Fisher Scientific, Waltham, MA, USA) and contained a final concentration of 50 µg/mL gentamycin (Lonza, Basel, Switzerland).

Proliferating cells were treated with 2,7-bis[2-(diethylamino)ethoxy]-9-fluorenone dihydrochloride (tilorone dihydrochloride; #220957, Sigma-Aldrich) at a concentration of 20 or 35 nM for 40 h.

Myoblasts were seeded with an equal number of cells ($1.8-2 \times 10^5$ cells/well), and after 24 h of proliferation, when 80-90% confluence was reached, the medium was changed to a differentiation medium containing DMEM supplemented with 2% horse serum (Sigma-Aldrich) and 50 µg/mL gentamicin to initiate differentiation. At the end of the 5-day long differentiation, well developed myotubes are formed (Keller-Pinter et al. 2018; Szabo et al. 2022). Differentiated myotubes were treated with 20 nM tilorone (2 or 5 h) and, in some studies, with 100 nM insulin (Humulin-R; Eli Lilly, Indianapolis, IN, USA) for an additional 10 min on the 5th day of differentiation.

3.2. Experimental animals

Male C57BL/6J mice (n=4; The Jackson Laboratory, Bar Harbor, ME, USA) at 12 weeks of age were used for the tilorone experiments.

Young adult (3-months-old) wild-type C57BL/6 mice were used for chronic, 4-week-long astaxanthin feeding experiments (8 were fed with astaxanthin supplemented chow and 8 were fed normal rodent chow). The special chow was prepared with the addition of 4 g/kg of AstaReal A1010 (dissolved in 100% ethanol) to the standard rodent pellet (protein 20%, carbohydrates 70%, fats 4%, fibers 5%, vitamins, micro- and macronutrients) for a final concentration of 0.02% astaxanthin. This concentration was chosen according to the literature (Aoi et al. 2008; Sztretye et al. 2020).

Animals were housed under conventional conditions at $23 \pm 2^\circ\text{C}$ with $50 \pm 10\%$ humidity and artificial lighting with a circadian cycle of 12 h. The semi-synthetic diet (VRF1; Akromom Ltd., Budapest, Hungary) and drinking water were available ad libitum to all animals. The

animal experiments were approved by the Ethical Committee for Animal Research, University of Debrecen, Hungary (1/2017/DEBÁB, 3-1/2019/DEMÁB). Laboratory animals were kept and treated in compliance with all applicable sections of the Hungarian Laws and animal welfare directions and regulations of the European Union.

3.3. Quantitative real-time (qRT)-PCR

To perform qRT-PCR, the RotorGene 3000 instrument (Qiagen, Hilden, Germany) was used with gene-specific primers, and the change in RNA levels was monitored using the SybrGreen protocol. According to the manufacturer's instructions, 1 µg of C2C12 total RNA was reverse-transcribed in a final volume of 30 µL using a High-Capacity cDNA Archive Kit (Thermo Fisher Scientific). The reverse transcription was performed in a thermo cycler according to the following protocol: 10 min at room temperature, 2 h at 37°C, 5 min at 4°C, and 10 min at 75°C for enzyme inactivation. After a 2-fold dilution, 1 µL of the diluted reaction mix was used as the template for qRT-PCR. Reactions were performed with qPCR BIO SyGreen Mix Lo-ROX mix (PCR Biosystems, London, UK) according to the manufacturer's instructions at a final primer concentration of 250 nM under the following conditions: 2 min at 95°C followed by 40 cycles of 95°C for 5 s and 60°C for 30 s. To check the quality of the products, melting point analysis was performed after each reaction. Primers were designed using the online Roche Universal Probe Library Assay Design Center, and verified the quality by Bioneer MS analysis (Daejeon, South Korea). Individual threshold cycle (C_t) values were normalized to the mean C_t values of *MmHprt* and *MmRpl27* as internal control genes. Relative gene expression levels are presented as $2^{-\Delta\Delta C_t}$. Information about the genes and the primers is provided in Table 1.

Table 1. List of investigated genes and primers used in qRT-PCR experiments.

Reference Sequence	Gene name	Description	Primers	
			Forward	Reverse
NM_007553.3	Bmp2	Bone morphogenetic protein 2	ttccatcacgaagaagccgt	ttccatcacgaagaagccgt
NM_007554.3	Bmp4	Bone morphogenetic protein 4	tctgcaggaaccaatggagc	aaaggctcagagaagctgcg
NM_007557.3	Bmp7	Bone morphogenetic protein 7	cgagacctccagatcacagt	cagcaagaagaggtccgact
NM_008109.3	GDF5 (Bmp14)	Growth differentiation factor 5, Bone morphogenetic protein 14	tcctaagctcttaaggagagc	aagtaccaggcacaagaaggt
NM_008540.2	Smad4	SMAD family member 4	attggatggagacttcagg	tgcttagttcattctgtgtagatca
NM_011400.3	Slc2a1 (GLUT1)	Solute carrier family 2 (facilitated glucose transporter), member 1	gatcccagcagcaagaaggt	tagccgaactgcagtgatcc
NM_001359114.1	Slc2a4 (GLUT4)	Solute carrier family 2 (facilitated glucose transporter), member 4	gctctgacgtaaggatgggg	tcaatcaccttctgtggggc
NM_013556.2	HPRT	Hypoxanthine guanine phosphoribosyl transferase	cctctcagaccgctttt	aacctgttcattcatcgctaa
NM_011289.3	RPL27	Ribosomal protein L27	tgaagggttagcgaagtg	tttcatgaacttcccatctc

3.4. Gel electrophoresis and immunoblotting

C2C12 cells were lysed in RIPA buffer (20 mM Tris-HCl pH 7.5, 150 mM NaCl, 1 mM Na₂EDTA, 1 mM EGTA, 1% NP-40, 1% sodium deoxycholate, 2.5 mM sodium pyrophosphate, 1 mM β -glycerophosphate, 1 mM Na₃VO₄, 1 μ g/mL leupeptin; #9806, Cell Signaling Technology, Danvers, MA, USA) supplemented with 1 mM NaF and protease inhibitors (#P8340, Sigma-Aldrich) as described earlier (Szabo et al. 2022).

Biceps femoris, and pectoralis muscles of control and astaxanthin-fed mice were homogenized in buffer containing 50 mM of Tris-HCl pH 7.6, 100 mM of NaCl, 10 mM of EDTA, 1 mM of NaF, 1 mM of Na₃VO₄, and protease inhibitor cocktail (#P8340, Sigma-Aldrich).

The cell lysates were centrifuged for 5 min, while the muscle homogenates were centrifuged for 10 minutes at 16,000 \times g at 4 °C to eliminate cellular debris, and then the supernatants were quantified for protein concentration using the bicinchoninic acid method (#23227; Thermo Fisher Scientific). Equal amounts of proteins were separated by SDS-polyacrylamide gel electrophoresis and transferred onto Protran nitrocellulose membranes (GE Healthcare Amersham™, Little Chalfont, UK). The membranes were blocked in Tris Buffered Saline (TBS) containing 5% skimmed milk and 0.1% Tween-20 (Sigma-Aldrich) for 1 h at room temperature.

The membranes were overnight incubated at 4°C with the following rabbit primary antibodies: phospho-mTOR (Ser2448 #5536), mTOR (#2983), phospho-AS160 (Thr642; #8881), AS160 (#2670), PGC-1 α (#2178), phospho-AMPK (Thr172 #2535), AMPK (#2532), phospho-Akt2 (Ser474; #8599), Akt2 (#3063), pSmad1/5/8 [Smad1 (Ser463/465)/Smad5 (Ser463/465)/Smad9 (Ser465/467); #13820], PPAR γ (#2435) and GAPDH (#2118), all from Cell Signaling Technology (Leiden, Netherland), except for GLUT1 (#PA1-46152, Thermo Fisher Scientific) and GLUT4 (#NBP1-49533, Novus Biologicals, Littleton, CO, USA) and mouse desmin (#M076029-2; DAKO; Agilent, Santa Clara, CA, USA). All were used with a dilution of 1:1000 except GAPDH, that was 1:5000. After that, membranes were incubated with the horseradish peroxidase (HRP) conjugated anti-IgG secondary antibodies [anti-mouse (P0161) and anti-rabbit (P0448)] from DAKO (Glostrup, Denmark).

Enhanced chemiluminescence HRP substrate (#K-12045 Advansta, San Jose, CA, USA) was used to activate peroxidase and the chemiluminescence signal was recorded using X-ray films (Agfa, Mortsel, Belgium), and finally, Quantity One (Bio-Rad, Hercules, CA,

USA) software was used to quantify the density of specific bands. Protein signals were always normalized against GAPDH on the same membrane.

3.5. Fluorescent staining and microscopy

For fluorescent staining, the samples were fixed with 4% paraformaldehyde (Molar Chemicals Kft., Halásztelek, Hungary) for 15 min at room temperature, permeabilized with 0.2% Triton X100 (Sigma-Aldrich), and blocked with 2% BSA (Sigma-Aldrich) in PBS. Rabbit anti-GLUT4 primary antibody (#ab654; Abcam, Cambridge, UK or #NBP1-49533; Bio-Techne, Minneapolis, MN, USA) followed by Alexa Fluor 488-conjugated secondary antibody (#711-545-152; Jackson ImmunoResearch, Ely, Cambridgeshire, UK) was used to visualize GLUT4.

To label the mitochondria, the cells were incubated with MitoTracker™ Deep Red FM (#M22426, Thermo Fisher Scientific) under normal conditions and then fixed with 4% paraformaldehyde (Molar Chemicals Kft.) for 15 min at room temperature. The nuclei were counterstained with Hoechst 33258 (#94403, Sigma-Aldrich).

Wide-field fluorescence images were obtained using a Nikon Eclipse Ni-U fluorescence microscope (Nikon Instruments Inc., Melville, NY, USA) with a 100× objective (Nikon CFI Plan Apo DM Lambda 100× Oil, NA = 1.45). Images were normalized to their background, then signal intensity was quantified and plotted normalized to control. The evaluation and conversion of the images to a heat maps were performed with ImageJ software (National Institutes of Health, Bethesda, MD, USA).

Leica DMI1 phase-contrast microscope (Leica Microsystems, Wetzlar, Germany) with a 10× objective (Leica Hi Plan 10×, NA = 0.28) was used to generate representative images to show the morphology of undifferentiated (myoblast) and differentiated (myotube) C2C12 cells.

3.6. *In vitro* ¹⁸F-fluoro-2-deoxyglucose (¹⁸FDG) uptake measurement

To monitor the uptake of the radioactive glucose analog ¹⁸FDG by myoblast cells, C2C12 cells were seeded into 6-well plates ($0.08\text{--}0.1 \times 10^6$ cells/well). After 24-26 h of culture, the monolayer surface was washed with DMEM containing 1 mM glucose and 20% FBS. The cells were incubated in the presence of 10 μCi (0.37 MBq) of ¹⁸FDG in 1 mL DMEM containing 1mM glucose and 20% FBS. The plates were incubated for 1 h at 37°C, then the solution was removed and the cell surface was washed twice with 2 mL room-temperature PBS. Finally, the

cells were harvested, resuspended and the radioactivity of the suspension was measured with Packard Cobra-II Auto Gamma Counter device.

Tilorone treatment was performed at concentrations of 20 and 35 nM for 40 hours. Tilorone was also present during ^{18}F FDG incubation. To test the role of GLUT1 in glucose uptake, tilorone-treated cultures were incubated with a GLUT1 inhibitor, BAY-876 (#SML1774; Sigma-Aldrich) 10 nM for 2 h.

To measure the ^{18}F FDG uptake of differentiated myotubes, cells were seeded into 6-well plates ($1.8\text{--}2 \times 10^5$ cells/well) for 24 h in growth medium (DMEM, 20% FBS). Then after confirming that the cells had reached 90% confluence, the medium was switched to a differentiation medium consisting of DMEM supplemented with 2% horse serum (Sigma-Aldrich) and differentiated continued for an additional 5 days. On the 5th day on differentiation, cell cultures were treated with 20 nM tilorone for 2 or 5 h and 100 nm insulin for 10 min (Humulin-R; Eli Lilly). ^{18}F FDG uptake was measured as described previously.

3.7. Assessment of mitochondrial oxygen consumption (O_2 flux) using high-resolution respirometry

To examine the respiration of different experimental groups, myoblasts (3×10^6 cells) were suspended in 2 mL MiR05 respiration medium (pH 7.1; oxygen solubility factor 0.92) and gently pipetted into the oxygraph chambers (Oxygraph-2k, Oroboros Instruments, Innsbruck, Austria). All measurements were performed in 2 mL of respiration medium under continuous magnetic stirring (750 rpm) at 37°C. To avoid limitation of O_2 on mitochondrial respiration, chamber O_2 concentrations were kept in the range of 50-200 μM without reoxygenation (Doerrier et al. 2018; Nászai et al. 2019).

In intact cells, after stable routine respiration (without exogenous substrates and ADP), ATP synthase (or complex V) was inhibited with oligomycin (Omy; 2.5 μM ; LEAK respiration) for blocking mitochondrial ATP synthesis. Maximal capacity of the electron transport system (ETS) was achieved with stepwise titration of protonophore (CCCP; final concentration: 0.25 μM /steps). Following complex I inhibition (with 0.5 μM rotenone), the electron transport system-independent respiration (or residual oxygen consumption; ROX) was determined in the presence of complex III inhibitor, antimycin A (2.5 μM). DatLab 7.3 software (Oroboros Instruments, Innsbruck, Austria) was used for display, respirometry data acquisition, and analysis.

3.8. Animal treatment and *in vivo* imaging

C57BL/6J mice were injected intraperitoneally with a dose of 25 mg tilorone/kg body weight. The treatment was repeated 3 days after the first injection, and the positron emission tomography / computed tomography (PET/CT) scans were performed before the first injection and after the second injection.

Mice were anaesthetized with 3% Forane using a dedicated small animal anaesthesia device and were injected with 10.2 ± 0.9 MBq of ^{18}F FDG in 100 μL saline via the lateral tail vein before treatment and after the second tilorone treatment. 50 min after radiotracer injection, whole-body PET/CT scans were performed in isoflurane anaesthesia using the preclinical *nanoScan PET/MRI* 1T device (Mediso LTD., Hungary). After the image reconstruction and PET image analysis, the standardized uptake value (SUV) was calculated by the following formula: $\text{SUV} = [\text{ROI activity (MBq/mL)}] / [\text{injected activity (MBq)} / \text{animal weight (g)}]$ (Kocsis et al. 2017).

3.9. Statistical analysis

Statistical evaluations were performed via Student's t-test or one-way analysis of variance (ANOVA) followed by Dunnett's or Sidak post-hoc test. GraphPad Prism 8.0 (GraphPad Software Inc., San Diego, CA, USA) was used for graphing and statistical analyses. The data are expressed as the mean + standard errors of the means (SEM) or the median (horizontal line in the box) with the 25th (lower whisker) and 75th (upper whisker) percentiles are plotted on box plots. The p value less than 0.05 was considered significantly different.

4. RESULTS

4.1. Tilorone increases BMP signaling in myoblasts

The work of Leppäranta and colleagues on mouse epithelial cells provides evidence that tilorone is capable of inducing the transcription of BMP2 and BMP7 (Leppäranta et al. 2013). Thus, our first step was to determine whether it is possible to induce the transcription of BMPs with tilorone treatment in mouse myoblast cells. The treatment time was selected based on Leppäranta's experiment, where 24- and 48-h treatments were effective (Leppäranta et al. 2013). qRT-PCR revealed that mRNA levels of BMP2, BMP4, BMP7, and BMP14 were elevated by both (20 and 35 nM) tilorone concentrations in myoblasts; however, BMP14 expression was only significantly increased by the higher concentration (Figure 4). It is also worth noting from the qPCR results that Smad4, which is one of the components of the BMP signaling pathway, showed a significant increase in transcription at both concentrations (Figure 4). Further, we found that tilorone treatment led to an increase in the phosphorylation of Smad1/5/8(Ser463/Ser456/Ser467) (Figure 5A, B), indicating the augmentation of BMP signaling.

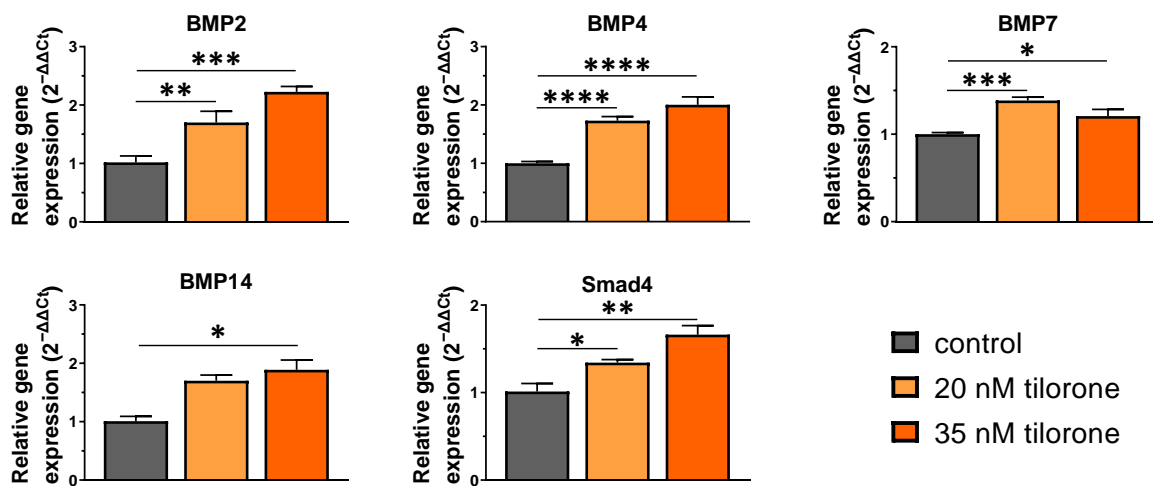


Figure 4. Transcriptional changes in bone morphogenetic protein (BMP) and Smad4 levels in C2C12 myoblast as the result of tilorone treatment. C2C12 myoblasts were treated with tilorone (40 h, 20 or 35 nM), and the gene expression of BMP2, BMP4, BMP7, BMP14, and Smad4 molecules was measured by qRT-PCR. Relative gene expression levels as $2^{-\Delta\Delta C_t}$ values using *MmHprt* and *MmRpl27* as housekeeping control genes, are presented. Data are reported as the mean + SEM (n= 3–4). *p < 0.05, **p < 0.01, ***p < 0.001, ****p < 0.0001.

4.2. Effect of tilorone on signaling molecules regulating GLUT4 translocation

As tilorone treatment enhanced the transcription of several BMPs and Smad4, and increased the phosphorylation of Smad1/5/8, we further investigated the impact of these proteins on insulin-dependent glucose uptake and assessed their regulatory role. BMP2 and BMP6 can sensitize adipocytes to insulin and enhance their glucose uptake (Schreiber et al. 2017). The C2C12 mouse skeletal muscle cell line is a widely studied and commonly used *in vitro* model for studying glucose homeostasis, insulin signaling mechanism, insulin resistance, GLUTs at the cellular and molecular levels (Mangnall, Bruce, and Fraser 1993; Tulipano, Spano, and Cocchi 2008; Wong, Al-Salami, and Dass 2020). Additionally, GLUT4 translocation has also been demonstrated in C2C12 myoblasts (Duan et al. 2017). We tested the expression and phosphorylation of skeletal muscle-specific Akt2, AMPK, and AS160, which play a prominent role in regulating the insulin-dependent and -independent translocation of GLUT4. Tilorone increased the phospho-Akt2(Ser474)/Akt2 and phospho-AMPK(Thr172)/AMPK ratios, and these changes were significant for 35 nM tilorone. The full amount of AS160 expression was decreased by both tilorone concentrations, and the phospho-AS160(Thr642)/AS160 ratio was increased (Figure 5A, B).

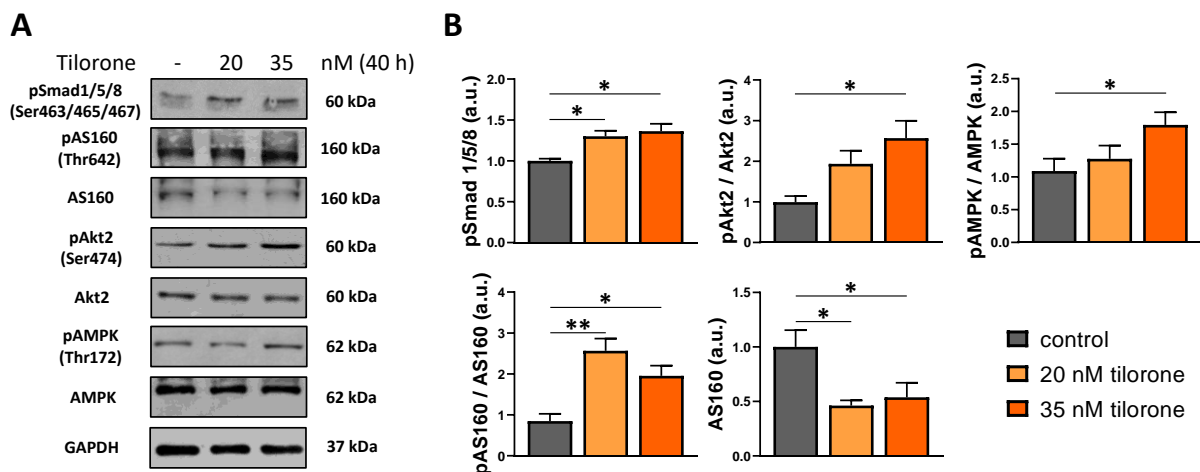


Figure 5. Changes in the BMP target Smad1/5/8 and in the molecules involved in the controlling of GLUT4 translocation in proliferating C2C12 cells as a result of tilorone treatment. (A) Representative Western blots depict the levels of phospho-Smad1/5/8(Ser463/Ser456/Ser467), phospho-AS160(Thr642), AS160, phospho-Akt2(Ser474), Akt2, phospho-AMPK(Thr172), and AMPK in proliferating C2C12 myoblasts following tilorone treatment (40h, 20 or 35 nM). GAPDH shows the equal loading of samples. (B) Quantification of the Western blot datas were normalized to the control and then the mean + SEM was plotted (n = 3–8). *p < 0.05, **p < 0.01. au, arbitrary unit

Following that, myoblasts were differentiated into myotubes *in vitro* (Figure 6A). To monitor the process of myoblast differentiation, we evaluated the amount of desmin, a muscle-specific intermediate filament. The increased level of desmin indicated the successful differentiation of the samples. The levels and phosphorylation of AS160(Thr642), the key regulator of GLUT4 translocation, were also examined on the fifth day of differentiation. Due to the observed effects of tilorone on myoblast differentiation (our unpublished data), we applied tilorone only for a short treatment in differentiated samples. In myotubes, 20 nM tilorone increased the phospho-AS160(Thr642)/AS160 ratio after either 2 and 5 h treatment (Figure 6B, C).

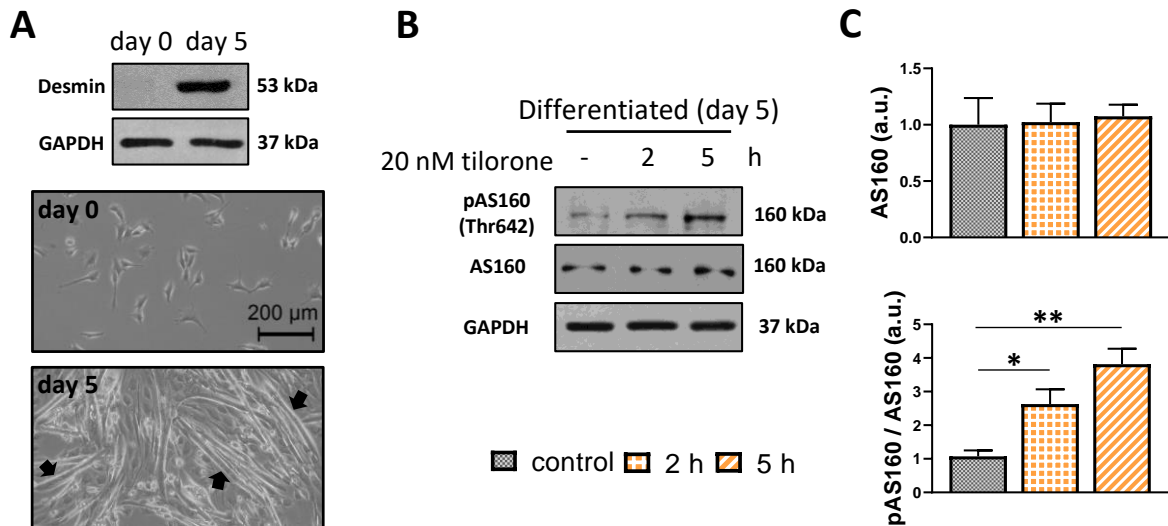


Figure 6. Phosphorylation changes of AS160 in differentiated myotubes after tilorone treatment. (A) Representative phase-contrast images of undifferentiated (proliferating) and differentiated C2C12 cells with $\times 10$ magnifications where arrows indicate myotubes. The representative immunoblot shows the change in the expression level of desmin in undifferentiated (Day 0) and in differentiated (Day 5) C2C12 cells. GAPDH was used as the loading control. (B) Representative Western blots depict the phospho- and total AS160 levels in differentiated C2C12 myotubes after tilorone treatment (2 or 5 h, 20 nM). GAPDH was used as a loading control. (C) Signals of proteins were normalized to the control and reported as mean + SEM (n = 3). *p < 0.05, **p < 0.01. au, arbitrary unit

4.3. Tilorone increases the expression of GLUTs and glucose uptake of C2C12 cells

Since increased phosphorylation of Akt2, AMPK, and AS160 favors GLUT4 translocation and glucose uptake, in the next step, we examined the intracellular expression of GLUT4 in tilorone-treated myoblasts using immunofluorescent staining and wide-field fluorescence microscopy. In addition to the original representative images, pseudocolor images

provide better visualization of the altered GLUT4 expression depicting the increased levels of GLUT4 fluorescence following tilorone treatment (Figure 7A). The high-intensity red and yellow areas were mainly adjacent to the nucleus in tilorone-treated cells (Figure 7A). Quantification of the whole GLUT4 fluorescence intensity of the cells revealed an increase in their GLUT4 content after tilorone treatment (Figure 7B).

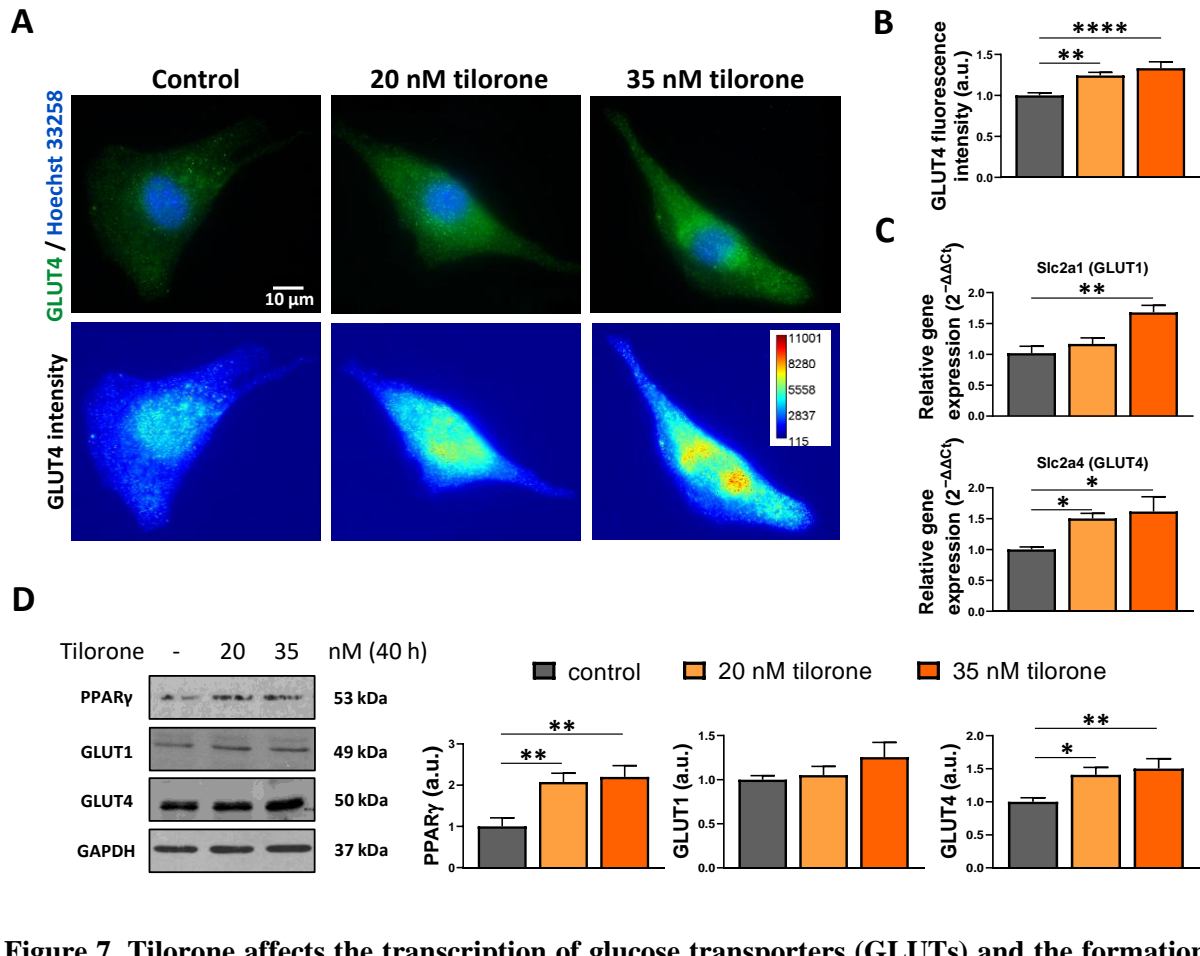


Figure 7. Tilorone affects the transcription of glucose transporters (GLUTs) and the formation of the GLUT4 protein in C2C12 myoblasts. C2C12 myoblasts were treated with tilorone (40 h, 20 or 35 nM). (A) Representative wide-field fluorescence images reveal the amount and distribution of GLUT4 following staining with Alexa Fluor 488 (green). DNA were stained by Hoechst 33258 (blue). Representative pseudocolor images depict GLUT4 signal intensity, corresponding to individual pixel intensities based on the calibration bar. (B) The mean intensity values of the cells were quantified, normalized to control, and compared following treatment. Data are reported as the mean + SEM (n = 3 independent experiments, 36–41 cells/treatment were quantified). (C) The levels of Scl2a1 (GLUT1) and Sclca4 (GLUT4) were studied by qRT-PCR and normalize to *MmHprt* and *MmRpl27* as internal control genes the results, then the relative gene expression levels were calculated using the $2^{-\Delta\Delta C_t}$ method. Data are reported as the mean + SEM (n = 3–4). (D) Representative western blots of PPAR γ , GLUT1, and GLUT4 protein expression. GAPDH was used as loading control. Quantification of the results normalized to control and reported as the mean + SEM (n = 3-8). *p < 0.05, **p < 0.01, ****p < 0.0001. au, arbitrary unit

Subsequently, qRT-PCR was conducted to examine the mRNA levels of myoblast-specific Slc2a1 (GLUT1) and Slc2a4 (GLUT4). It was found that treatment with various concentrations of tilorone resulted in increased levels of both Slc2a1 and Slc2a4 transcripts (Figure 7C). GLUT1 and GLUT4 protein levels were also analyzed by Western blot. While the level of GLUT1 were tendentially increased, the amount of GLUT4 protein increased at both concentrations (Figure 7D). Schreiber et al. demonstrated in mouse adipocytes that Smad1/5/8 and Smad4 can transcriptionally activate PPAR γ , which is a critical regulator of GLUT4 expression (Schreiber et al. 2017). Therefore, using the Western blot technique, we also examined the expression of PPAR γ , and we detected an increase in response to the two concentrations of tilorone we used (Figure 7D).

Since we observed elevated levels of GLUTs and intense activation of Akt2/AS160 signaling that regulate GLUT4 translocation, radiolabelled glucose analog ^{18}F FDG uptake of C2C12 cells was also measured. Our results revealed a 1.5-fold increase in ^{18}F FDG uptake after 20 nM tilorone treatment, and this uptake was further amplified by the higher concentration (Figure 8A). To determine the contribution of GLUT1 and GLUT4 to glucose uptake, we treated the cells with BAY-876, a specific inhibitor of GLUT1, after preincubation with tilorone. The BAY-876 treatment reduced cellular ^{18}F FDG uptake, indicating that GLUT1 is involved in tilorone-mediated glucose uptake (Figure 8B).

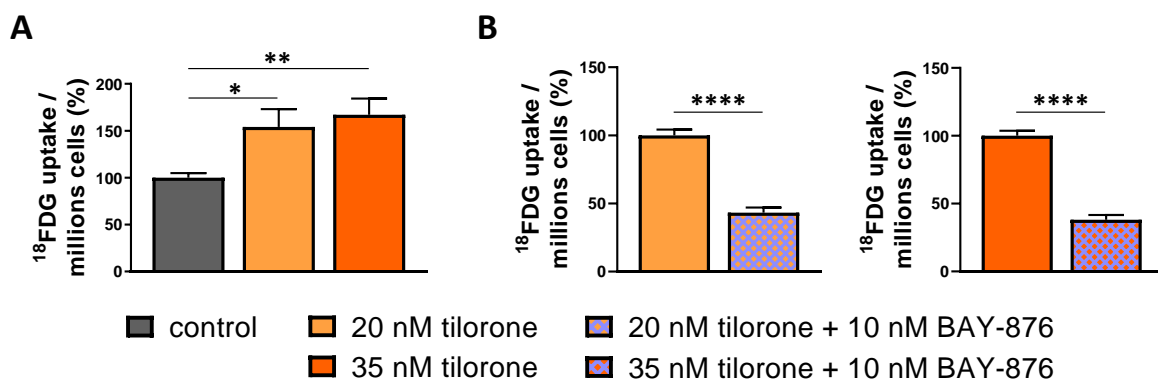


Figure 8. Changes in ^{18}F FDG uptake after tilorone treatment by C2C12 cells. (A) Changes in ^{18}F FDG uptake by C2C12 myoblasts as a result of tilorone treatment (24 h, 20 or 35 nM). ^{18}F FDG uptake is expressed as percentage of 1×10^6 myoblasts relative to the control. (B) The effect of BAY-876 (2 h, 10 nM), a GLUT1 inhibitor, on ^{18}F FDG uptake of tilorone-treated (24 h; 20 or 35 nM) C2C12 myoblasts. ^{18}F FDG uptake is expressed as percentage of 1×10^6 myoblasts relative to tilorone treated cells. Results are reported as the mean + SEM (n = 5–7). *p < 0.05, **p < 0.01, ****p < 0.0001.

4.4. Tilorone increases ^{18}F FDG uptake of myotubes and enhances insulin effect

Based on the previous results, tilorone improved glucose uptake in myoblasts, so the next investigation focused on whether tilorone has an insulin-sensitizing effect on myotubes. To assess this, a critical element of insulin-mediated signaling, the phosphorylation of Akt2, was measured using Western blot technique. As expected, Akt2(Ser474) phosphorylation was significantly increased upon insulin treatment in myotubes (Figure 9A, B). Furthermore, tilorone treatment further augmented the insulin-induced phospho-Akt2(Ser474)/Akt2 ratio, indicating the insulin-sensitizing effect of tilorone (Figure 9A, B).

After that, the ^{18}F FDG uptake of the myotubes was examined on the fifth day of differentiation. We observed increased ^{18}F FDG uptake of myotubes after tilorone treatment (5 h). Insulin increased the ^{18}F FDG uptake of control and tilorone-treated (2 or 5 h tilorone administration) groups. Notably, tilorone administration (5 h) further boosted the insulin-mediated ^{18}F FDG uptake of myotubes (Figure 9C).

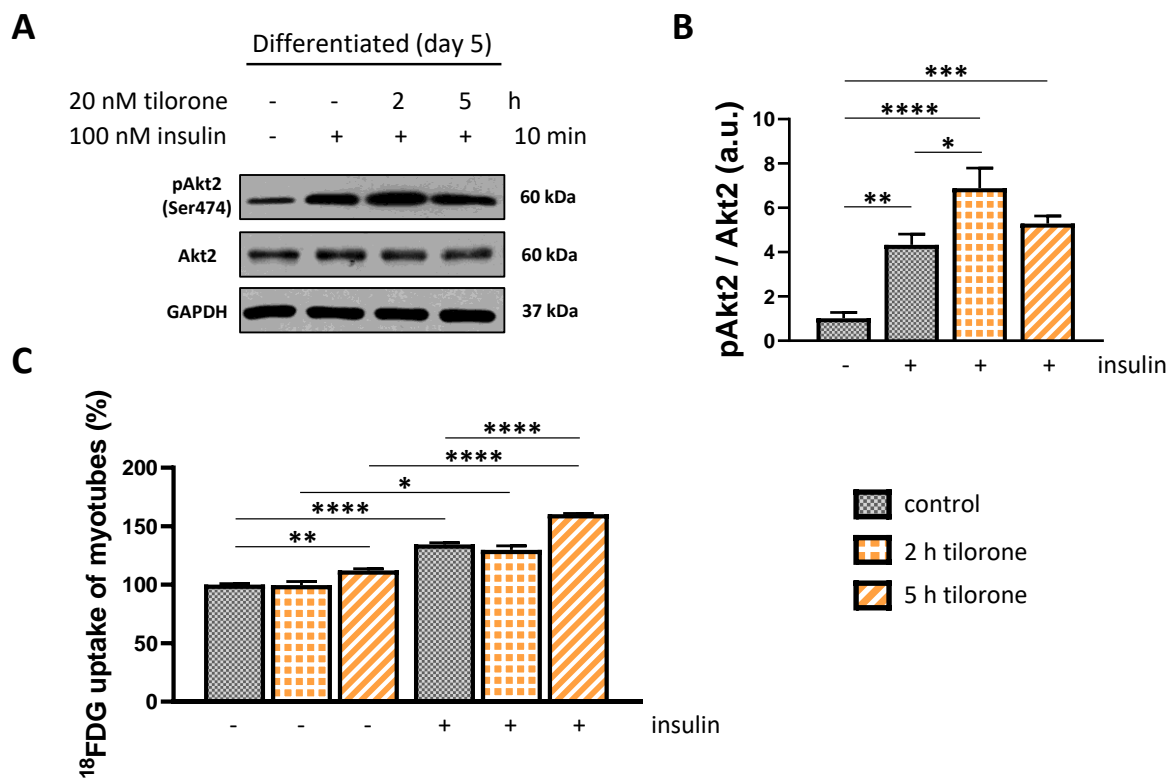


Figure 9. The influence of tilorone on insulin sensitivity and ^{18}F FDG uptake by myotubes. (A) Illustrative western blots depict the levels of phospho-Akt2 (Ser474), Akt2, and GAPDH in differentiated C2C12 myotubes after tilorone pretreatment (2 or 5 h, 20 nM) followed by insulin administration (100 nM, 10 min). GAPDH used as loading control. (B) Quantification of the western blot results, data normalized to untreated control and reported as the mean + SEM (n= 3–4). (C) The radioactively labeled glucose analog ^{18}F FDG uptake of C2C12 myotubes following tilorone (2 or 5 h, 20

nM) administration and with or without insulin (10 min 100 nM) treatment. ^{18}F FDG uptake is expressed as a percentage of the untreated control group. Results are reported as the mean + SEM ($n = 4$); * $p < 0.05$, ** $p < 0.01$, *** $p < 0.001$, **** $p < 0.0001$. au, arbitrary unit

4.5. Effects of tilorone treatment on mitochondrial function in myoblasts

To determine whether increased glucose uptake by cells affects the mitochondrial respiratory chain and indirectly the production of oxidative ATP, the oxygen consumption of C2C12 cells was investigated by high-resolution respirometry. Routine (baseline), proton leak, ETS (representing maximal respiration capacity), and ROX values are presented in a representative measurement plot in Figure 10A. Compared to the control group, treatment with 20 or 35 nM tilorone resulted in a significant decrease in routine respiration in intact myoblasts. Additionally, tilorone reduced ATP-linked respiration (difference between routine and leak respiration), which was evident from the unchanged leak values (Figure 10B).

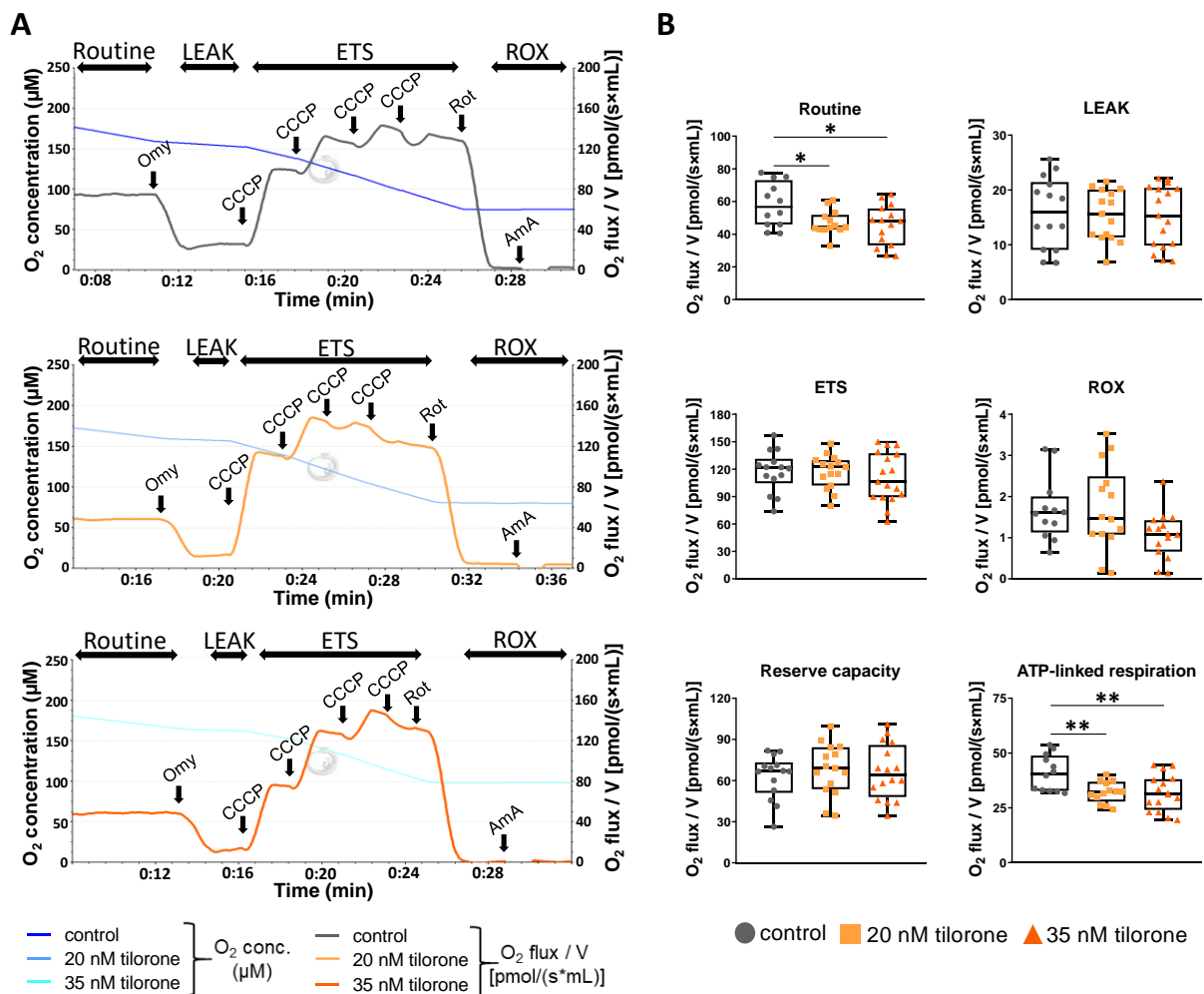


Figure 10. Effect of tilorone on mitochondrial respiration in C2C12 myoblasts. (A) On the representative experimental figures of the mitochondrial respiration measurements, the lines illustrate

chamber O₂ concentrations and mitochondrial O₂ flux in control and tilorone treated (40 h, 20 or 35 nM) cells. Maximal electron transport system (ETS) capacity was achieved via stepwise titration of an uncoupler (CCCP). (B) Measured routine respiration, LEAK state, maximal ETS capacity, residual oxygen consumption (ROX), reserve capacity, and ATP-linked respiration are presented as O₂ flux/V (pmol/[s × mL]). The box plots demonstrate the median (horizontal line in the box) and the 25th (lower whisker) and 75th (upper whisker) percentiles (n = 12–17). AmA, antimycin A; CCCP, carbonyl cyanide m-chlorophenyl hydrazone; Omy, oligomycin; Rot, rotenone

Observing changes in mitochondrial function, we investigated PGC-1 α , which regulates mitochondrial biogenesis, and assessed the total amount of mitochondria in the cells. The protein level of PGC-1 α analysed by Western blot did not show any change after treatment with 20 or 35 nM tilorone (Figure 11A). To achieve total amount of mitochondria in the cells, we visualized mitochondria using the specific fluorescent dye MitoTracker™ Deep Red FM, which passively diffuses across the plasma membrane of living cells and accumulates in active mitochondria (Figure 11B). We measured the total fluorescent intensity of the cells and found no difference between control and tilorone-treated cells (Figure 11C), indicating that the mitochondrial number did not change following tilorone treatment.

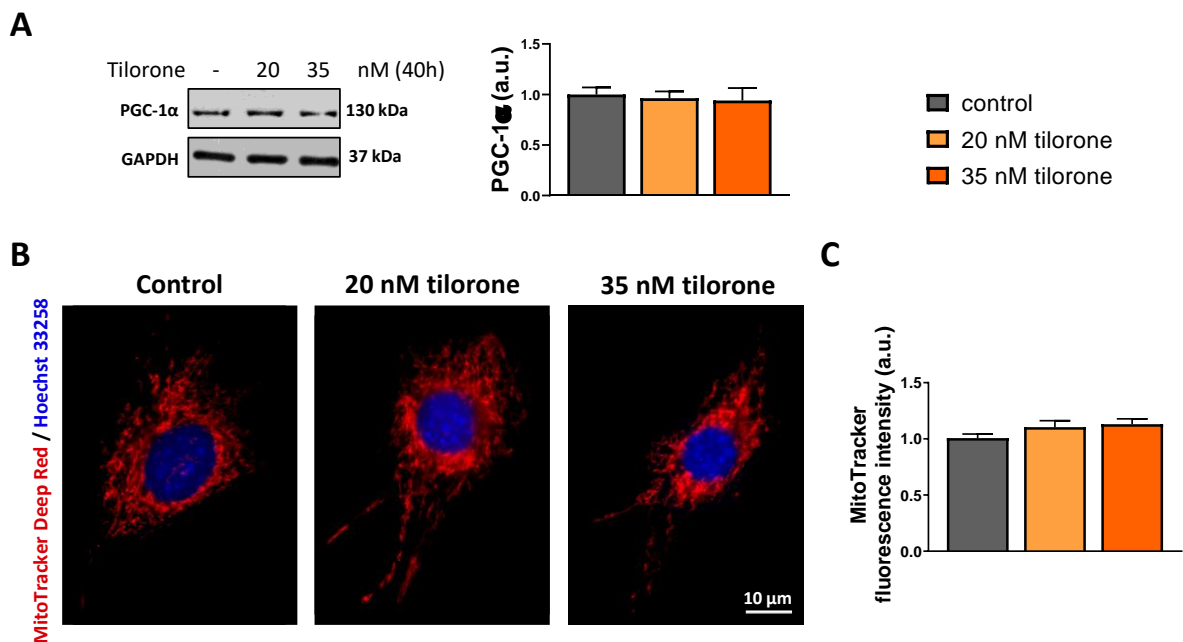


Figure 11. Effect of tilorone on the amount of mitochondria in C2C12 myoblasts. (A) Representative western blot image of PGC-1 α expression and GAPDH as a loading control. To quantify the results, the data were normalized to the control and then the mean + SEM was plotted (n = 5). (B) Representative images depict mitochondria labeled with MitoTracker Deep Red FM (red). Nuclei were stained by Hoechst 33258 (blue). (C) The fluorescence signal intensity of MitoTracker Deep Red FM staining was measured in the individual cells, and the total intensity values of the cells were compared. The results were normalized to control and reported as the mean + SEM (n = 3–4 independent experiments, 49–65 cells/treatment). *p < 0.05, **p < 0.01.; au, arbitrary unit

4.6. Tilorone administration increases ^{18}F FDG uptake *in vivo*

Based on the increased glucose uptake observed in skeletal muscle myoblasts and myotubes *in vitro*, we proceeded to investigate the effect of systemic tilorone administration on *in vivo* ^{18}F FDG uptake using PET/CT imaging. The selected treatment concentration was determined based on previous *in vivo* experiments and pharmacokinetics evaluation of tilorone (Leppäranta et al. 2013). The distribution of radiolabelled glucose in C57BL/6 mice was examined by PET/CT scans (Figure 12A). By performing quantitative analysis of the ^{18}F FDG-PET images, we observed a significant increase in the average SUV (Standardized Uptake Value) of skeletal muscle, adipose tissue, and liver following tilorone treatment, indicating enhanced radiotracer uptake in these tissues. The ^{18}F FDG accumulation was similar in tilorone-treated skeletal muscle, adipose tissues, and liver (Figure 12B). Among the examined tissues, heart exhibited the highest basal glucose uptake; however, it did not increase after tilorone treatment (Figure 12B).

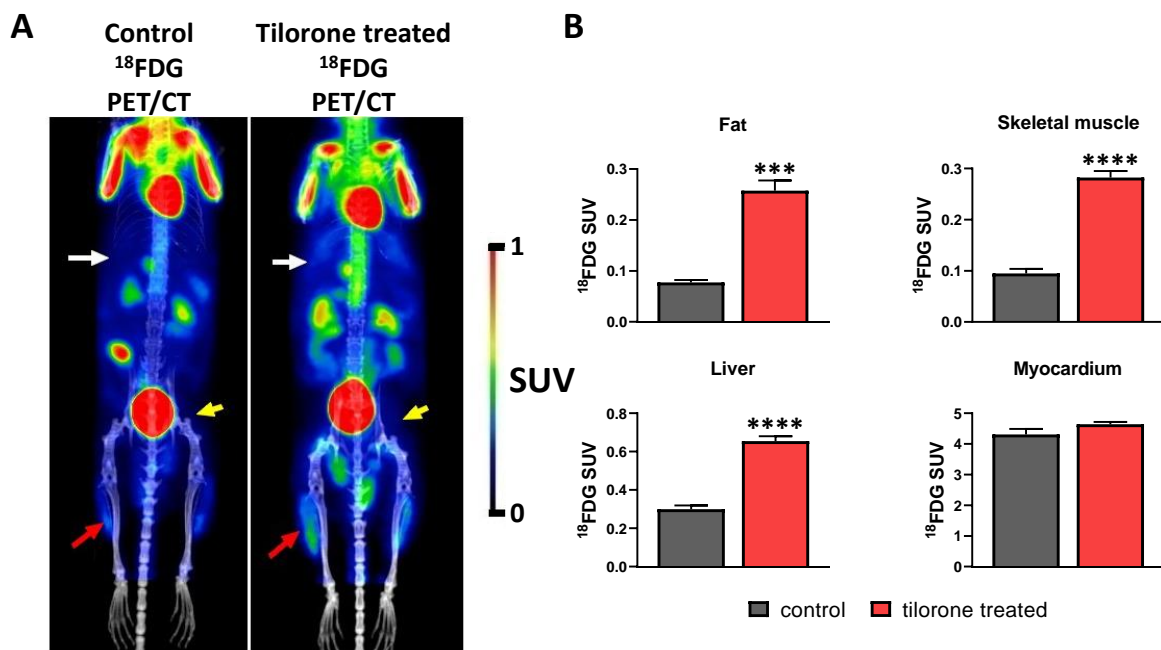


Figure 12. *In vivo* ^{18}F FDG uptake in C57BL/6 mice after tilorone treatment. (A) Representative decay-corrected ^{18}F FDG-PET/CT MIP (maximum intensity projection) images of the same C57BL/6 mouse before (left panel) and after twice repeated tilorone vaccination (25 mg/kg) (right panel). White arrows: liver, yellow arrows: fat, red arrows: muscle. (B) Quantitative analysis of ^{18}F FDG uptake of selected tissues (fat, liver, skeletal muscle, myocardium). Datas are reported as the mean of standardized uptake value (SUV) + SEM (n = 4); ***p < 0.001, ****p < 0.0001.

4.7. Astaxanthin feeding influences the activation of signaling molecules affecting skeletal muscle metabolism

Due to their size, skeletal muscles are responsible for a significant part of the metabolism of the entire body. Therefore, we aimed to investigate whether the astaxanthin diet affects proteins regulating skeletal muscle metabolism. Astaxanthin is known to accumulate in skeletal muscle (Aoi et al. 2003); therefore, the effects of long-term astaxanthin administration on representative muscles known to be involved in force production such as the hindlimb (biceps femoris muscle) or forelimb (pectoral muscle) muscles of the mice were studied. The levels and phosphorylation status of proteins involved in glucose uptake, regulation of cellular energy level, protein synthesis, and cell survival were also analysed.

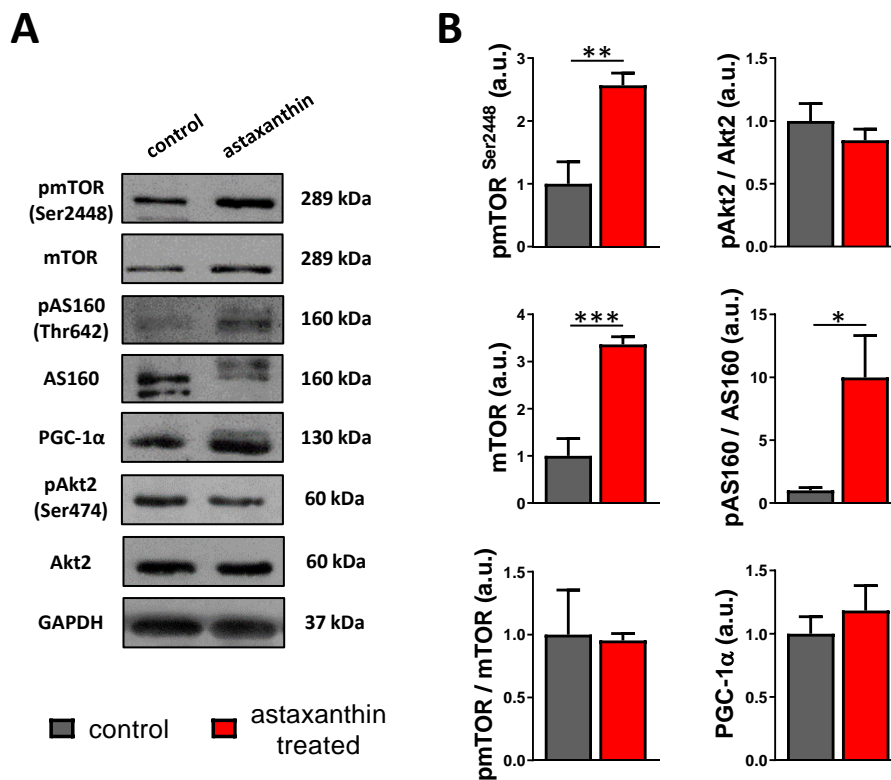


Figure 13. Effects of astaxanthin feeding on the levels of signaling proteins in biceps muscles. (A) Representative Western blots depict the levels of phosphor-mTOR(Ser2448), mTOR, phospho-AS160(Thr642), AS160, PGC-1 α , phospho-Akt2(Ser474) and Akt2. GAPDH used as loading control. (B) Statistical analysis of changes in signaling protein expression of the biceps femoris muscle. Quantification of the results is reported as mean + SEM (n = 3–4); * p < 0.05, ** p < 0.01, *** p < 0.001. au, arbitrary unit

In both of the two examined muscles, the biceps femoris and the pectoralis muscle, an increase in mTOR(Ser2448) phosphorylation was observed as a result of astaxanthin feeding

(Figure 13, 14). At the same time, the amount of total mTOR also showed an increase, therefore the phospho-mTOR(Ser2448)/mTOR ratio did not change significantly after astaxanthin treatment (Figure 13, 14). Although the Akt2 and the phospho-Akt2(Ser474)/Akt2 ratio did not change significantly in the studied samples, as only a mild elevation could be observed in pectoral muscles. Astaxanthin feeding significantly increased phospho-AS160(Thr642)/AS160 ratio in both biceps femoris and pectoral muscle samples (Figure 13, 14). The expression of PGC-1 α showed only a slight increase in the biceps femoris and pectoralis muscle samples following astaxanthin treatment (Figure 12A, B).

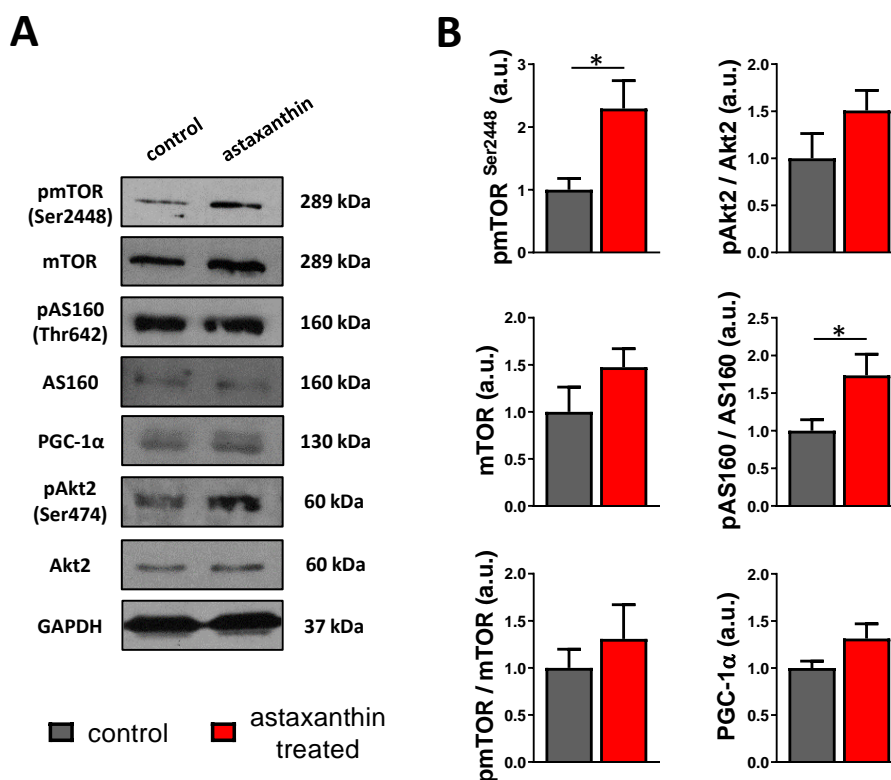


Figure 14. Effects of astaxanthin feeding on the levels of signaling proteins in pectoral muscles. (A) Representative Western blots depict the levels of phosphor-mTOR(Ser2448), mTOR, phospho-AS160(Thr642), AS160, PGC-1 α , phospho-Akt2(Ser474), Akt2 and GAPDH. GAPDH used as loading control. (B) statistical analysis of changes in signaling protein expression of the pectoral muscles. Quantification of the results is reported as mean + SEM (n = 3–4); * p < 0.05. au, arbitrary unit

5. DISCUSSION

The ever-increasing number of T2DM patients makes it increasingly urgent to find new and more effective treatment options for the disease (Whiting et al. 2011; H. Sun et al. 2022). Therefore, it is important to examine as many possible agents as possible for their effect in regulating glucose homeostasis.

Tilorone possesses a broad array of biological activities beyond its antiviral effect. In addition to ameliorating pulmonary fibrosis in a mouse model (Leppäranta et al. 2013), tilorone has also been shown to potentially provide a new therapeutic option for the treatment of fibrosis associated with heart failure (Horlock et al. 2021). Additionally, in tumor-bearing mice, it was demonstrated that the effect of tilorone depends on the BMP-Smad1/5/8 signaling pathway (Sartori et al. 2021). As a consequence, tilorone is capable of preventing muscle wasting and the function of the neuromuscular junction, which was confirmed in tumor-bearing mice (Sartori et al. 2021). Nevertheless, this finding does not rule out the existence of other potential targets for tilorone. In a previous study, a high-throughput drug screen identified the synthetic small-molecule compound tilorone has been shown to enhance the transcription of BMPs and increase the expression of the BMP target gene *Id3* (inhibitor of differentiation-3) in pulmonary epithelial cells *in vitro*. Moreover, it was observed to enhance Smad1 phosphorylation *in vivo* (Leppäranta et al. 2013). BMPs are known to play a role in insulin sensitization, glucose uptake, carbohydrate and lipid metabolism, as well as the regulation of mitochondrial function (Schreiber et al. 2017; Yu et al. 2017; Kohler et al. 2023). Therefore, we conducted investigations into the effects of tilorone on glucose uptake and metabolism both *in vitro* and *in vivo*. Several studies investigated the effect of tilorone on different cell types and at different concentrations. And because tilorone is used as an antiviral agent, we selected the concentration used in this study in line with its antiviral application (Lane and Ekins 2020).

In epithelial cells, tilorone has been found to enhance the transcription of BMP2 and BMP7, but not BMP4 (Leppäranta et al. 2013). However, in our experiment, we observed increased transcription of BMP2, BMP4, BMP7, and BMP14 in C2C12 myoblasts after tilorone treatment. Moreover, we noticed increased Smad1/5/8 phosphorylation and increased Smad4 transcription, indicating the enhanced BMP signaling due to tilorone.

Schreiber and colleagues successfully activated the Smad1/5/8 and Smad4 signaling pathways with BMP2 and BMP6 treatment, and these molecules increased the amount of GLUT4 by PPAR γ in 3T3-L1 adipocytes (Schreiber et al. 2017). In our experiments, tilorone

also increased the level of PPAR γ . PPAR γ is involved in regulating cell differentiation, glucose and lipid metabolism, lipid storage and mobilization (Janani and Ranjitha Kumari 2015), as well as mitochondrial biogenesis through PGC-1 α (Jamwal, Blackburn, and Elsworth 2020). Via another pathway, BMP14 can activate Sirt1, which deacetylates and thus activates PPAR γ (D. Wang et al. 2018). All of the BMPs we examined (i.e., BMP2, BMP4, BMP7, and BMP14) can positively regulate PPAR γ . Several targets of active PPAR γ include the Slc2a4 (GLUT4) gene (Wu et al. 1998; Armoni, Harel, and Karnieli 2007). Importantly, PPAR γ agonists have emerged as effective insulin sensitizers in the treatment of type 2 diabetes. The PPAR γ agonist TZD drugs have been criticized due to their harmful side effects (Huan et al. 2019).

Importantly, we observed that tilorone treatment affects both insulin-dependent (via GLUT4 translocation) and insulin-independent (via GLUT1) glucose uptake of myoblasts. GLUT1 is an insulin-independent transporter, and thus, it is essentially released into the plasma membrane of cells. The presence of GLUT1 in skeletal muscle was previously reported as the predominant GLUT isoform in myoblasts (Zhao and Keating 2007). The specific inhibition of GLUT1 markedly decreased (more than 50 % inhibition) the ¹⁸FDG uptake of tilorone treated cells indicating the involvement of GLUT1 in glucose uptake. However, it should also be taken into account that increasing the amount of GLUT4 alone would not be sufficient to increase glucose uptake. This is supported by the fact that treatment with BMP2 and BMP6 alone increased the amount of GLUT4 through PPAR γ , but did not promote GLUT4 translocation (Schreiber et al. 2017). The initiation of GLUT4 translocation can be attributed to the BMP7, which is capable of activating the PI3K/PDK1/Akt pathway, thereby enhancing GLUT4 translocation to the plasma membrane and increasing glucose uptake in adipose tissue and muscle (Chattopadhyay et al. 2017). Our results are completely consistent with these works, as the increased GLUT4 levels and activated Akt2/AS160 signaling together contribute to increased GLUT4-mediated glucose uptake, which is a result of tilorone simultaneously triggering the activation of multiple BMPs (summarized in Figure 12). However, it is important to note that we did not specifically evaluate GLUT4 at the plasma membrane. This is due to the limitations of using C2C12 cells as a model for studying directly the GLUT4 translocation.

Akt2/AS160 signaling plays a crucial role in regulating GLUT4 translocation. The phospho-AS160(Thr642)/AS160 ratio increased in both myoblasts and myotubes following tilorone treatment. However, the total AS160 level decreased in myoblasts after tilorone administration, but not in myotubes. Importantly, we applied tilorone to myoblasts for 40 h, which might have resulted in a negative feedback effect following increased glucose uptake, leading to the decreased level of total AS160 protein. The 40 h tilorone treatment allowed

sufficient time for quantitative protein changes in myoblasts, while the shorter treatment periods (2 or 5 h) on myotubes mainly facilitated faster phosphorylation changes.

Skeletal muscle is one of the most energy-demanding tissues in the human body. The transcription factor PGC-1 α plays a central role in the regulation of cellular energy metabolism by maintaining mitochondrial biogenesis and oxidative metabolism (Liang and Ward 2006). According to our results, the amount of active mitochondria did not change after tilorone treatment; however, both the routine and ATP-linked respiration values decreased despite the increased glucose uptake by the cells. This is particularly interesting because BMP7 overexpression has been described to enhance mitochondrial activity (basal respiration, ATP turnover, and respiratory capacity) and decrease MitoTracker Deep Red staining, indicating high uncoupling efficiency (Townsend et al. 2013). Our inconsistency with these results can be resolved by the fact that the studies were performed on brown adipocytes, which have a completely different uncoupling protein (UCP) profile compared to skeletal muscle (Boss et al. 1997; Fleury et al. 1997). The reduced mitochondrial function may explain the increased glucose uptake. It is worth noting that besides inducing BMPs, tilorone may have other cellular effects. Together, these effects could reduce ATP-linked respiration in mitochondria, possibly resulting in an increased intracellular AMP/ATP ratio. Elevated levels of AMP inhibit AS160 via AMPK and subsequently activate GLUT4 translocation (Huang and Czech 2007). This assumption is supported by the increased phospho-AMPK(Thr172)/AMPK ratio observed in cells treated with higher concentrations of tilorone.

Multiple studies have explored the role of BMPs in mitochondrial function and their effect on mitochondrial quantity in different tissues. In brown pre-adipocytes, BMP4 treatment led to a decrease in PGC-1 α mRNA levels while increasing PPAR γ 1 transcription (Modica et al. 2016). In line with this, the expression of PGC-1 α was reduced in the brown adipose tissue of BMP-4 overexpressing transgenic mice without a change in the number of mitochondria, while the transcription of these genes was increased in white adipose tissue (Qian et al. 2013). Based on these findings, BMP4 plays a role in mitochondrial functions, albeit in a strongly tissue-specific manner. And the BMP7, which, as mentioned above, enhances mitochondrial respiration in brown adipocytes, not by increasing the quantity of mitochondria, despite the elevated levels of PPAR γ (Townsend et al. 2013). Increased mitochondrial oxygen consumption was also detected after BMP2 treatment in human chondrocytes (C. Wang et al. 2018). Our results are partly consistent with this data; however, it is important to note that we examined the effect of tilorone treatment, which induces multiple BMPs simultaneously, and these BMPs may counteract each other's effects.

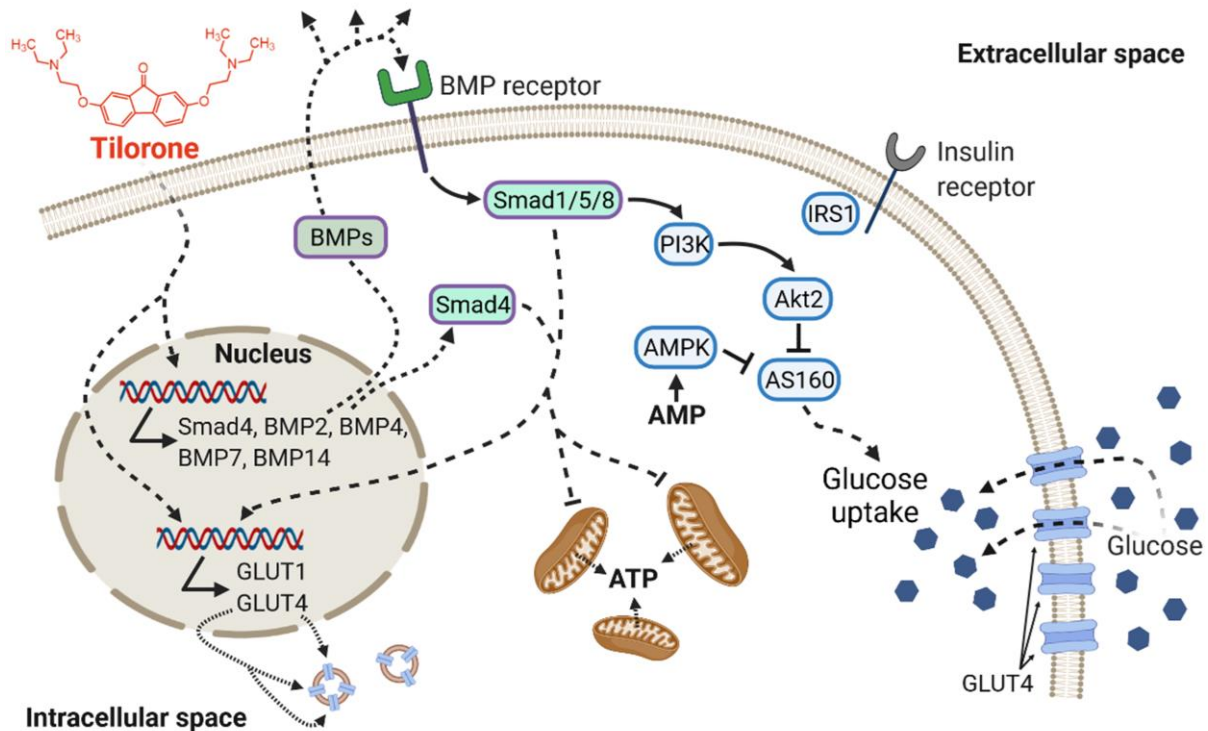


Figure 12. Schematic summary of the effects of tilorone on signaling pathways and glucose uptake. Tilorone induces the transcription of BMP2, BMP4, BMP7, and BMP14, and enhances the activity of the BMP pathway by increasing the phosphorylation of Smad1/5/8 and expression of Smad4. This activation leads to increased levels of glucose transporters (GLUT1 and GLUT4) and activation of the Akt2/AS160 pathway, both contributing to enhanced glucose uptake. Additionally, tilorone's effects on decreasing mitochondrial respiration and ATP-linked processes further support increased glucose uptake. The figure was created using BioRender.com. Akt, protein kinase B; AMP, adenosine monophosphate; AMPK, AMP-activated protein kinase; AS160, Akt substrate of 160 kDa; ATP, adenosine triphosphate; BMP, bone morphogenetic proteins; GLUT, glucose transporter; IRS1, insulin receptor substrate 1; PI3K, phosphoinositide-3-kinase.

Since it is known that oxidative stress plays a role in the development of insulin resistance and T2DM (Abdali, Samson, and Grover 2015; Tangvarasittichai 2015), we also investigated the role of an antioxidant, astaxanthin, in terms of molecules that regulate glucose uptake. Our data suggest that astaxanthin exerts new signaling effects which can greatly influence skeletal muscle metabolism.

Our investigations mainly aimed to explore the possibility of enhancing glucose uptake in skeletal muscles. There are several inducers of GLUT4 translocation; however, AS160 is an indispensable element in the regulation of GLUT4 membrane translocation (Thong, Bilan, and Klip 2007). Thus, the increased phosphorylation of AS160 is an essential signal for the glucose uptake of skeletal muscle and adipose tissue. In previous *in vitro* work on L6 myoblasts, it has been reported that astaxanthin treatment was able to enhance GLUT4 translocation and glucose uptake by restoring the redox balance (Ishiki et al. 2013). In an *in vivo* experiment, the role of

astaxanthin also was studied in mice, which were fed a high-fat, high-fructose diet. Among their results, it can be found that astaxanthin treatment was able to restore both Akt phosphorylation and the amount of GLUT4, which had deteriorated due to the diet (Arunkumar, Bhuvaneshwari, and Anuradha 2012). During our study, where we examined a long-term effect with 4 weeks of astaxanthin feeding, we observed a significant increase in the phospho-AS160(Thr642)/AS160 ratio in both the biceps femoris and pectoralis muscle samples (Gönczi et al. 2022). The increased phosphorylation of AS160(Thr642) can explain the beneficial effects of astaxanthin to improve insulin sensitivity. In the case of insulin resistance and type-2 diabetes mellitus the cellular amount of GLUT4 is decreased (Schreiber et al. 2017) and its translocation is impaired (Jaldin-Fincati et al. 2017); therefore, the promising results suggesting an increase in GLUT4 translocation imply the possibility of lowering blood glucose levels. The increased phospho-AS160(Thr642)/AS160 ratio following astaxanthin feeding presumably increases intracellular glucose levels and, consequently enhancing energy levels, and enabling cells to improve protein synthesis and muscle mass gain. This idea is further supported by an increase in mTOR phosphorylation in the astaxanthin-fed group, since mTOR stimulates protein synthesis and inhibits autophagy (X. M. Ma and Blenis 2009; Y. Feng, Yao, and Klionsky 2015). In our investigations, we found that astaxanthin feeding increased the phosphorylation of mTOR(Ser2448) in the biceps femoris and pectoralis muscles. However, the total amount of mTOR also increased along with the level of phosphorylation, resulting in no significant change in the phospho-mTOR(Ser2448)/mTOR ratio after astaxanthin treatment.

As we have already written about PGC-1 α above, this molecule is an extremely important, essential transcriptional coactivator in energy metabolism and the main regulator of mitochondrial biogenesis (Liang and Ward 2006). Moreover, PGC-1 α also increases GLUT4 levels and has multiple roles in the pathogenesis of T2DM (Soyal et al. 2006; Ruegsegger et al. 2018). In our experiments, the expression of PGC-1 α slightly increased in biceps femoris and pectoralis muscle samples following astaxanthin administration, which is close to a previous work, where PGC-1 α was significantly elevated in skeletal muscle samples following astaxanthin intake in mice (Liu et al. 2014). Although increased phosphorylation of Akt was described in L6 muscle cells following astaxanthin administration (Ishiki et al. 2013), however, the phospho-Akt2(Ser474)/Akt2 ratio measured by us did not show any significant change compared to the control. The discrepancy from the results projected by some literature data could be due to the possibility that the *in vivo* treatment we applied might have triggered systemic effects that were not considered in this study. On the other hand, it is also possible

that in a healthy organism, additional antioxidants do not further enhance normal metabolism at the cellular level. However, at the organism level, astaxanthin treatment is capable of improving blood glucose levels after OGTT and HbA1c values in healthy middle-aged people, including those with prediabetes (Urakaze et al. 2021). Thus, increased intake of the antioxidant, such as astaxanthin, can aid in the prevention of diabetes development and provide an effective treatment option for improving existing pathological conditions.

Summing up all these findings, we concluded that tilorone treatment is capable of upregulating BMP expression and activating the BMP signaling. The simultaneous activation of multiple BMPs induce widespread changes in skeletal muscle cells. Tilorone treatment leads to elevated levels of GLUT1 and GLUT4, activates crucial molecules involved in GLUT4 translocation regulation, and ultimately increases glucose uptake in the cells. Tilorone treatment reduces both basal and ATP-linked respiration without altering mitochondrial quantity. Additionally, it sensitizes myotubes to insulin-induced glucose uptake.

Tilorone can alter the glucose access of skeletal muscle cells both under *in vitro* and *in vivo* conditions, as confirmed by glucose analog ^{18}F FDG uptake measurements at the levels of myoblasts, myotubes, and skeletal muscle tissue. Moreover, tilorone increases the uptake of ^{18}F FDG by the liver and the other GLUT4-specific tissue, adipose tissue. However, a precise determination of the molecular mechanisms taking place here is still necessary. Given that the BMP pathway holds promise as a drug target for insulin resistance and diabetes, it becomes essential to investigate the potential therapeutic impact of tilorone on these conditions. Additionally, exploring tilorone's efficacy in skeletal muscle disorders characterized by disrupted BMP signaling is warranted. This study has the potential to broaden the application of tilorone, an already available medication.

Another subject of our investigation, astaxanthin, could also be a promising agent in relation to insulin resistance and diabetes. Astaxanthin has long been proven as a potent antioxidant, protecting cells against oxidative stress. Our findings suggest that it significantly influences the regulation of AS160, a central player in GLUT4 translocation regulation. While tilorone is available as a drug, the significant advantage of astaxanthin is its widespread presence in marine life, making it accessible through seafood and dietary supplements on store shelves. Thus, astaxanthin could serve as a valuable supplement, though not a replacement, for a healthy and balanced diet.

6. CONCLUSION

The regulation of GLUT4 translocation is a multifactorial process. Numerous molecules and signaling pathways are already known to be indispensable for the translocation of GLUT4 to the plasma membrane, allowing glucose uptake and energy production within cells. However, the connections between these pathways and other signaling molecules and routes are the subjects of investigation even in nowadays.

Our research also looked for connections between existing mechanisms and found an antiviral agent, tilorone, which is related to the regulation of glucose uptake by skeletal muscle cells through the inducing effect of BMP. The combined effect of BMPs reinforces each other and can increase the amount and translocation of GLUT4 in skeletal muscle cells, as well as the uptake of glucose. On the other hand, it is a question of what other mechanisms tilorone has an effect on, which may affect glucose uptake or mitochondrial functions.

Despite the fact that ROS naturally forms during the process of energy production, it has numerous negative effects on cellular metabolism, such as glucose uptake. Understanding to what extent and in which cases the elimination of generated ROS with antioxidants brings about significant changes in skeletal muscle glucose uptake is also of great importance. It is possible that even in healthy individuals, a powerful antioxidant like astaxanthin can only moderately enhance the regulation of glucose uptake in skeletal muscle, however, its preventive effect can be significant.

The results obtained from tilorone and astaxanthin treatments can bring mankind closer to the understanding of GLUT4 translocation and glucose uptake. Finally, this knowledge may one day provide a definitive solution to prevent and cure diabetes.

FUNDING

This research was supported by the National Research, Development and Innovation Office of Hungary [grant numbers: GINOP-2.3.2-15-2016-00040 (MYOTeam), EFOP-3.6.2-16-2017-00006, NKFI FK 134684, and NKFI K 132446]. Project no. TKP2021-EGA-28 has been implemented with the support provided by the Ministry of Innovation and Technology of Hungary from the National Research, Development and Innovation Fund, financed under the TKP2021-EGA funding scheme. The work was further supported by the János Bolyai Research Scholarship of the Hungarian Academy of Sciences (BO/00734/19/5) and UNKP-21-5-SZTE-571 New National Excellence Program of the Ministry for Innovation and Technology Sciences.

ACKNOWLEDGEMENTS

Here I would like to express my gratitude and thanks to all those who helped me navigate this bumpy road during the many years of work on my PhD studies.

To begin, I would like to express my gratitude to Professor László Dux Head of the Multidisciplinary Doctoral School and former Head of the Department of Biochemistry, and Tamás Bálint Csont, the current head of the Department of Biochemistry, for giving me the opportunity to work at the Institute in recent years.

I am grateful to my supervisor, Anikó Keller-Pintér, for her tireless support and professional guidance, which accompanied my PhD years.

I would like to express my gratitude to Professor László Csernoch and Professor Balázs Pál and his research team for the opportunity to work together.

I would also like to thank my co-authors György Trencsényi and Judit P. Szabo for the ^{18}F FDG measurements, László Juhász for his measurements on Oroboros, Ágnes Zvara and László G. Puskás for the qRT-PCR measurements.

I also owe a special thanks to Kitti Szabó, Dániel Becsky, Erzsébet Rádi and Zita Makráné Felhő for the great working atmosphere and mutual support. I would also like to thank the current members of our working group for their joint work: Enikő Tóth, Barnabás Horváth, Norman Noel Tanner, Dóra Julianna Szabó, Ágnes Szalenko-Tőkés and Éva Tóth; and former colleagues: Annamária Petrilla, Balázs Szenczi-Kaszás, Szuzina Fazekas.

Furthermore, I would like to thank all the members of the Biochemistry Institute. I received generous technical support and assistance from Ildikó Engi, Tünde Bodnár and Imre Ocsovszki.

I am grateful to my biology teacher, Katalin Szontagh, for making me like this field through her interesting lessons. And to my former supervisor, Ágnes Szepesi, for arousing my curiosity about the scientific career with our brainstorming sessions.

I express my heartfelt gratitude to my close friends and teachers. However, my deepest appreciation and thanks go to my family for their unwavering support, patience, and love, which they have always provided throughout my life.

REFERENCES

- Abdali, Daniyal, Sue E. Samson, and Ashok Kumar Grover. 2015. "How Effective Are Antioxidant Supplements in Obesity and Diabetes?" *Medical Principles and Practice* 24 (3): 201–15. <https://doi.org/10.1159/000375305>.
- Alessi, Dario R, Stephen R James, C Peter Downes, Andrew B Holmes, Piers R J Gaffney, Colin B Reese, and Philip Cohen. 1997. "Characterization of a 3-Phosphoinositide-Dependent Protein Kinase Which Phosphorylates and Activates Protein Kinase Ba." *Current Biology* 7 (4): 261–69.
- Aoi, Wataru, Yuji Naito, Kunihiro Sakuma, Masashi Kuchide, Harukuni Tokuda, Takashi Maoka, Shinya Toyokuni, Shigenori Oka, Masahiro Yasuhara, and Toshikazu Yoshikawa. 2003. "Astaxanthin Limits Exercise-Induced Skeletal and Cardiac Muscle Damage in Mice." *Antioxidants & Redox Signaling* 5 (1): 139–44. <https://doi.org/10.1089/152308603321223630>.
- Aoi, Wataru, Yuji Naito, Yoshikazu Takanami, Takeshi Ishii, Yukari Kawai, Satomi Akagiri, Yoji Kato, Toshihiko Osawa, and Toshikazu Yoshikawa. 2008. "Astaxanthin Improves Muscle Lipid Metabolism in Exercise via Inhibitory Effect of Oxidative CPT I Modification." *Biochemical and Biophysical Research Communications* 366 (4): 892–97. <https://doi.org/10.1016/J.BBRC.2007.12.019>.
- Arkan, Melek C., Andrea L. Hevener, Florian R. Greten, Shin Maeda, Zhi Wei Li, Jeffrey M. Long, Anthony Wynshaw-Boris, Giuseppe Poli, Jerrold Olefsky, and Michael Karin. 2005. "IKK- β Links Inflammation to Obesity-Induced Insulin Resistance." *Nature Medicine* 2005 11:2 11 (2): 191–98. <https://doi.org/10.1038/nm1185>.
- Armoni, Michal, Chava Harel, and Eddy Karnieli. 2007. "Transcriptional Regulation of the GLUT4 Gene: From PPAR- γ and FOXO1 to FFA and Inflammation." *Trends in Endocrinology & Metabolism* 18 (3): 100–107. <https://doi.org/10.1016/J.TEM.2007.02.001>.
- Arunkumar, Elumalai, Saravanan Bhuvanewari, and Carani Venkatraman Anuradha. 2012. "An Intervention Study in Obese Mice with Astaxanthin , a Marine Carotenoid – Effects on Insulin Signaling and pro-Inflammatory Cytokines." *Food & Function* 3 (2): 120–26. <https://doi.org/10.1039/C1FO10161G>.

- Baron, A. D., G. Brechtel, P. Wallace, and S. V. Edelman. 1988. "Rates and Tissue Sites of Non-Insulin- and Insulin-Mediated Glucose Uptake in Humans." *https://doi.org/10.1152/Ajpendo.1988.255.6.E769* 255 (6).
<https://doi.org/10.1152/AJPENDO.1988.255.6.E769>.
- Bhuvaneswari, Saravanan, and Carani Venkatraman Anuradha. 2012. "Astaxanthin Prevents Loss of Insulin Signaling and Improves Glucose Metabolism in Liver of Insulin Resistant Mice." *Canadian Journal of Physiology and Pharmacology* 90 (11): 1544–52.
<https://doi.org/10.1139/y2012-119>.
- Birben, E., Umit Murat Sahiner, Cansin Sackesen, Serpil Erzurum, and Omer Kalayci. 2012. "Oxidative Stress and Antioxidant Defense." *The World Allergy Organization Journal* 5 (1): 9. <https://doi.org/10.1097/WOX.0B013E3182439613>.
- Bjørklund, Geir, Amin Gasmi, Larysa Lenchyk, Mariia Shanaida, Saba Zafar, Pavan Kumar Mujawdiya, Roman Lysiuk, Halyna Antonyak, Sadaf Noor, Muhammad Akram, Kateryna Smetanina, Salva Piscopo, Taras Upyr, and Massimiliano Peana. 2022. "The Role of Astaxanthin as a Nutraceutical in Health and Age-Related Conditions." *Molecules* 2022, Vol. 27, Page 7167 27 (21): 7167.
<https://doi.org/10.3390/MOLECULES27217167>.
- Boss, Olivier, Sonia Samec, Ariane Paoloni-Giacobino, Colette Rossier, Abdul Dulloo, Josiane Seydoux, Patrick Muzzin, and Jean Paul Giacobino. 1997. "Uncoupling Protein-3: A New Member of the Mitochondrial Carrier Family with Tissue-Specific Expression." *FEBS Letters* 408 (1): 39–42. [https://doi.org/10.1016/S0014-5793\(97\)00384-0](https://doi.org/10.1016/S0014-5793(97)00384-0).
- Bouzakri, Karim, and Juleen R. Zierath. 2007. "MAP4K4 Gene Silencing in Human Skeletal Muscle Prevents Tumor Necrosis Factor- α -Induced Insulin Resistance." *Journal of Biological Chemistry* 282 (11): 7783–89. <https://doi.org/10.1074/jbc.M608602200>.
- Chan, Kung chi, Shih chueh Chen, and Pei chi Chen. 2019. "Astaxanthin Attenuated Thrombotic Risk Factors in Type 2 Diabetic Patients." *Journal of Functional Foods* 53 (February): 22–27. <https://doi.org/10.1016/J.JFF.2018.12.012>.
- Chattopadhyay, Tandrika, Rajiv Ranjan Singh, Sarika Gupta, and Avadhesh Surolia. 2017. "Bone Morphogenetic Protein-7 (BMP-7) Augments Insulin Sensitivity in Mice with Type II Diabetes Mellitus by Potentiating PI3K/AKT Pathway." *Biofactors* 43 (2): 195–

209. <https://doi.org/10.1002/biof.1334>.
- Chen, Yao, Bingwei Ma, Xingchun Wang, Xiaojuan Zha, Chunjun Sheng, Peng Yang, and Shen Qu. 2021. "Potential Functions of the BMP Family in Bone, Obesity, and Glucose Metabolism." *Journal of Diabetes Research* 2021. <https://doi.org/10.1155/2021/6707464>.
- Dai, Shuhan, Jiachen Zang, and Chenyan Lv. 2022. "Distribution, Purification, and Delivery of Astaxanthin in Food System." *J Food Sci Technol* 7: 456–67.
- DeFronzo, Ralph A, and Devjit Tripathy. 2009. "Skeletal Muscle Insulin Resistance Is the Primary Defect in Type 2 Diabetes." *Diabetes Care* 32 (suppl 2): S157–63.
- Doerrier, Carolina, Luiz F Garcia-Souza, Gerhard Krumschnabel, Yvonne Wohlfarter, András T Mészáros, and Erich Gnaiger. 2018. "High-Resolution FluoRespirometry and OXPHOS Protocols for Human Cells, Permeabilized Fibers from Small Biopsies of Muscle, and Isolated Mitochondria." In *Mitochondrial Bioenergetics*, 31–70. Springer.
- Duan, Yehui, Fengna Li, Wenlong Wang, Qiuping Guo, Chaoyue Wen, and Yulong Yin. 2017. "Alteration of Muscle Fiber Characteristics and the AMPK-SIRT1-PGC-1 α Axis in Skeletal Muscle of Growing Pigs Fed Low-Protein Diets with Varying Branched-Chain Amino Acid Ratios." *Oncotarget* 8 (63): 107011.
- Eguez, Lorena, Adrian Lee, Jose A Chavez, Cristinel P Miinea, Susan Kane, Gustav E Lienhard, and Timothy E McGraw. 2005. "Full Intracellular Retention of GLUT4 Requires AS160 Rab GTPase Activating Protein." *Cell Metabolism* 2 (4): 263–72.
- Ekins, Sean, Mary A Lingerfelt, Jason E Comer, Alexander N Freiberg, Jon C Mirsalis, Kathleen O'Loughlin, Anush Harutyunyan, Claire McFarlane, Carol E Green, and Peter B Madrid. 2018. "Efficacy of Tilorone Dihydrochloride against Ebola Virus Infection." *Antimicrobial Agents and Chemotherapy* 62 (2).
- Ekpe, Lawson, Kenneth Inaku, and Victor Ekpe. 2018. "Antioxidant Effects of Astaxanthin in Various Diseases—A Review." *J. Mol. Pathophysiol* 7 (1): 1–6.
- Feng, Weihong, Yanxia Wang, Na Guo, Pu Huang, and Yang Mi. 2020. "Effects of Astaxanthin on Inflammation and Insulin Resistance in a Mouse Model of Gestational Diabetes Mellitus." *Dose-Response* 18 (2). <https://doi.org/10.1177/1559325820926765>.
- Feng, Yuchen, Zhiyuan Yao, and Daniel J. Klionsky. 2015. "How to Control Self-Digestion:

- Transcriptional, Post-Transcriptional, and Post-Translational Regulation of Autophagy.” *Trends in Cell Biology*. Elsevier. <https://doi.org/10.1016/j.tcb.2015.02.002>.
- Fleury, Christophe, Maria Neverova, Sheila Collins, Serge Raimbault, Odette Champigny, Corinne Levi-Meyrueis, Frederic Bouillaud, Michael F. Seldin, Richard S. Surwit, Daniel Ricquier, and Craig H. Warden. 1997. “Uncoupling Protein-2: A Novel Gene Linked to Obesity and Hyperinsulinemia.” *Nature Genetics* 15:3 15 (3): 269–72. <https://doi.org/10.1038/ng0397-269>.
- Forbes, Josephine M., and Mark E. Cooper. 2013. “Mechanisms of Diabetic Complications.” *Physiological Reviews*. American Physiological Society Bethesda, MD. <https://doi.org/10.1152/physrev.00045.2011>.
- Frontera, Walter R., and Julien Ochala. 2015. “Skeletal Muscle: A Brief Review of Structure and Function.” *Behavior Genetics*. Springer New York LLC. <https://doi.org/10.1007/s00223-014-9915-y>.
- Fuchs, Elaine, and Helen M. Blau. 2020. “Tissue Stem Cells: Architects of Their Niches.” *Cell Stem Cell* 27 (4): 532–56. <https://doi.org/10.1016/J.STEM.2020.09.011>.
- Fulco, Marcella, Yana Cen, Po Zhao, Eric P. Hoffman, Michael W. McBurney, Anthony A. Sauve, and Vittorio Sartorelli. 2008. “Glucose Restriction Inhibits Skeletal Myoblast Differentiation by Activating SIRT1 through AMPK-Mediated Regulation of Nampt.” *Developmental Cell* 14 (5): 661–73. <https://doi.org/10.1016/j.devcel.2008.02.004>.
- Furuichi, Yasuro, Yuki Kawabata, Miho Aoki, Yoshitaka Mita, Nobuharu L. Fujii, and Yasuko Manabe. 2021. “Excess Glucose Impedes the Proliferation of Skeletal Muscle Satellite Cells Under Adherent Culture Conditions.” *Frontiers in Cell and Developmental Biology* 9 (March): 341. <https://doi.org/10.3389/fcell.2021.640399>.
- Gönczi, Mónika, Andrea Csemer, László Szabó, Mónika Sztretye, János Fodor, Krisztina Pocsai, Kálmán Szenthe, Anikó Keller-Pintér, Zoltán Márton Köhler, Péter Nánási, Norbert Szentandrassy, Balázs Pál, and László Csernoch. 2022. “Astaxanthin Exerts Anabolic Effects via Pleiotropic Modulation of the Excitable Tissue.” *International Journal of Molecular Sciences* 23 (2): 917. <https://doi.org/10.3390/ijms23020917>.
- Goto, Satoru, Kentaro Kogure, Kazutoyo Abe, Yukari Kimata, Katsuhiko Kitahama, Eiji Yamashita, and Hiroshi Terada. 2001. “Efficient Radical Trapping at the Surface and

- inside the Phospholipid Membrane Is Responsible for Highly Potent Antiperoxidative Activity of the Carotenoid Astaxanthin.” *Biochimica et Biophysica Acta (BBA) - Biomembranes* 1512 (2): 251–58. [https://doi.org/10.1016/S0005-2736\(01\)00326-1](https://doi.org/10.1016/S0005-2736(01)00326-1).
- Guiu-Jurado, Esther, Mark Unthan, Nina Böhler, Matthias Kern, Kathrin Landgraf, Arne Dietrich, Dorit Schleinitz, Karen Ruschke, Nora Klöting, Mathias Faßhauer, Anke Tönjes, Michael Stumvoll, Antje Körner, Peter Kovacs, and Matthias Blüher. 2016. “Bone Morphogenetic Protein 2 (BMP2) May Contribute to Partition of Energy Storage into Visceral and Subcutaneous Fat Depots.” *Obesity* 24 (10): 2092–2100. <https://doi.org/10.1002/OBY.21571>.
- Herman, Rok, Nika Aleksandra Kravos, Mojca Jensterle, Andrej Janež, and Vita Dolžan. 2022. “Metformin and Insulin Resistance: A Review of the Underlying Mechanisms behind Changes in GLUT4-Mediated Glucose Transport.” *International Journal of Molecular Sciences* 2022, Vol. 23, Page 1264 23 (3): 1264. <https://doi.org/10.3390/IJMS23031264>.
- Holman, N, B Young, and R Gadsby. 2015. “Current Prevalence of Type 1 and Type 2 Diabetes in Adults and Children in the UK.” *Diabetic Medicine* 32 (9): 1119–20. <https://doi.org/10.1111/dme.12791>.
- Hong, Oak-Kee, Soon-Jib Yoo, Jang-Won Son, Mee-Kyoung Kim, Ki-Hyun Baek, Ki-Ho Song, Bong-Yun Cha, Hanjoong Jo, and Hyuk-Sang Kwon. 2016. “High Glucose and Palmitate Increases Bone Morphogenic Protein 4 Expression in Human Endothelial Cells.” *The Korean Journal of Physiology & Pharmacology* 20 (2): 169. <https://doi.org/10.4196/kjpp.2016.20.2.169>.
- Horlock, Duncan, David M. Kaye, Catherine E. Winbanks, Xiao Ming Gao, Helen Kiriazis, Daniel G. Donner, Paul Gregorevic, Julie R. McMullen, and Bianca C. Bernardo. 2021. “Old Drug, New Trick: Tilorone, a Broad-Spectrum Antiviral Drug as a Potential Anti-Fibrotic Therapeutic for the Diseased Heart.” *Pharmaceuticals* 2021, Vol. 14, Page 263 14 (3): 263. <https://doi.org/10.3390/PH14030263>.
- Hotamisligil, Gökhan S., Pascal Peraldi, Adriane Budavari, Ramsey Ellis, Morris F. White, and Bruce M. Spiegelman. 1996. “IRS-1-Mediated Inhibition of Insulin Receptor Tyrosine Kinase Activity in TNF- α - and Obesity-Induced Insulin Resistance.” *Science* 271 (5249): 665–68. <https://doi.org/10.1126/SCIENCE.271.5249.665>.

- Huan, Yi, Xuan Pan, Jun Peng, Chunming Jia, Sujuan Sun, Guoliang Bai, Xing Wang, Tian Zhou, Rongcui Li, Shuainan Liu, Caina Li, Quan Liu, Zhanzhu Liu, and Zhufang Shen. 2019. "A Novel Specific Peroxisome Proliferator-activated Receptor γ (PPAR γ) Modulator YR4-42 Ameliorates Hyperglycaemia and Dyslipidaemia and Hepatic Steatosis in Diet-induced Obese Mice." *Diabetes, Obesity & Metabolism* 21 (11): 2553. <https://doi.org/10.1111/DOM.13843>.
- Huang, Shaohui, and Michael P. Czech. 2007. "The GLUT4 Glucose Transporter." *Cell Metabolism* 5 (4): 237–52. <https://doi.org/10.1016/j.cmet.2007.03.006>.
- Ishiki, Manabu, Yasuhiro Nishida, Hiroshi Ishibashi, Tsutomu Wada, Shiho Fujisaka, Akiko Takikawa, Masaharu Urakaze, Toshiyasu Sasaoka, Isao Usui, and Kazuyuki Tobe. 2013. "Impact of Divergent Effects of Astaxanthin on Insulin Signaling in L6 Cells." *Endocrinology* 154 (8): 2600–2612. <https://doi.org/10.1210/EN.2012-2198>.
- Ishikura, Shuhei, Philip J Bilan, and Amira Klip. 2007. "Rabs 8A and 14 Are Targets of the Insulin-Regulated Rab-GAP AS160 Regulating GLUT4 Traffic in Muscle Cells." *Biochemical and Biophysical Research Communications* 353 (4): 1074–79.
- Itani, Samar I., Neil B. Ruderman, Frank Schmieder, and Guenther Boden. 2002. "Lipid-Induced Insulin Resistance in Human Muscle Is Associated with Changes in Diacylglycerol, Protein Kinase C, and I κ B- α ." *Diabetes* 51 (7): 2005–11. <https://doi.org/10.2337/diabetes.51.7.2005>.
- Jäer, Sibylle, Christoph Handschin, Julie St-Pierre, and Bruce M Spiegelman. 2007. "AMP-Activated Protein Kinase (AMPK) Action in Skeletal Muscle via Direct Phosphorylation of PGC-1 α ." *Proceedings of the National Academy of Sciences of the United States of America* 104 (29): 12017–22. <https://doi.org/10.1073/pnas.0705070104>.
- Jaldin-Fincati, Javier R., Martin Pavarotti, Scott Frendo-Cumbo, Philip J. Bilan, and Amira Klip. 2017. "Update on GLUT4 Vesicle Traffic: A Cornerstone of Insulin Action." *Trends in Endocrinology & Metabolism* 28 (8): 597–611. <https://doi.org/10.1016/j.tem.2017.05.002>.
- Jamwal, Sumit, Jennifer Blackburn, and John D Elsworth. 2020. "PPAR γ /PGC1 α Signaling as a Potential Therapeutic Target for Mitochondrial Biogenesis in Neurodegenerative Disorders." *Pharmacology & Therapeutics*, 107705.

- Janani, C, and B.D. Ranjitha Kumari. 2015. "PPAR Gamma Gene – A Review." *Diabetes & Metabolic Syndrome: Clinical Research & Reviews* 9 (1): 46–50.
<https://doi.org/10.1016/j.dsx.2014.09.015>.
- JeBailey, Lellean, Oshrit Wanono, Wenyan Niu, Jessica Roessler, Assaf Rudich, and Amira Klip. 2007. "Ceramide- and Oxidant-Induced Insulin Resistance Involve Loss of Insulin-Dependent Rac-Activation and Actin Remodeling in Muscle Cells." *Diabetes* 56 (2): 394–403. <https://doi.org/10.2337/DB06-0823>.
- Kahn, Barbara B, and Timothy E. McGraw. 2010. "Rosiglitazone, PPAR γ , and Type 2 Diabetes." *New England Journal of Medicine* 363 (27): 2667–69.
<https://doi.org/10.1056/NEJMcibr1012075>.
- Katz, Ehud, Eva Margalith, and Bela Winer. 1976. "Inhibition of Herpesvirus Deoxyribonucleic Acid and Protein Synthesis by Tilorone Hydrochloride." *Antimicrobial Agents and Chemotherapy* 9 (1): 189–95.
- Keller-Pinter, Aniko, Kitti Szabo, Tamas Kocsis, Ferenc Deak, Imre Ocsovszki, Agnes Zvara, Laszlo Puskas, Laszlo Szilak, Laszlo Dux, Aniko Keller-Pinter, Kitti Szabo, Tamas Kocsis, Ferenc Deak, Imre Ocsovszki, Agnes Zvara, Laszlo Puskas, Laszlo Szilak, and Laszlo Dux. 2018. "Syndecan-4 Influences Mammalian Myoblast Proliferation by Modulating Myostatin Signalling and G1/S Transition." *FEBS Letters* 592 (18): 3139–51. <https://doi.org/10.1002/1873-3468.13227>.
- Kim, Min Soo, and Wook Jin. 2020. "TrkB-Induced Inhibition of R-SMAD/SMAD4 Activation Is Essential for TGF- β -Mediated Tumor Suppressor Activity." *Cancers* 2020, Vol. 12, Page 1048 12 (4): 1048. <https://doi.org/10.3390/CANCERS12041048>.
- Kocsis, Tamas, Gyorgy Trencsenyi, Kitti Szabo, Julia Aliz Baan, Geza Muller, Luca Mendler, Ildiko Garai, Hans Reinauer, Ferenc Deak, Laszlo Dux, and Aniko Keller-Pinter. 2017. "Myostatin Propeptide Mutation of the Hypermuscular Compact Mice Decreases the Formation of Myostatin and Improves Insulin Sensitivity." *American Journal of Physiology - Endocrinology and Metabolism* 312 (3): E150–60.
<https://doi.org/10.1152/ajpendo.00216.2016>.
- Kohler, Zoltan M., Gyorgy Trencsenyi, Laszlo Juhasz, Agnes Zvara, Judit P. Szabo, Laszlo Dux, Laszlo G. Puskas, Laszlo Rovo, and Aniko Keller-Pinter. 2023. "Tilorone Increases Glucose Uptake in Vivo and in Skeletal Muscle Cells by Enhancing

- Akt2/AS160 Signaling and Glucose Transporter Levels.” *Journal of Cellular Physiology* 238 (5): 1080–94. <https://doi.org/10.1002/JCP.30998>.
- Krueger, Russell F, and Gerald D Mayer. 1970. “Tilorone Hydrochloride: An Orally Active Antiviral Agent.” *Science* 169 (3951): 1213–14.
- Kuang, Shihuan, Kazuki Kuroda, Fabien Le Grand, and Michael A. Rudnicki. 2007. “Asymmetric Self-Renewal and Commitment of Satellite Stem Cells in Muscle.” *Cell* 129 (5): 999–1010. <https://doi.org/10.1016/J.CELL.2007.03.044>.
- Kuhn, Richard, and Nils Andreas Sörensen. 1938. “Über Astaxanthin Und Ovoverdin.” *Berichte Der Deutschen Chemischen Gesellschaft (A and B Series)* 71 (9): 1879–88. <https://doi.org/10.1002/CBER.19380710918>.
- Lai, Tso Ting, Chung May Yang, and Chang Hao Yang. 2020. “Astaxanthin Protects Retinal Photoreceptor Cells against High Glucose-Induced Oxidative Stress by Induction of Antioxidant Enzymes via the PI3K/Akt/Nrf2 Pathway.” *Antioxidants* 2020, Vol. 9, Page 729 9 (8): 729. <https://doi.org/10.3390/ANTIOX9080729>.
- Lane, Thomas R., and Sean Ekins. 2020. “Toward the Target: Tilorone, Quinacrine, and Pyronaridine Bind to Ebola Virus Glycoprotein.” *ACS Medicinal Chemistry Letters* 11 (8): 1653–58. <https://doi.org/10.1021/acsmchemlett.0c00298>.
- Lee, Jongsoon, and Paul F Pilch. 1994. “The Insulin Receptor: Structure, Function, and Signaling.” *American Journal of Physiology-Cell Physiology* 266 (2): C319–34.
- Leppäranta, Outi, Jussi M Tikkanen, Maxim M Bespalov, Katri Koli, and Marjukka Myllärniemi. 2013. “Bone Morphogenetic Protein–Inducer Tilorone Identified by High-Throughput Screening Is Antifibrotic In Vivo.” *American Journal of Respiratory Cell and Molecular Biology* 48 (4): 448–55.
- Leto, Dara, and Alan R Saltiel. 2012. “Regulation of Glucose Transport by Insulin: Traffic Control of GLUT4.” *Nature Reviews Molecular Cell Biology* 13 (6): 383–96.
- Liang, Huiyun, and Walter F Ward. 2006. “PGC-1 α : A Key Regulator of Energy Metabolism.” *Advances in Physiology Education*.
- Liu, Po Hung, Wataru Aoi, Maki Takami, Hitomi Terajima, Yuko Tanimura, Yuji Naito, Yoshito Itoh, and Toshikazu Yoshikawa. 2014. “The Astaxanthin-Induced Improvement in Lipid Metabolism during Exercise Is Mediated by a PGC-1 α Increase in Skeletal

- Muscle.” *Journal of Clinical Biochemistry and Nutrition* 54 (2): 86–89.
<https://doi.org/10.3164/JCBN.13-110>.
- Loginova, S Ia, A V Koval’chuk, S V Borisevich, S I Syromiatnikova, G V Borisevich, Iu I Pashchenko, R A Khamitov, V A Maksimov, and A M Shuster. 2004. “Antiviral Activity of an Interferon Inducer Amixin in Experimental West Nile Fever.” *Voprosy Virusologii* 49 (2): 8.
- Ma, Jinhui, Yuko Nakagawa, Itaru Kojima, and Hiroshi Shibata. 2014. “Prolonged Insulin Stimulation Down-Regulates GLUT4 through Oxidative Stress-Mediated Retromer Inhibition by a Protein Kinase CK2-Dependent Mechanism in 3T3-L1 Adipocytes.” *Journal of Biological Chemistry* 289 (1): 133–42.
<https://doi.org/10.1074/jbc.M113.533240>.
- Ma, Xiaojun, and John Blenis. 2009. “Molecular Mechanisms of mTOR-Mediated Translational Control.” *Nature Reviews Molecular Cell Biology* 10 (5): 307–18.
<https://doi.org/10.1038/nrm2672>.
- Mangnall, D., C. Bruce, and R. B. Fraser. 1993. “Insulin-Stimulated Glucose Uptake in C2C12 Myoblasts.” *Biochemical Society Transactions* 21 (4): 438S–438S.
<https://doi.org/10.1042/BST021438S>.
- Maoka, Takashi. 2011. “Carotenoids in Marine Animals.” *Marine Drugs* 2011, Vol. 9, Pages 278–293 9 (2): 278–93. <https://doi.org/10.3390/MD9020278>.
- Massagué, Joan, Joan Seoane, and David Wotton. 2005. “Smad Transcription Factors.” *Genes & Development* 19 (23): 2783–2810.
- Meo, Sergio Di, Susanna Iossa, and Paola Venditti. 2017. “Skeletal Muscle Insulin Resistance: Role of Mitochondria and Other ROS Sources.” *Journal of Endocrinology* 233 (1): R15–42. <https://doi.org/10.1530/JOE-16-0598>.
- Merz, Karla E., Ragadeepthi Tunduguru, Miwon Ahn, Vishal A. Salunkhe, Rajakrishnan Veluthakal, Jinhee Hwang, Supriyo Bhattacharya, Erika M. McCown, Pablo A. Garcia, Chunxue Zhou, Eunjin Oh, Stephanie M. Yoder, Jeffrey S. Elmendorf, and Debbie C. Thurmond. 2022. “Changes in Skeletal Muscle PAK1 Levels Regulate Tissue Crosstalk to Impact Whole Body Glucose Homeostasis.” *Frontiers in Endocrinology* 13 (February): 821849. <https://doi.org/10.3389/fendo.2022.821849>.

- Miki, Wataru. 1991. "Biological Functions and Activities of Animal Carotenoids." *Pure and Applied Chemistry* 63 (1): 141–46.
- Modica, Salvatore, Leon G Straub, Miroslav Balaz, Wenfei Sun, Lukas Varga, Patrik Stefanicka, Milan Profant, Eric Simon, Heike Neubauer, and Barbara Ukropcova. 2016. "Bmp4 Promotes a Brown to White-like Adipocyte Shift." *Cell Reports* 16 (8): 2243–58.
- Nászai, Anna, Emil Terhes, József Kaszaki, Mihály Boros, and László Juhász. 2019. "Ca²⁺ N It Be Measured? Detection of Extramitochondrial Calcium Movement With High-Resolution Fluorescence Respirometry." *Scientific Reports* 9 (1): 1–13.
- Nehlin, Jan O., Marlene Just, Arild C. Rustan, and Michael Gaster. 2011. "Human Myotubes from Myoblast Cultures Undergoing Senescence Exhibit Defects in Glucose and Lipid Metabolism." *Biogerontology* 12 (4): 349–65. <https://doi.org/10.1007/s10522-011-9336-5>.
- Newsholme, Philip, Vinicius Fernandes Cruzat, Kevin Noel Keane, Rodrigo Carlessi, and Paulo Ivo Homem De Bittencourt. 2016. "Molecular Mechanisms of ROS Production and Oxidative Stress in Diabetes." *Biochemical Journal* 473 (24): 4527–50. <https://doi.org/10.1042/BCJ20160503C>.
- Nishimura, Tomoki, Tadashi Okobira, Andrew M Kelly, Naohiko Shimada, Yoichi Takeda, and Kazuo Sakurai. 2007. "DNA Binding of Tilorone: ¹H NMR and Calorimetric Studies of the Intercalation." *Biochemistry* 46 (27): 8156–63.
- Nomiyama, Takashi, Yasuhiro Igarashi, Hikari Taka, Reiko Mineki, Toyoyoshi Uchida, Takeshi Ogihara, Jong Bock Choi, Hiroshi Uchino, Yasushi Tanaka, Hiroshi Maegawa, Atsunori Kashiwagi, Kimie Murayama, Ryuzo Kawamori, and Hirotaka Watada. 2004. "Reduction of Insulin-Stimulated Glucose Uptake by Peroxynitrite Is Concurrent with Tyrosine Nitration of Insulin Receptor Substrate-1." *Biochemical and Biophysical Research Communications* 320 (3): 639–47. <https://doi.org/10.1016/J.BBRC.2004.06.019>.
- Oakhill, Jonathan S., Rohan Steel, Zhi-Ping Ping Chen, John W. Scott, Naomi Ling, Shanna Tam, and Bruce E. Kemp. 2011. "AMPK Is a Direct Adenylate Charge-Regulated Protein Kinase." *Science* 332 (6036): 1433–35. <https://doi.org/10.1126/science.1200094>.

- Owen, Mark R., Elena Doran, and Andrew P. Halestrap. 2000. "Evidence That Metformin Exerts Its Anti-Diabetic Effects through Inhibition of Complex 1 of the Mitochondrial Respiratory Chain." *Biochemical Journal* 348 (Pt 3): 607. <https://doi.org/10.1042/0264-6021:3480607>.
- Pääsuke, Reedik, Margus Eimre, Andres Piirsoo, Nadežda Peet, Liidia Laada, Lumme Kadaja, Mart Roosimaa, Mati Pääsuke, Aare Märtsen, Enn Seppet, and Kalju Paju. 2016. "Proliferation of Human Primary Myoblasts Is Associated with Altered Energy Metabolism in Dependence on Ageing in Vivo and in Vitro." *Oxidative Medicine and Cellular Longevity* 2016. <https://doi.org/10.1155/2016/8296150>.
- Patel, Anil Kumar, Vaibhav Sunil Tambat, Chiu Wen Chen, Ajeet Singh Chauhan, Prashant Kumar, Akash Pralhad Vadrade, Chun Yung Huang, Cheng Di Dong, and Reeta Rani Singhania. 2022. "Recent Advancements in Astaxanthin Production from Microalgae: A Review." *Bioresource Technology* 364 (November): 128030. <https://doi.org/10.1016/J.BIORTECH.2022.128030>.
- Pauk, Martina, Tatjana Bordukalo-Niksic, Jelena Brkljacic, Vishwas M. Paralkar, Amy L. Brault, Ivo Dumic-Cule, Fran Borovecki, Lovorka Grgurevic, and Slobodan Vukicevic. 2019. "A Novel Role of Bone Morphogenetic Protein 6 (BMP6) in Glucose Homeostasis." *Acta Diabetologica* 56 (3): 365–71. <https://doi.org/10.1007/s00592-018-1265-1>.
- Pessler, D, A Rudich, and N Bashan. 2001. "Oxidative Stress Impairs Nuclear Proteins Binding to the Insulin Responsive Element in the GLUT4 Promoter." *Diabetologia* 44: 2156–64.
- Price, Nathan L., Ana P. Gomes, Alvin J.Y. Ling, Filipe V. Duarte, Alejandro Martin-Montalvo, Brian J. North, Beamon Agarwal, Lan Ye, Giorgio Ramadori, Joao S. Teodoro, Basil P. Hubbard, Ana T. Varela, James G. Davis, Behzad Varamini, Angela Hafner, Ruin Moaddel, Anabela P. Rolo, Roberto Coppari, Carlos M. Palmeira, et al. 2012. "SIRT1 Is Required for AMPK Activation and the Beneficial Effects of Resveratrol on Mitochondrial Function." *Cell Metabolism* 15 (5): 675–90. <https://doi.org/10.1016/J.CMET.2012.04.003>.
- Puhl, Ana C., Ethan J. Fritch, Thomas R. Lane, Longping V. Tse, Boyd L. Yount, Carolina Q. Sacramento, Natalia Fintelman-Rodrigues, Tatyana Almeida Tavella, Fabio Trindade

- Maranhão Costa, Stuart Weston, James Logue, Matthew Frieman, Lakshmanane Premkumar, Kenneth H. Pearce, Brett L. Hurst, Carolina Horta Andrade, James A. Levi, Nicole J. Johnson, Samantha C. Kisthardt, et al. 2021. “Repurposing the Ebola and Marburg Virus Inhibitors Tilorone, Quinacrine, and Pyronaridine: In Vitro Activity against SARS-CoV-2 and Potential Mechanisms.” *ACS Omega* 6 (11): 7454–68. <https://doi.org/10.1021/acsomega.0c05996>.
- Qian, Shu-Wen, Yan Tang, Xi Li, Yuan Liu, You-You Zhang, Hai-Yan Huang, Rui-Dan Xue, Hao-Yong Yu, Liang Guo, and Hui-Di Gao. 2013. “BMP4-Mediated Brown Fat-like Changes in White Adipose Tissue Alter Glucose and Energy Homeostasis.” *Proceedings of the National Academy of Sciences* 110 (9): E798–807.
- Racioppi, Luigi, and Anthony R Means. 2012. “Calcium/Calmodulin-Dependent Protein Kinase Kinase 2: Roles in Signaling and Pathophysiology.” *Journal of Biological Chemistry* 287 (38): 31658–65.
- Ratan, Rajiv R., Ambreena Siddiq, Leila Aminova, Brett Langley, Stephen McConoughey, Ksenia Karpisheva, Hsin Hwa Lee, Thomas Carmichael, Harley Kornblum, Giovanni Coppola, Daniel H. Geschwind, Ahmet Hoke, Natalya Smirnova, Cameron Rink, Sashwati Roy, Chandan Sen, Michael S. Beattie, Ron P. Hart, Martin Grumet, et al. 2008. “Small Molecule Activation of Adaptive Gene Expression: Tilorone or Its Analogs Are Novel Potent Activators of Hypoxia Inducible Factor-1 That Provide Prophylaxis against Stroke and Spinal Cord Injury.” In *Annals of the New York Academy of Sciences*, 1147:383–94. John Wiley & Sons, Ltd. <https://doi.org/10.1196/annals.1427.033>.
- Rauch, Cyril, and Paul T. Loughna. 2005. “C2C12 Skeletal Muscle Cells Exposure to Phosphatidylcholine Triggers IGF-1 Like-Responses.” *Cellular Physiology and Biochemistry* 15 (5): 211–24. <https://doi.org/10.1159/000086408>.
- Richter, Erik A., and Mark Hargreaves. 2013. “Exercise, GLUT4, and Skeletal Muscle Glucose Uptake.” <https://doi.org/10.1152/Physrev.00038.2012> 93 (3): 993–1017. <https://doi.org/10.1152/PHYSREV.00038.2012>.
- Rizwan, Huma, Sweta Pal, Silpa Sabnam, and Arttatrana Pal. 2020. “High Glucose Augments ROS Generation Regulates Mitochondrial Dysfunction and Apoptosis via Stress Signalling Cascades in Keratinocytes.” *Life Sciences* 241 (January): 117148.

<https://doi.org/10.1016/J.LFS.2019.117148>.

- Ruegsegger, Gregory N, Ana L Creo, Tiffany M Cortes, Surendra Dasari, and K Sreekumaran Nair. 2018. "Altered Mitochondrial Function in Insulin-Deficient and Insulin-Resistant States." *The Journal of Clinical Investigation* 128 (9): 3671–81.
- Saeedi, Pouya, Inga Petersohn, Paraskevi Salpea, Belma Malanda, Suvi Karuranga, Nigel Unwin, Stephen Colagiuri, Leonor Guariguata, Ayesha A. Motala, Katherine Ogurtsova, Jonathan E. Shaw, Dominic Bright, and Rhys Williams. 2019. "Global and Regional Diabetes Prevalence Estimates for 2019 and Projections for 2030 and 2045: Results from the International Diabetes Federation Diabetes Atlas, 9th Edition." *Diabetes Research and Clinical Practice* 157 (November): 107843.
<https://doi.org/10.1016/j.diabres.2019.107843>.
- Sáez, Guillermo T, and Nuria Están-Capell. 2017. "Antioxidant Enzymes BT - Encyclopedia of Cancer." In , edited by Manfred Schwab, 288–94. Berlin, Heidelberg: Springer Berlin Heidelberg. https://doi.org/10.1007/978-3-662-46875-3_7210.
- Sakamoto, Kei, and Geoffrey D Holman. 2008. "Emerging Role for AS160/TBC1D4 and TBC1D1 in the Regulation of GLUT4 Traffic." *American Journal of Physiology-Endocrinology And Metabolism* 295 (1): E29–37.
- Sanvee, Gerda M., Miljenko V. Panajatovic, Jamal Bouitbir, and Stephan Krähenbühl. 2019. "Mechanisms of Insulin Resistance by Simvastatin in C2C12 Myotubes and in Mouse Skeletal Muscle." *Biochemical Pharmacology* 164 (June): 23–33.
<https://doi.org/10.1016/J.BCP.2019.02.025>.
- Sartori, Roberta, Adam Hagg, Sandra Zampieri, Andrea Armani, Catherine E. Winbanks, Laís R. Viana, Mouna Haidar, Kevin I. Watt, Hongwei Qian, Camilla Pezzini, Pardis Zanganeh, Bradley J. Turner, Anna Larsson, Gianpietro Zanchettin, Elisa S. Pierobon, Lucia Moletta, Michele Valmasoni, Alberto Ponzoni, Shady Attar, et al. 2021. "Perturbed BMP Signaling and Denervation Promote Muscle Wasting in Cancer Cachexia." *Science Translational Medicine* 13 (605).
<https://doi.org/10.1126/scitranslmed.aay9592>.
- Sartori, Roberta, Elija Schirwis, Bert Blaauw, Sergia Bortolanza, Jinghui Zhao, Elena Enzo, Amalia Stantzou, Etienne Mouisel, Luana Toniolo, and Arnaud Ferry. 2013. "BMP Signaling Controls Muscle Mass." *Nature Genetics* 45 (11): 1309–18.

- Satoh, Takaya, and Nobuyuki Takenaka. 2019. "A Critical Role for the Small GTPase Rac1 in Insulin Signaling That Regulates Glucose Uptake in Skeletal Muscle." *Research on Chemical Intermediates* 45 (11): 5389–97.
- Saxton, Robert A., and David M. Sabatini. 2017. "mTOR Signaling in Growth, Metabolism, and Disease." *Cell*. Cell Press. <https://doi.org/10.1016/j.cell.2017.02.004>.
- Schreiber, Isabelle, Gina Dörpholz, Claus-Eric Eric Ott, Bjørt Kragesteen, Nancy Schanze, Cory Thomas Lee, Josef Köhrle, Stefan Mundlos, Karen Ruschke, and Petra Knaus. 2017. "BMPs as New Insulin Sensitizers: Enhanced Glucose Uptake in Mature 3T3-L1 Adipocytes via PPAR γ and GLUT4 Upregulation." *Scientific Reports* 7 (1): 1–13. <https://doi.org/10.1038/s41598-017-17595-5>.
- Shen, Liang, Junwei Niu, Chunhua Wang, Baoying Huang, Wenling Wang, Na Zhu, Yao Deng, Huijuan Wang, Fei Ye, and Shan Cen. 2019. "High-Throughput Screening and Identification of Potent Broad-Spectrum Inhibitors of Coronaviruses." *Journal of Virology* 93 (12).
- Snezhkina, Anastasiya V., Anna V. Kudryavtseva, Olga L. Kardymon, Maria V. Savvateeva, Nataliya V. Melnikova, George S. Krasnov, and Alexey A. Dmitriev. 2020. "ROS Generation and Antioxidant Defense Systems in Normal and Malignant Cells." *Oxidative Medicine and Cellular Longevity*. Hindawi Limited. <https://doi.org/10.1155/2019/6175804>.
- Soyal, S., F. Krempler, H. Oberkofler, and W. Patsch. 2006. "PGC-1 α : A Potent Transcriptional Cofactor Involved in the Pathogenesis of Type 2 Diabetes." *Diabetologia* 49 (7): 1477–88. <https://doi.org/10.1007/S00125-006-0268-6>.
- Stahmann, Nadine, Angela Woods, David Carling, and Regine Heller. 2006. "Thrombin Activates AMP-Activated Protein Kinase in Endothelial Cells via a Pathway Involving Ca²⁺/Calmodulin-Dependent Protein Kinase Kinase β ." *Molecular and Cellular Biology* 26 (16): 5933–45.
- Stuart, Charles A., Gary Wen, W. Clay Gustafson, and E. Aubrey Thompson. 2000. "Comparison of GLUT1, GLUT3, and GLUT4 mRNA and the Subcellular Distribution of Their Proteins in Normal Human Muscle." *Metabolism: Clinical and Experimental* 49 (12): 1604–9. <https://doi.org/10.1053/meta.2000.18559>.

- Stuart, Charles A., Deling Yin, Mary E.A. Howell, Rhesa J. Dykes, John J. Laffan, and Arny A. Ferrando. 2006. "Hexose Transporter MRNAs for GLUT4, GLUT5, and GLUT12 Predominate in Human Muscle." *American Journal of Physiology - Endocrinology and Metabolism* 291 (5): 1067–73. <https://doi.org/10.1152/ajpendo.00250.2006>.
- Sun, Hong, Pouya Saeedi, Suvi Karuranga, Moritz Pinkepank, Katherine Ogurtsova, Bruce B. Duncan, Caroline Stein, Abdul Basit, Juliana C.N. Chan, Jean Claude Mbanya, Meda E. Pavkov, Ambady Ramachandaran, Sarah H. Wild, Steven James, William H. Herman, Ping Zhang, Christian Bommer, Shihchen Kuo, Edward J. Boyko, et al. 2022. "IDF Diabetes Atlas: Global, Regional and Country-Level Diabetes Prevalence Estimates for 2021 and Projections for 2045." *Diabetes Research and Clinical Practice* 183 (January): 109119. <https://doi.org/10.1016/J.DIABRES.2021.109119>.
- Sun, Yi, Philip J Bilan, Zhi Liu, and Amira Klip. 2010. "Rab8A and Rab13 Are Activated by Insulin and Regulate GLUT4 Translocation in Muscle Cells." *Proceedings of the National Academy of Sciences* 107 (46): 19909–14.
- Szabo, Kitti, Daniel Varga, Attila Gergely Vegh, Ning Liu, Xue Xiao, Lin Xu, Laszlo Dux, Miklos Erdelyi, Laszlo Rovo, and Aniko Keller-Pinter. 2022. "Syndecan-4 Affects Myogenesis via Rac1-Mediated Actin Remodeling and Exhibits Copy-Number Amplification and Increased Expression in Human Rhabdomyosarcoma Tumors." *Cellular and Molecular Life Sciences* 79 (2): 1–21. <https://doi.org/10.1007/s00018-021-04121-0>.
- Sztretye, Mónika, Beatrix Dienes, Mónika Gönczi, Tamás Czirják, László Csernoch, László Dux, Péter Szentesi, and Anikó Keller-Pintér. 2019. "Astaxanthin: A Potential Mitochondrial-Targeted Antioxidant Treatment in Diseases and with Aging." *Oxidative Medicine and Cellular Longevity* 2019. <https://doi.org/10.1155/2019/3849692>.
- Sztretye, Mónika, Zoltán Singlár, László Szabó, Ágnes Angyal, Norbert Balogh, Faranak Vakilzadeh, Péter Szentesi, Beatrix Dienes, and László Csernoch. 2020. "Improved Tetanic Force and Mitochondrial Calcium Homeostasis by Astaxanthin Treatment in Mouse Skeletal Muscle." *Antioxidants* 2020, Vol. 9, Page 98 9 (2): 98. <https://doi.org/10.3390/ANTIOX9020098>.
- Tangvarasittichai, Surapon. 2015. "Oxidative Stress, Insulin Resistance, Dyslipidemia and Type 2 Diabetes Mellitus." *World Journal of Diabetes* 6 (3): 456.

<https://doi.org/10.4239/WJD.V6.I3.456>.

Thong, Farah S.L., Philip J. Bilan, and Amira Klip. 2007. "The Rab GTPase-Activating Protein AS160 Integrates Akt, Protein Kinase C, and AMP-Activated Protein Kinase Signals Regulating GLUT4 Traffic." *Diabetes* 56 (2): 414–23.

<https://doi.org/10.2337/DB06-0900>.

Tomic, Dunya, Jonathan E. Shaw, and Dianna J. Magliano. 2022. "The Burden and Risks of Emerging Complications of Diabetes Mellitus." *Nature Reviews Endocrinology*. Nature Publishing Group. <https://doi.org/10.1038/s41574-022-00690-7>.

Townsend, Kristy L., Ding An, Matthew D. Lynes, Tian Lian Huang, Hongbin Zhang, Laurie J. Goodyear, and Yu Hua Tseng. 2013. "Increased Mitochondrial Activity in BMP7-Treated Brown Adipocytes, Due to Increased CPT1- and CD36-Mediated Fatty Acid Uptake." *https://Home.Liebertpub.Com/Ars* 19 (3): 243–57.

<https://doi.org/10.1089/ARS.2012.4536>.

Tulipano, Giovanni, Pier Franco Spano, and Daniela Cocchi. 2008. "Effects of Olanzapine on Glucose Transport, Proliferation and Survival in C2C12 Myoblasts." *Molecular and Cellular Endocrinology* 292 (1–2): 42–49. <https://doi.org/10.1016/J.MCE.2008.04.010>.

Urakaze, Masaharu, Chikaaki Kobashi, Yukihiro Satou, Kouichi Shigeta, Masahiro Toshima, Masatoshi Takagi, Jiro Takahashi, and Hiroshi Nishida. 2021. "The Beneficial Effects of Astaxanthin on Glucose Metabolism and Modified Low-Density Lipoprotein in Healthy Volunteers and Subjects with Prediabetes." *Nutrients* 2021, Vol. 13, Page 4381 13 (12): 4381. <https://doi.org/10.3390/NU13124381>.

Urist, Marshall R. 1965. "Bone: Formation by Autoinduction." *Science* 150 (3698): 893–99. <https://doi.org/10.1126/SCIENCE.150.3698.893>.

Vanhaesebroeck, Bart, Len Stephens, and Phillip Hawkins. 2012. "PI3K Signalling: The Path to Discovery and Understanding." *Nature Reviews Molecular Cell Biology* 13 (3): 195–203.

Wang, Cuicui, Richard M Silverman, Jie Shen, and Regis J O'Keefe. 2018. "Distinct Metabolic Programs Induced by TGF-B1 and BMP2 in Human Articular Chondrocytes with Osteoarthritis." *Journal of Orthopaedic Translation* 12: 66–73.

Wang, Dan, Xinhao Jiang, Aiqing Lu, Min Tu, Wei Huang, and Ping Huang. 2018. "BMP14



- Induces Tenogenic Differentiation of Bone Marrow Mesenchymal Stem Cells in Vitro.” *Experimental and Therapeutic Medicine* 16 (2): 1165–74.
- Whiting, David R., Leonor Guariguata, Clara Weil, and Jonathan Shaw. 2011. “IDF Diabetes Atlas: Global Estimates of the Prevalence of Diabetes for 2011 and 2030.” *Diabetes Research and Clinical Practice* 94 (3): 311–21.
<https://doi.org/10.1016/J.DIABRES.2011.10.029>.
- Won, Jong Chul. 2021. “Thiazolidinediones (TZDs),” 131–41. https://doi.org/10.1007/978-981-16-5123-6_11.
- Wong, Chun Y, Hani Al-Salami, and Crispin R Dass. 2020. “C2C12 Cell Model: Its Role in Understanding of Insulin Resistance at the Molecular Level and Pharmaceutical Development at the Preclinical Stage.” *Journal of Pharmacy and Pharmacology* 72 (12): 1667–93.
- Wu, Zhidan, Yuhong Xie, Ron F Morrison, N L Bucher, and Stephen R Farmer. 1998. “PPAR γ Induces the Insulin-Dependent Glucose Transporter GLUT4 in the Absence of C/EBP α during the Conversion of 3T3 Fibroblasts into Adipocytes.” *The Journal of Clinical Investigation* 101 (1): 22–32.
- Yap, Kah Heng, Gan Sook Yee, Mayuren Candasamy, Swee Ching Tan, Shadab Md, Abu Bakar Abdul Majeed, and Subrat Kumar Bhattamisra. 2020. “Catalpol Ameliorates Insulin Sensitivity and Mitochondrial Respiration in Skeletal Muscle of Type-2 Diabetic Mice through Insulin Signaling Pathway and Ampk/Sirt1/Pgc-1 α /Ppar- γ Activation.” *Biomolecules* 10 (10): 1–21. <https://doi.org/10.3390/biom10101360>.
- Yu, Yong, Ayse Sena Mutlu, Harrison Liu, and Meng C Wang. 2017. “High-Throughput Screens Using Photo-Highlighting Discover BMP Signaling in Mitochondrial Lipid Oxidation.” *Nature Communications* 8 (1): 1–11.
- Zhao, Feng-Qi, and Aileen F Keating. 2007. “Functional Properties and Genomics of Glucose Transporters.” *Current Genomics* 8 (2): 113–28.
- Zhou, Gaochao, Robert Myers, Ying Li, Yuli Chen, Xiaolan Shen, Judy Fenyk-Melody, Margaret Wu, John Ventre, Thomas Doebber, and Nobuharu Fujii. 2001. “Role of AMP-Activated Protein Kinase in Mechanism of Metformin Action.” *The Journal of Clinical Investigation* 108 (8): 1167–74.

- Zimmet, Paul, KGMM Alberti, and Jonathan Shaw. 2001. "Global and Societal Implications of the Diabetes Epidemic." *Nature* 414 (6865): 782–87.
- Zorzano, Antonio, César Fandos, and Manuel Palacín. 2000. "Role of Plasma Membrane Transporters in Muscle Metabolism." *Biochemical Journal* 349 (3): 667–88. <https://doi.org/10.1042/BJ3490667>.
- Zou, Ming-Hui, Xiu-Yun Hou, Chao-Mei Shi, Daisuke Nagata, Kenneth Walsh, and Richard A. Cohen. 2002. "Modulation by Peroxynitrite of Akt- and AMP-Activated Kinase-Dependent Ser1179 Phosphorylation of Endothelial Nitric Oxide Synthase." *Journal of Biological Chemistry* 277 (36): 32552–57. <https://doi.org/10.1074/jbc.M204512200>.

ANNEX

I.

Tilorone increases glucose uptake in vivo and in skeletal muscle cells by enhancing Akt2/AS160 signaling and glucose transporter levels

Zoltan M. Kohler¹  | Gyorgy Trencsenyi² | Laszlo Juhasz³ | Agnes Zvara⁴ | Judit P. Szabo² | Laszlo Dux¹ | Laszlo G. Puskas⁴ | Laszlo Rovo⁵ | Aniko Keller-Pinter¹ 

¹Department of Biochemistry, Albert Szent-Gyorgyi Medical School, University of Szeged, Szeged, Hungary

²Department of Medical Imaging, Division of Nuclear Medicine and Translational Imaging, Faculty of Medicine, University of Debrecen, Debrecen, Hungary

³Institute of Surgical Research, Albert Szent-Gyorgyi Medical School, University of Szeged, Szeged, Hungary

⁴Laboratory of Functional Genomics, Biological Research Centre, Eotvos Lorand Research Network, Szeged, Hungary

⁵Department of Oto- Rhino-Laryngology and Head and Neck Surgery, University of Szeged, Szeged, Hungary

Correspondence

Aniko Keller-Pinter, Department of Biochemistry, Albert Szent-Gyorgyi Medical School, University of Szeged, Dom Sq 9, H-6720 Szeged, Hungary.
Email: keller.aniko@med.u-szeged.hu

Funding information

National Research, Development and Innovation Office of Hungary; National Research, Development and Innovation Fund; János Bolyai Research Scholarship of the Hungarian Academy of Sciences; New National Excellence Program of the Ministry for Innovation and Technology Sciences; University of Szeged Open Access Fund

Abstract

Skeletal muscle plays a major role in whole-body glucose metabolism. Insulin resistance in skeletal muscle is characterized by decreased insulin-stimulated glucose uptake resulting from impaired intracellular trafficking and decreased glucose transporter 4 (GLUT4) expression. In this study, we illustrated that tilorone, a low-molecular-weight antiviral agent, improves glucose uptake in vitro and in vivo. Tilorone increased bone morphogenetic protein (BMP) signaling in C2C12 myoblasts, the transcription of multiple BMPs (BMP2, BMP4, BMP7, and BMP14), Smad4 expression, and the phosphorylation of BMP-mediated Smad1/5/8. The activation of Akt2/AS160 (TBC1D4) signaling, the critical regulator of GLUT4 translocation, was also increased, as well as the levels of GLUT4 and GLUT1, leading to enhanced uptake of the radioactively labeled glucose analog ¹⁸F-fluoro-2-deoxyglucose (¹⁸FDG). However, this excess glucose content did not result in increased ATP formation by mitochondrial respiration; both basal and ATP-linked respiration were diminished, thereby contributing to the induction of AMPK. In differentiated myotubes, AS160 phosphorylation and ¹⁸FDG uptake also increased. Moreover, tilorone administration further increased insulin-stimulated phosphorylation of Akt2 and glucose uptake of myotubes indicating an insulin-sensitizing effect. Importantly, during in vivo experiments, the systemic administration of tilorone resulted in increased ¹⁸FDG uptake of skeletal muscle, liver, and adipose tissue in C57BL/6 mice. Our results provide new perspectives for the treatment of type 2 diabetes, which has a limited number of treatments that regulate protein expression or translocation.

KEYWORDS

BMP, GLUT, insulin sensitivity, mitochondria, skeletal muscle, tilorone

This is an open access article under the terms of the Creative Commons Attribution-NonCommercial-NoDerivs License, which permits use and distribution in any medium, provided the original work is properly cited, the use is non-commercial and no modifications or adaptations are made.

© 2023 The Authors. *Journal of Cellular Physiology* published by Wiley Periodicals LLC.

1 | INTRODUCTION

Approximately 40% of the human body is composed of skeletal muscle, which is responsible for 90% of glucose elimination after meals (DeFronzo & Tripathy, 2009). The primary glucose transporter (GLUT) in skeletal muscle and adipose tissue is GLUT4, which is responsible for insulin-stimulated glucose uptake and metabolism (Huang & Czech, 2007). GLUT4 is a member of the solute carrier family 2 (Slc2) gene family, which includes GLUT1–12 (Joost et al., 2002). Beyond GLUT4, skeletal muscle also express GLUT1 transporters. The relative amounts of GLUT4 and GLUT1 in skeletal muscles depend on the developmental stage, and GLUT1 plays a major role in glucose transport in C2C12 myoblasts (Rauch & Loughna, 2005; Zorzano et al., 2000).

When insulin binds to insulin receptors on the surface of skeletal muscle cells, activation of the phosphoinositide-3-kinase (PI3K)/protein kinase B (Akt)/Akt substrate of 160 kDa (AS160; also known as TBC1D4) pathway leads to the translocation of GLUT4-containing vesicles from the cytosol to the cell membrane and consequently glucose uptake (Leto & Saltiel, 2012). Akt regulates the Rab GTPase-activating protein (GAP) AS160, which regulates the activity of the small GTPases Rab8a, Rab13, and Rab14 in muscle cells (Ishikura et al., 2007; Sun et al., 2010). These Rab GTPases bind to static (MICAL-L2, α -actinin-4, actin filaments) and motile (MyoVa) effectors that allow mobilization of the GLUT4 vesicle (Jaldin-Fincati et al., 2017). In contrast, GLUT1 is an insulin-independent transporter and constitutively localizes in the plasma membrane.

The prevalence of diabetes mellitus (DM) is increasing at an alarming rate worldwide. Over a 10-year period starting in 2009, the estimated number of people (20–79 years old) living with diabetes increased dramatically by 62% from 285 to 463 million (Saeedi et al., 2019). In addition, half of all patients with diabetes (50.1%) have not been diagnosed (Saeedi et al., 2019). Over 90% of cases of DM are type 2 DM (T2DM) (Holman et al., 2015; Zimmet et al., 2001). Insulin resistance and a lack of proper insulin secretion are the causes of T2DM, also known as non-insulin-dependent DM. Insulin resistance can be defined as impaired insulin sensitivity and glucose uptake (Reaven, 1988). The only drug that directly targets GLUT4 translocation regulatory elements to improve glucose uptake by tissues is metformin (1,1-dimethylbiguanide hydrochloride), a biguanide derivative. Metformin can increase cellular glucose uptake through AMP-activated protein kinase (AMPK) (Zhou et al., 2001), which serves as the energy sensor of the cells (Hardie et al., 2012). Insulin sensitizers, such as thiazolidinediones (TZDs), are also effective oral medications for diabetes. TZDs are agonists of the nuclear receptor peroxisome proliferator-activated receptor- γ (PPAR γ) and thereby improve glucose metabolism (Kahn & McGraw, 2010; Won, 2021).

Bone morphogenetic proteins (BMPs) are cytokines of the transforming growth factor- β family that bind to dedicated BMP receptors, which in turn phosphorylate BMP-responsive Smad1/5/8 transcription factors. Activated Smad1/5/8 forms a complex with Smad4 and then translocate into the nucleus, in which they act as

transcriptional regulators (Massagué et al., 2005). Smad1/5/8 is an important positive regulator of mature muscle fibers (Sartori et al., 2013). The role of BMPs in glucose uptake is also known. Specifically, serum BMP7 levels are decreased in type 2 diabetes models, and BMP7 enhances glucose uptake of muscle and adipose tissue through PDK1/PI3K/Akt activation and GLUT4 translocation (Chattopadhyay et al., 2017). Treatment of ob/ob mice with BMP6 leads to decreases in serum lipid and glucose levels (Pauk et al., 2019). Moreover, BMP2 and BMP6 were reported as insulin sensitizers, and BMP2 and BMP6 treatment increased glucose uptake in adipocytes by upregulating PPAR γ and GLUT4 (Schreiber et al., 2017).

The synthetic low-molecular-weight molecule tilorone dihydrochloride (hereafter tilorone) induces BMP signaling and increases the expression of BMP2 and BMP7 in epithelial cells (Leppäranta et al., 2013). The antiviral effect of the oral drug has been known since the 1970s (Krueger & Mayer, 1970), and the drug is marketed as an antiviral agent in some countries for various viral indications, such as influenza, acute respiratory viral infection, viral hepatitis, and viral encephalitis (Ekins et al., 2018). It remains effective against several viruses at present, such as herpes simplex virus, West Nile virus, Ebola virus (Ekins et al., 2018; Katz et al., 1976; Loginova et al., 2004), and human coronaviruses including MERS-CoV (Shen et al., 2019) and SARS-CoV-2 (Puhl et al., 2021).

Because tilorone can enhance the transcription of BMPs in epithelial cells (Leppäranta et al., 2013), and BMPs might participate in insulin sensitization, glucose uptake, carbohydrate, and lipid metabolism (Schreiber et al., 2017; Yu et al., 2017), we aimed to study the effects of tilorone on signaling of myoblasts and myotubes, and for glucose uptake in vitro and in vivo. In this study, we demonstrated that tilorone induces the expression of BMPs in skeletal muscle cells and enhances the activity of BMP signaling by increasing the phosphorylation of Smad1/5/8 and expression of Smad4. The increased activation of the Akt2/AS160 pathway and the enhanced expression of GLUTs resulted in improved glucose uptake independently of insulin. Moreover, we demonstrated the insulin-sensitizing effect of tilorone by increasing insulin-mediated Akt2 phosphorylation and glucose uptake.

2 | MATERIALS AND METHODS

2.1 | Cell culture, differentiation, and treatment

Murine C2C12 myoblasts (ATCC) were grown in high-glucose Dulbecco's modified Eagle's medium (DMEM) (4.5 g/L glucose with glutamine and pyruvate; Corning) containing 20% fetal bovine serum (Gibco/Thermo Fisher Scientific) and supplemented with 50 μ g/mL gentamicin (Lonza). To induce differentiation, myoblasts were grown at 80%–90% confluency and then the medium was switched to differentiation medium containing DMEM supplemented with 2% horse serum (Sigma-Aldrich) and 50 μ g/mL gentamicin. Proliferating cells were treated with 2,7-bis[2-(diethylamino)ethoxy]-9-fluorenone dihydrochloride (tilorone dihydrochloride; #220957; Sigma-Aldrich)

at a concentration of 20 or 35 nM for 40 h. Differentiated myotubes were treated with 20 nM tilorone (2 or 5 h) followed by 100 nM insulin (Humulin-R; Eli Lilly) for 10 min on the 5th day of differentiation.

2.2 | Experimental animals

12 weeks old, male C57BL/6J mice ($n = 4$; The Jackson Laboratory) were used for the experiments. Animals were housed under conventional conditions at $23 \pm 2^\circ\text{C}$ with $50 \pm 10\%$ humidity and artificial lighting with a circadian cycle of 12 h. The semisynthetic diet (VRF1; Akromon Ltd.) and drinking water were available ad libitum to all animals. The animal experiments were authorized by the Ethical Committee for Animal Research, University of Debrecen, Hungary (1/2017/DEBÁB). Laboratory animals were kept and treated in compliance with all applicable sections of the Hungarian Laws and animal welfare directions and regulations of the European Union.

2.3 | Quantitative real-time (qRT)-PCR

qRT-PCR was performed using a RotorGene 3000 instrument (Qiagen) with gene-specific primers and the SybrGreen protocol to monitor gene expression. One microgram of C2C12 total RNA was reverse-transcribed in a final volume of 30 μL using a High-Capacity cDNA Archive Kit (Thermo Fisher Scientific) according to the manufacturer's instructions. The reverse transcription protocol was as follows: 10 min at room temperature, 2 h at 37°C , 5 min on ice, and 10 min at 75°C for enzyme inactivation. These steps were performed in a thermal cycler. After a twofold dilution, 1 μL of the diluted reaction mix was used as the template for qRT-PCR. Reactions were performed with qPCR BIO SyGreen Mix Lo-ROX mix (PCR

Biosystems) according to the manufacturer's instructions at a final primer concentration of 250 nM under the following conditions: 2 min at 95°C followed by 40 cycles of 95°C for 5 s and 60°C for 30 s. Melting temperature analysis was performed after each reaction to check the quality of the products. Primers were designed using the online Roche Universal Probe Library Assay Design Center. The quality of the primers was verified via MS analysis by Bioneer (Daejeon). Individual threshold cycle (C_t) values were normalized to the mean C_t values of *MmHprt* and *MmRpl27* as internal control genes. Relative gene expression levels are presented as $2^{-\Delta\Delta C_t}$ values. Information about the genes and the primers is presented in Table 1.

2.4 | Immunoblotting

C2C12 cells were lysed in RIPA buffer (20 mM Tris-HCl pH 7.5, 150 mM NaCl, 1 mM Na_2EDTA , 1 mM EGTA, 1% NP-40, 1% sodium deoxycholate, 2.5 mM sodium pyrophosphate, 1 mM β -glycerophosphate, 1 mM Na_3VO_4 , 1 $\mu\text{g}/\text{mL}$ leupeptin; #9806; Cell Signaling Technology) supplemented with 1 mM sodium fluoride and a protease inhibitor cocktail (#P8340; Sigma-Aldrich).

First, the lysates were centrifuged at $16,000\times g$ for 5 min at 4°C , and then protein levels were determined using the bicinchoninic acid method (#23227; Thermo Fisher Scientific). Equal amounts of proteins were separated via sodium dodecyl sulfate-polyacrylamide gel electrophoresis and transferred to Protran nitrocellulose membrane (GE Healthcare). The membranes were blocked in tris buffered saline containing 5% skimmed milk and 0.1% Tween-20 (Sigma-Aldrich) for 1 h at room temperature. Then, the membranes were incubated at 4°C overnight with the following rabbit polyclonal primary antibodies: phospho-AS160 (Thr642; #8881), AS160 (#2670), PGC-1 α (#2178), phospho-AMPK (Thr172; #2535), AMPK (#2532), phospho-Akt2 (Ser474; #8599), Akt2 (#3063), phospho-

TABLE 1 List of investigated genes and primers used in qRT-PCR experiments.

Reference sequence	Gene name	Description	Primers	
			Forward	Reverse
NM_007553.3	Bmp2	Bone morphogenetic protein 2	ttccatcacgaagaagccgt	ttccatcacgaagaagccgt
NM_007554.3	Bmp4	Bone morphogenetic protein 4	tctgcaggaaccaatggagc	aaaggctcagagaagctcg
NM_007557.3	Bmp7	Bone morphogenetic protein 7	cgagacctccagatcacagt	cagcaagaagaggtccgact
NM_008109.3	GDF5 (Bmp14)	Growth differentiation factor 5, bone morphogenetic protein 14	tcctaagctctttaaggagagc	aagtcaccaggcacaaggt
NM_008540.2	Smad4	SMAD family member 4	attggatggacgacttcagg	tgcttagttcattctgtgatcatc
NM_011400.3	Slc2a1 (GLUT1)	Solute carrier family 2 (facilitated glucose transporter), member 1	gatcccagcagcaagaaggt	tagccgaactgcagtgatcc
NM_001359114.1	Slc2a4 (GLUT4)	Solute carrier family 2 (facilitated glucose transporter), member 4	gctctgacgtaaggatgggg	tcaatcacctctgtggggc
NM_013556.2	HPRT	Hypoxanthine guanine phosphoribosyl transferase	cctcctcagaccgctttt	aacctggtcatcatcgctaa
NM_011289.3	RPL27	Ribosomal protein L27	tgaaggttagcggaagtgc	tttcatgaactgccatctc

Abbreviations: BMP, bone morphogenetic protein; GLUT, glucose transporter; qRT-PCR, quantitative real-time PCR.

Smad1/5/8 (Smad1 [Ser463/465]/Smad5 [Ser463/465]/Smad9 [Ser465/467]; #13820), PPAR γ (#2435), and GAPDH (#2118), all from Cell Signaling Technology, desmin (#M076029-2; DAKO; Agilent), GLUT1 (#PA1-46152; Thermo Fisher Scientific), or GLUT4 (#NBP1-49533; Novus Biologicals). Membranes were subsequently incubated with the horseradish peroxidase-conjugated anti-rabbit IgG secondary antibody (#P0448) from DAKO. Peroxidase activity was developed using the enhanced chemiluminescence (#K-12045 Advanta) procedure and the chemiluminescence signal was recorded using X-ray films (Agfa). On the scanned X-ray films, bands were selected with uniformed square ROIs (region of interest) using the BioRad Quantity One Analysis Software (Bio-Rad). Then, using the "Volume Analysis Report" function, we obtained the intensity of the selected area normalized to the background.

2.5 | Assessment of mitochondrial oxygen consumption using high-resolution respirometry

To assess respiration after 40 h of tilorone treatment, intact C2C12 myoblasts (3×10^6 cells) were suspended in MiRO5 respiration medium (pH 7.1; oxygen solubility factor 0.92) and gently pipetted into oxygraph chambers (Oxygraph-2k; Oroboros Instruments). All measurements were performed in 2 mL of respiration medium under continuous magnetic stirring (750 rpm) at 37°C. To avoid the effects of low O₂ levels on mitochondrial respiration, chamber O₂ concentrations were kept in the range of 50–200 μ M without reoxygenation (Doerrier et al., 2018; Nászai et al., 2019). After stable routine respiration (without exogenous substrates and ADP), ATP synthase was inhibited with oligomycin (2.5 μ M; leak respiration). The capacity of the electron transport system (ETS) was maximized via the stepwise titration of a protonophore (carbonyl cyanide *m*-chlorophenylhydrazone [CCCP]; final concentration: 0.25 μ M/step). Following complex I inhibition (with 0.5 μ M rotenone), ETS-independent respiration (or residual oxygen consumption [ROX]) was determined in the presence of the complex III inhibitor antimycin A (2.5 μ M). DatLab 7.3 software (Oroboros Instruments) was used for online display, respirometry data acquisition, and analysis.

2.6 | Fluorescent staining and microscopy

For anti-GLUT4 immunofluorescence, the samples were fixed with 4% paraformaldehyde (Molar Chemicals Kft.) for 15 min at room temperature, permeabilized with 0.2% Triton X100 (Sigma-Aldrich), and blocked with 2% bovine serum albumin (Sigma-Aldrich) in PBS. Rabbit polyclonal anti-GLUT4 primary antibody (#NBP1-49533; Bio-Techne) was visualized with the appropriate Alexa Fluor 488-conjugated secondary antibody (#711-545-152; Jackson ImmunoResearch).

To label the mitochondria, the cells were incubated with MitoTracker™ Deep Red FM (#M22426; Thermo Fisher Scientific) and then fixed with 4% paraformaldehyde (Molar Chemicals Kft.) for

15 min at room temperature. The nuclei were counterstained with Hoechst 33258 (#94403; Sigma-Aldrich).

Wide-field fluorescence images were obtained using a Nikon Eclipse Ni-U fluorescence microscope (Nikon Instruments Inc.) with a $\times 100$ objective (Nikon CFI Plan Apo DM Lambda $\times 100$ Oil, NA = 1.45). Following background correction, the images were evaluated, and heat maps were generated using ImageJ software (National Institutes of Health).

Leica DMI1 phase-contrast microscope (Leica Microsystems) with a $\times 10$ objective (Leica Hi Plan $\times 10$, NA = 0.28) was used to obtain representative images demonstrating the morphology of the undifferentiated and differentiated C2C12 cells.

2.7 | Measurement of ¹⁸F-fluoro-2-deoxyglucose (¹⁸FDG) uptake in vitro

To monitor the uptake of the radioactive glucose analog ¹⁸FDG, by cells, C2C12 cells were seeded into six-well plates ($0.08\text{--}0.1 \times 10^6$ cells/well) in 2 mL of culture medium containing 20 or 35 nM tilorone. After 24 h of culture, the monolayer surface was washed with DMEM containing 1 mM glucose and 20% FBS. To test the role of GLUT1 in glucose uptake, tilorone-treated cultures were incubated with a GLUT1 inhibitor, BAY-876 (#SML1774; Sigma-Aldrich; 10 nM, 2 h). ¹⁸FDG (10 μ Ci [0.37 MBq]) in 1 mL of DMEM containing 1 mM glucose and 20% FBS was added to each well. In the samples preincubated with tilorone, the concentration of tilorone (20 or 35 nM) was maintained throughout the incubation period. The plates were incubated for 60 min at 37°C, the incubation solution was removed, and the cell surface was washed twice with 2 mL of room-temperature PBS. The cells were harvested and resuspended, and the radioactivity of the suspension was measured using a Packard Cobra-II Auto Gamma Counter device.

To measure the ¹⁸FDG uptake of differentiated myotubes, C2C12 cells were seeded into six-well plates ($1.8\text{--}2 \times 10^5$ cells/well) for 24 h in growth medium, and then, differentiation was induced by shifting the cells into differentiation medium containing 2% horse serum (Sigma-Aldrich). On the 5th day on differentiation, cell cultures were treated with 20 nM tilorone for 2 or 5 h and 100 nm insulin for 10 min (Humulin-R; Eli Lilly). Then, ¹⁸FDG uptake was measured as described previously.

2.8 | Animal treatment and in vivo imaging

C57BL/6 mice were injected intraperitoneally with 25 mg tilorone/kg body weight. The treatment was repeated 3 days after the first injection and PET/CT scans were performed on the day after the second tilorone injection.

Mice were anaesthetized with 3% Forane using a dedicated small animal anesthesia device and were injected with 10.2 ± 0.9 MBq of ¹⁸FDG in 100 μ L saline via the lateral tail vein before and after the

second tilorone treatment. 50 min after radiotracer injection, whole-body PET/CT scans were performed in isoflurane anesthesia using the preclinical *nanoScan PET/CT* device (Mediso LTD). After the image reconstruction and PET image analysis, the standardized uptake value (SUV) was calculated using the following formula: $SUV = (\text{ROI activity [MBq/mL]} / (\text{injected activity [MBq]} / \text{animal weight [g]}))$ (Kocsis et al., 2014).

2.9 | Statistical analysis

Statistical significance between groups was analyzed via Student's *t*-test or one-way analysis of variance followed by Dunnett's post hoc test. GraphPad Prism 8.0 (GraphPad Software Inc.) was used for graphing and statistical analyses. The data are expressed as the mean + SEM or the median (horizontal line in the box) with the 25th (lower whisker) and 75th (upper whisker) percentiles are plotted on box plots. $p < 0.05$ denoted statistical significance.

3 | RESULTS

3.1 | Tilorone increases BMP signaling in myoblasts

Leppäranta et al. (2013) demonstrated the ability of tilorone to enhance the transcription of BMP2 and BMP7 in mouse epithelial cells. Thus, we first examined whether this effect could be induced in mouse myoblasts. The treatment time we chose was based on Leppäranta's experiment, 24 and 48 h, which

were effective (Leppäranta et al., 2013). qRT-PCR revealed that mRNA levels of BMP2, BMP4, BMP7, and BMP14 were elevated by both (20 and 35 nM) concentrations in myoblasts; however, BMP14 expression was only significantly increased by the higher concentration (Figure 1). Moreover, the transcription of Smad4, a component of the BMP signaling pathway, was significantly increased by both concentrations (Figure 1). Further, we found that tilorone treatment increased the phosphorylation of Smad1/5/8 (Figure 2a,b), indicating the enhancement of BMP signaling.

3.2 | Effect of tilorone on signaling molecules regulating GLUT4 translocation

Because the transcription of several BMPs and Smad4 and phosphorylation of Smad1/5/8 were enhanced by tilorone treatment, we also examined whether these proteins affect insulin-dependent glucose uptake and assessed its regulation. BMP2 and BMP6 can sensitize adipocytes to insulin and enhance glucose uptake (Schreiber et al., 2017). The C2C12 mouse skeletal muscle cell line is a well-documented and *in vitro* used model for studying glucose homeostasis, insulin signaling mechanism, insulin resistance, GLUTs at the cellular and molecular levels (Mangnall et al., 1993; Tulipano et al., 2008; Wong et al., 2020). Moreover, GLUT4 translocation was also demonstrated in C2C12 myoblasts (Duan et al., 2017). We tested the expression and phosphorylation of skeletal muscle-specific Akt2, AMPK, and AS160, which regulate the insulin-dependent translocation of GLUT4. Tilorone increased the phospho-Akt2 (Ser474)/Akt2 and phospho-AMPK (Thr172)/AMPK ratios, and

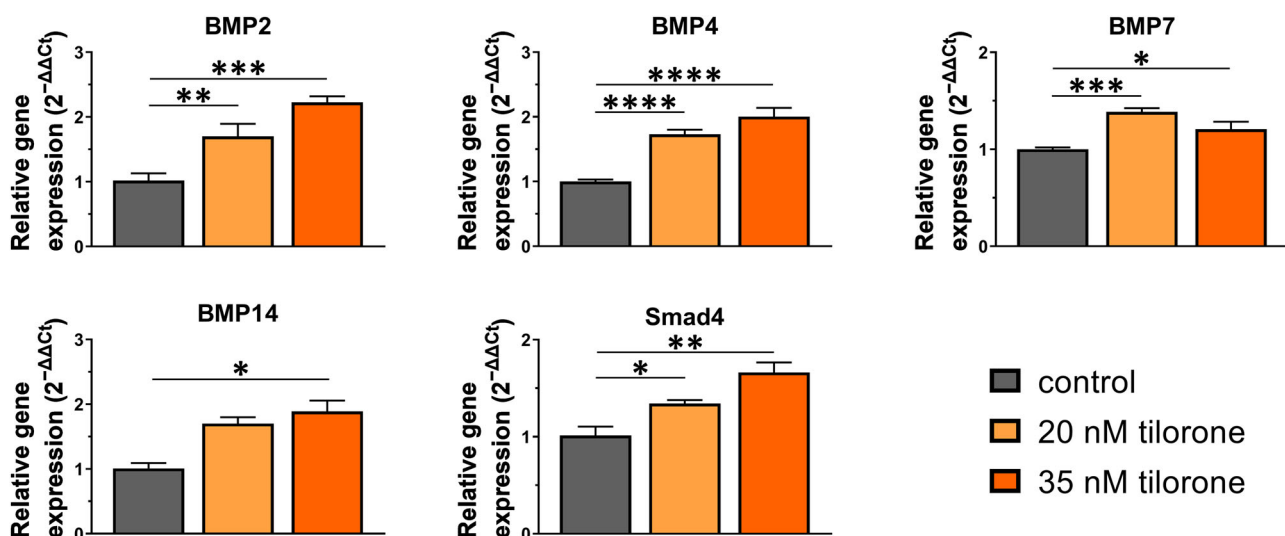


FIGURE 1 Tilorone increases bone morphogenetic protein (BMP) and Smad4 expression in myoblasts. C2C12 myoblasts were treated with 20 or 35 nM tilorone for 40 h, and the gene expression of BMP2, BMP4, BMP7, BMP14, and Smad4 molecules was measured by quantitative real-time PCR. Relative gene expression levels as $2^{-\Delta\Delta C_t}$ values using *MmHprt* and *MmRpl27* as internal control genes, are presented. Data are reported as the mean + SEM ($n = 3-4$). * $p < 0.05$, ** $p < 0.01$, *** $p < 0.001$, **** $p < 0.0001$. BMP, bone morphogenetic protein.

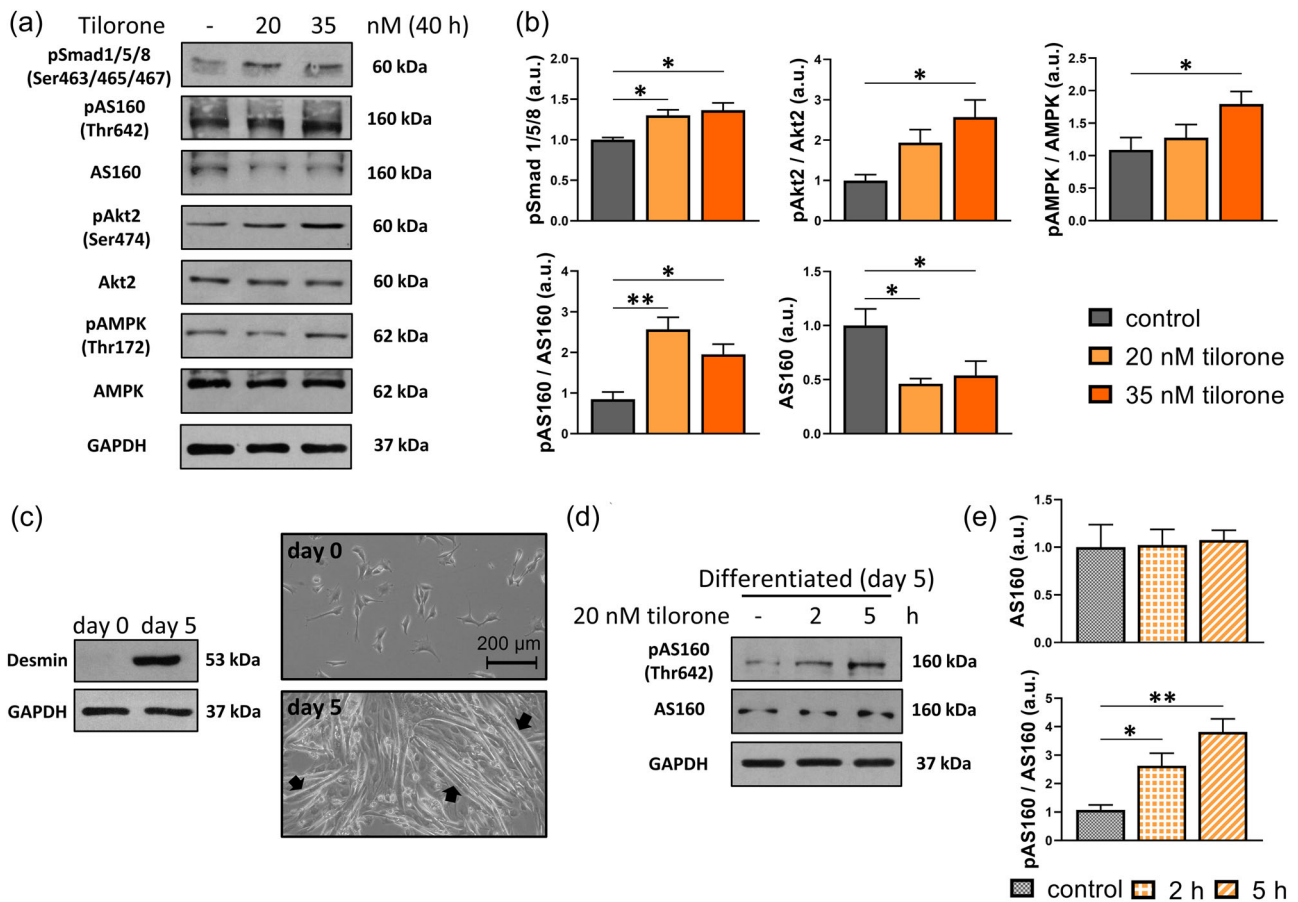


FIGURE 2 Effect of tilorone treatment on the activity of signaling molecules. Activation of bone morphogenetic protein (BMP) pathway was represented by phospho-Smad1/5/8 (Ser463/Ser456/Ser467) levels, and the activation of the signaling pathway (protein kinase B [Akt2]), AS160 regulating glucose transporter 4 (GLUT4) translocation was also studied. (a) Representative Western blots depict the levels of phospho-Smad1/5/8 (Ser463/Ser456/Ser467), phospho-AS160 (Thr642), AS160, phospho-Akt2 (Ser474), Akt2, phospho-AMPK(Thr172), and AMPK in proliferating C2C12 cells following 40 h tilorone treatment. GAPDH was used as a loading control. (b) Quantification of the Western blot results normalized to control and reported as the mean + SEM ($n = 3-8$ independent experiments). (c) Representative phase-contrast images of undifferentiated (proliferating) and differentiated C2C12 cells at $\times 10$ magnifications. Arrows mark the myotubes. Representative immunoblot shows the expression levels of desmin in undifferentiated (Day 0) and differentiated (Day 5) C2C12 cells. GAPDH was used as the loading control. (d) Representative Western blots depict the phospho- and total AS160 levels in differentiated C2C12 myotubes after 2 or 5 h of 20 nM tilorone treatment. GAPDH was used as a loading control. (e) For quantifying the western blot results, data were normalized to the control and reported as mean + SEM ($n = 3$ independent experiments). * $p < 0.05$, ** $p < 0.01$. AMPK, AMP-activated protein kinase; au, arbitrary unit.

these changes were significant for 35 nM tilorone. AS160 expression was decreased by both tilorone concentrations, and the phospho-AS160/AS160 ratio was increased (Figure 2a,b).

Subsequently, myoblasts were differentiated into myotubes in vitro (Figure 2c). To monitor the process of myoblast differentiation, we evaluated the amount of desmin, a muscle-specific intermediate filament. The level of desmin increased, indicating the appropriate differentiation of the samples. The levels and phosphorylation of AS160, the key regulator of GLUT4 translocation, were also examined on the fifth day of differentiation. Because tilorone affects myoblast differentiation as well (our unpublished data); therefore, we applied tilorone only for a short treatment in differentiated samples. In myotubes, 20 nM tilorone increased the phospho-AS160/AS160 ratio after either 2 or 5 h treatment (Figure 2d,e).

3.3 | Tilorone increases the expression of GLUTs and glucose uptake of C2C12 cells

Because the increased phosphorylation of Akt2, AMPK, and AS160 favors GLUT4 translocation and glucose uptake, we next studied the intracellular expression of GLUT4 in myoblasts exposed to tilorone via immunofluorescence staining and wide-field fluorescent microscopy. In addition to the original representative images, pseudocolor images provide better visualization of the altered GLUT4 expression depicting the increased levels of GLUT4 fluorescence following tilorone treatment (Figure 3a). The high-intensity red and yellow areas were mainly adjacent to the nucleus in tilorone-treated cells (Figure 3a). Quantification of the whole GLUT4 fluorescence intensity of the cells illustrated that their GLUT4 content increased after tilorone treatment (Figure 3b).

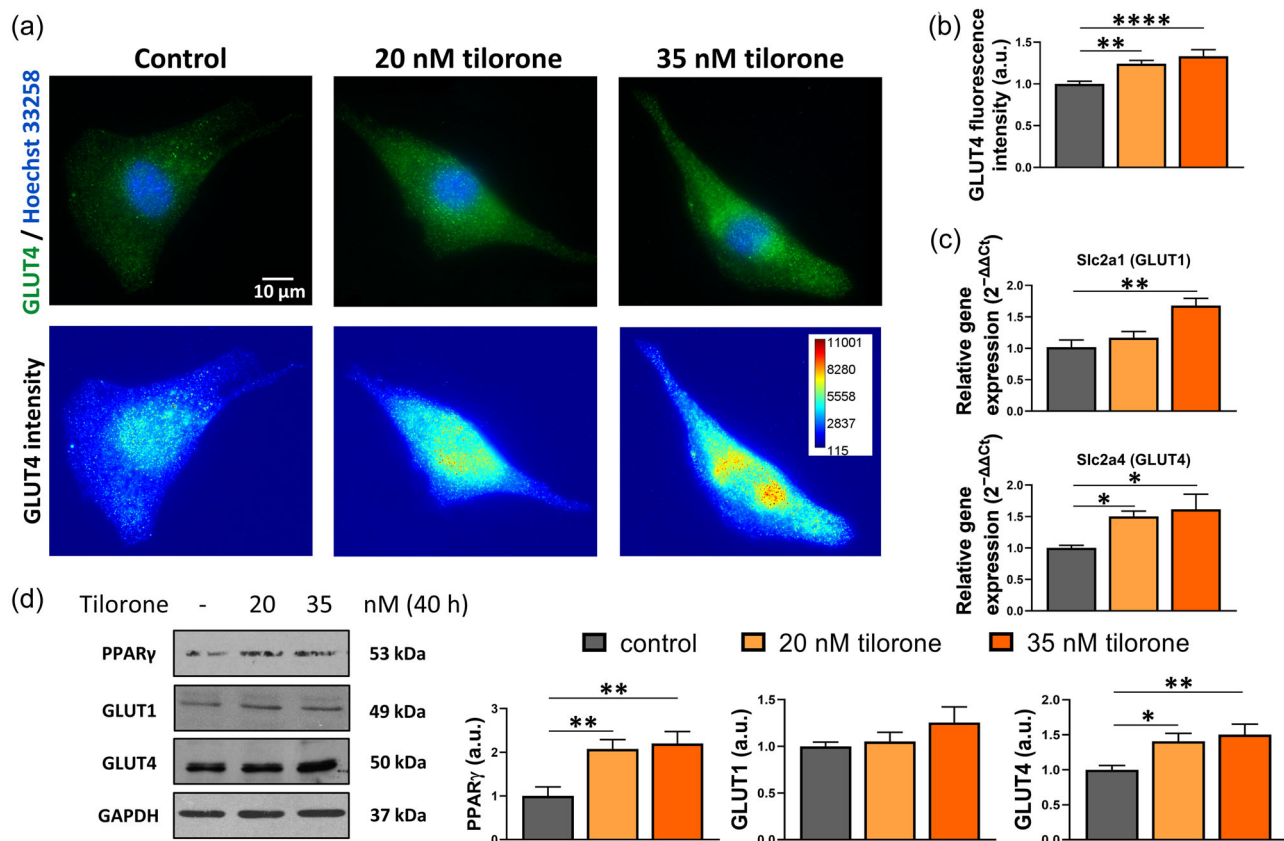


FIGURE 3 Tilorone increases the expression of glucose transporters (GLUTs). (a) Representative wide-field fluorescence images reveal the distribution of GLUT4 following staining with Alexa Fluor 488 (green). Nuclei were stained by Hoechst 33258 (blue). Representative pseudocolor images depict the GLUT4 signal intensity. The color was assigned to each pixel based on the pixel intensity value according to the calibration bar. (b) The mean intensity values of the cells were quantified, normalized to control, and compared following tilorone treatment. Data are reported as the mean + SEM ($n = 3$ independent experiments, 36–41 cells/treatment were quantified). (c) The levels of Slc2a1 (GLUT1) and Slc2a4 (GLUT4) were studied by quantitative real-time PCR. The housekeeping genes MmHprt and MmRpl27 were used as internal controls to normalize qRT-PCR results, and relative gene expression levels were calculated using the $2^{-\Delta\Delta C_t}$ method. Data are reported as the mean + SEM ($n = 3$ –4 independent experiments). (d) Representative western blots of PPAR γ , GLUT1, and GLUT4 protein expression. GAPDH was used as an internal control. Quantification of the results normalized to control and reported as the mean + SEM (GLUT1: $n = 3$, PPAR γ and GLUT4: $n = 8$ independent experiments). * $p < 0.05$, ** $p < 0.01$, **** $p < 0.0001$. au, arbitrary unit; PPAR γ , peroxisome proliferator-activated receptor- γ .

Subsequently, qRT-PCR was performed to check the mRNA levels of myoblast-specific Slc2a1 (GLUT1) and Slc2a4 (GLUT4). We found that the levels of both the Slc2a1 and Slc2a4 transcripts were increased by treatment with different concentrations of tilorone (Figure 3c). GLUT1 and GLUT4 protein levels were also analyzed by Western blot. GLUT1 levels were tendentially increased following tilorone treatment, and we detected a significant increase in GLUT4 protein levels at 35 nM tilorone concentration (Figure 3d). From the research of Schreiber et al. (2017) using mouse adipocytes, we know that Smad1/5/8 and Smad4 can transcriptionally activate PPAR γ , which is a critical regulator of GLUT4 expression. We thus examined the expression of PPAR γ by Western blot technique and detected an increase in both tilorone concentrations (Figure 3d).

Because we observed increased levels of GLUTs and strong activation of Akt2/AS160 signaling that regulate GLUT4 translocation, radiolabeled glucose analog ^{18}F FDG uptake of C2C12 cells was also measured. Our results revealed a 1.5-fold increase in ^{18}F FDG

uptake after 20 nM tilorone treatment, and this uptake was further increased by the higher concentration (Figure 4a). To separate the rate of glucose uptake via GLUT1 or GLUT4, we applied BAY-876, a GLUT1-specific inhibitor to the cells after preincubation with tilorone. BAY-876 treatment decreased the ^{18}F FDG uptake of the cells indicating the involvement of GLUT1 in tilorone-mediated glucose uptake (Figure 4b).

3.4 | Tilorone increases ^{18}F FDG uptake of myotubes and enhances insulin effect

Because tilorone increased glucose uptake in myoblasts, next we examined whether tilorone exhibits an insulin sensitizing effect on myotubes. The phosphorylation of Akt2, a critical element of insulin-mediated signaling, was significantly increased following insulin treatment, as expected (Figure 5a,b). Administration of

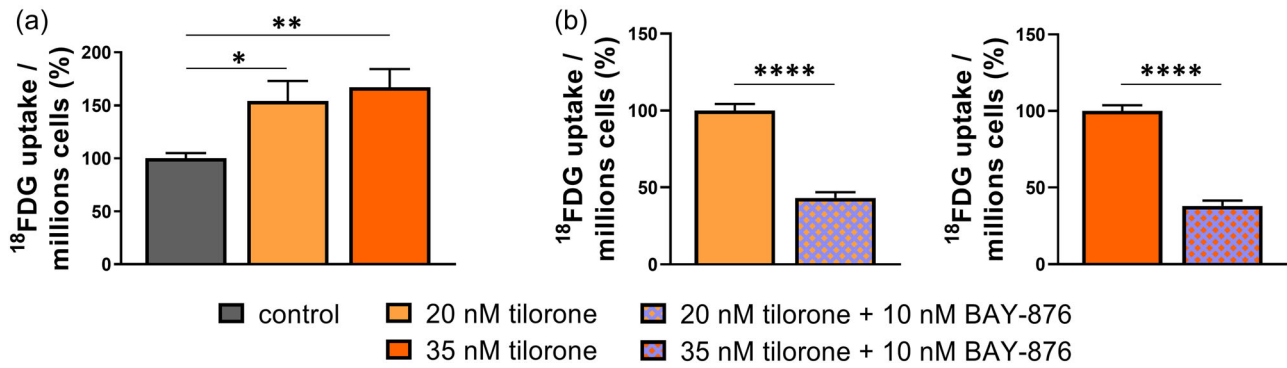


FIGURE 4 Tilorone increases ¹⁸F-fluoro-2-deoxyglucose (¹⁸FDG) uptake by C2C12 cells. (a) Rate of uptake of the radioactively labeled glucose analog ¹⁸FDG by C2C12 myoblasts following 20 or 35 nM tilorone treatment (24 h). ¹⁸FDG uptake is expressed as percentage of 1×10^6 myoblasts relative to the control. (b) The effect of BAY-876 (2 h, 10 nM), a GLUT1 inhibitor, on ¹⁸FDG uptake of tilorone-treated (24 h; 20 or 35 nM) C2C12 myoblasts. ¹⁸FDG uptake is expressed as percentage of 1×10^6 myoblasts relative to tilorone treated cells. Results are reported as the mean + SEM ($n = 5-7$ independent experiments). * $p < 0.05$, ** $p < 0.01$, *** $p < 0.0001$. GLUT, glucose transporter.

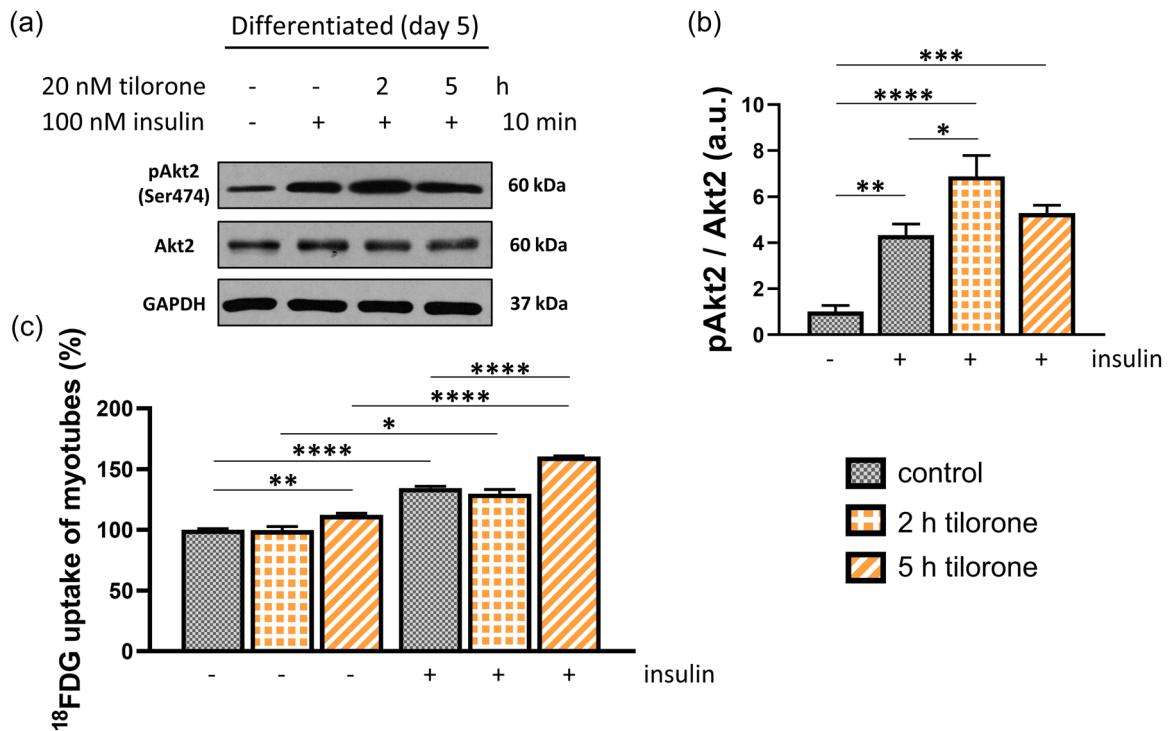


FIGURE 5 Tilorone increases insulin effect and improves ¹⁸FDG uptake in myotubes. (a) Representative Western blots depict the levels of phospho-Akt2 (Ser474), Akt2, and GAPDH in differentiated C2C12 myotubes after tilorone pretreatment (20 nM, 2 or 5 h) followed by insulin administration (100 nM, 10 min). GAPDH shows the equal loading of samples. (b) Quantification of the western blot results, data normalized to untreated control and reported as the mean + SEM ($n = 3-4$ independent experiments); * $p < 0.05$, ** $p < 0.01$, *** $p < 0.001$, **** $p < 0.0001$. (c) The radioactively labeled glucose analog ¹⁸FDG uptake of C2C12 myotubes following 20 nM tilorone (2 or 5 h) administration and with or without insulin (10 min 100 nM) treatment. ¹⁸FDG uptake is expressed as a percentage of the untreated control group. Results are reported as the mean + SEM ($n = 4$ independent experiments); * $p < 0.05$, ** $p < 0.01$, **** $p < 0.0001$.

tilorone further increased the insulin-induced phospho-Akt2/ Akt2 ratio indicating the insulin-sensitizer effect of tilorone (Figure 5a,b).

Next, we examined the ¹⁸FDG uptake of myotubes on the fifth day of differentiation. We observed increased ¹⁸FDG uptake

of myotubes after tilorone treatment (5 h). Insulin increased the ¹⁸FDG uptake of control and tilorone-treated (2 or 5 h tilorone administration) groups. Moreover, tilorone administration (5 h) increased the insulin-mediated ¹⁸FDG uptake of myotubes (Figure 5c).

3.5 | Effects of tilorone treatment on mitochondrial function in myoblasts

To determine whether the elevated glucose uptake of the cells was associated with changes in the mitochondrial respiratory chain, the oxygen consumption of C2C12 cells was examined via high-resolution respirometry. Routine (baseline), proton leak, ETS (representing maximal respiration capacity), and ROX values are presented in a representative measurement plot in Figure 6a. Compared to the control group findings, treatment with 20 or 35 nM tilorone significantly decreased routine respiration in intact myoblasts. In addition, tilorone reduced ATP-linked respiration (difference between routine and leak respiration) based on the unchanged leak values (Figure 6b). Following oligomycin treatment, the oxygen consumption represents the level of proton leak in the cells. No significant difference in the maximal capacity of ETS and ROX was observed following treatment. Mitochondrial reserve capacity (respiration reserve), the difference between the respiratory capacity and basal respiration, is the “spare” respiratory capacity important for cellular responses to stress and preventing oxidant-induced mitochondrial dysfunction (Dranka et al., 2010). In our experiments, the mitochondrial reserve capacity did not change after tilorone administration.

As we observed changes of mitochondrial function, we next studied the expression of PPAR γ coactivator 1 alpha (PGC-1 α) which regulates mitochondrial biogenesis, and total number of mitochondria in the cells was also evaluated. The PGC-1 α protein levels did not change following either 20 or 35 nM tilorone treatment (Figure 6c) analyzed by western blot. To achieve total number of mitochondria in the cells, we visualized mitochondria using the specific fluorescent dye MitoTracker™ Deep Red FM, which passively diffuses across the plasma membrane of living cells and accumulates in active mitochondria (Figure 6d). We measured the total fluorescent intensity of the cells and found no difference between control and tilorone-treated cells (Figure 6e), indicating that the mitochondrial number did not change following tilorone treatment.

3.6 | Tilorone administration increases ¹⁸FDG uptake in vivo

Considering the increased glucose uptake of skeletal muscle myoblasts in vitro, we next examined the effect of systemic tilorone administration on in vivo ¹⁸FDG uptake using PET/CT imaging. The treatment concentration we chose was based on earlier in vivo experiments and pharmacokinetics evaluation of tilorone (Leppäranta et al., 2013). The distribution of radiolabelled glucose in C57BL/6 mice was examined by PET/CT scans (Figure 7a). By the quantitative analysis ¹⁸FDG-PET images, we found significant increases in the SUV mean of skeletal muscle, adipose tissue, and liver following tilorone treatment, indicating the increased radiotracer uptake of these tissues. The ¹⁸FDG accumulation was comparable in tilorone treated skeletal muscle, adipose tissues, and liver (Figure 7b). Among

the examined tissues, heart exhibited the highest basal glucose uptake; however, it did not increase after tilorone treatment (Figure 7b).

4 | DISCUSSION

The synthetic small-molecule compound tilorone can enhance the transcription of BMPs in epithelial cells (Leppäranta et al., 2013). BMPs might participate in insulin sensitization, glucose uptake, carbohydrate and lipid metabolism, and the regulation of mitochondrial function (Schreiber et al., 2017; Yu et al., 2017); therefore, we examined the effects of tilorone on glucose uptake and metabolism in vitro and in vivo. As the number of people with T2DM is continuously increasing, there is an urgent need for new therapeutic strategies and to identify new drug candidates that increase glucose uptake.

Tilorone first was used as a broad-spectrum antiviral agent in the 1970s. The mechanism through which tilorone mediates its effect is not completely understood. Tilorone is able to induce transcriptional changes (Ratan et al., 2008); and a possible explanation of the mechanism of its action is that tilorone can intercalate into DNA thereby affecting the expression of genes (Nishimura et al., 2007). Earlier a high-throughput drug screen identified tilorone as a BMP-inducing agent. Tilorone was shown to induce BMP genes and the expression of the BMP target gene *Id3* (inhibitor of differentiation-3) in pulmonary epithelial cells in vitro, and to increase *Smad1* phosphorylation in vivo (Leppäranta et al., 2013). In the muscles of tumor-bearing mice, it was also proved that tilorone effect is dependent on the BMP-*Smad1/5/8* signaling pathway (Sartori et al., 2021). However, this does not exclude other possible target genes for tilorone.

In epithelial cells, tilorone has been found to increase the transcription of BMP2 and BMP7, but not BMP4 (Leppäranta et al., 2013). We observed increased BMP2, BMP4, BMP7, and BMP14 transcription in C2C12 myoblasts following tilorone administration. Moreover, we observed increased *Smad1/5/8* phosphorylation and increased *Smad4* transcription following tilorone treatment, indicating the enhanced BMP signaling. Several studies investigated the effect of tilorone on different cell types. In this study, we used a tilorone concentration comparable to the antiviral concentration of tilorone (Lane & Ekins, 2020).

Tilorone possesses a broad array of biological activities beyond its antiviral effect. In addition to alleviating pulmonary fibrosis in a mouse model (Leppäranta et al., 2013), a recent publication demonstrated that tilorone represents a potential novel therapy for fibrosis associated with heart failure (Horlock et al., 2021), and can also prevent muscle wasting and preserve the function of neuromuscular junction of tumor-bearing mice (Sartori et al., 2021). Since the *Smad1/5/8*-mediated BMP signaling was identified as an important regulator of muscle homeostasis affecting skeletal muscle size or the function of neuromuscular junction, the potential therapeutic application of tilorone in muscle wasting diseases of different origin might be an interesting perspective.

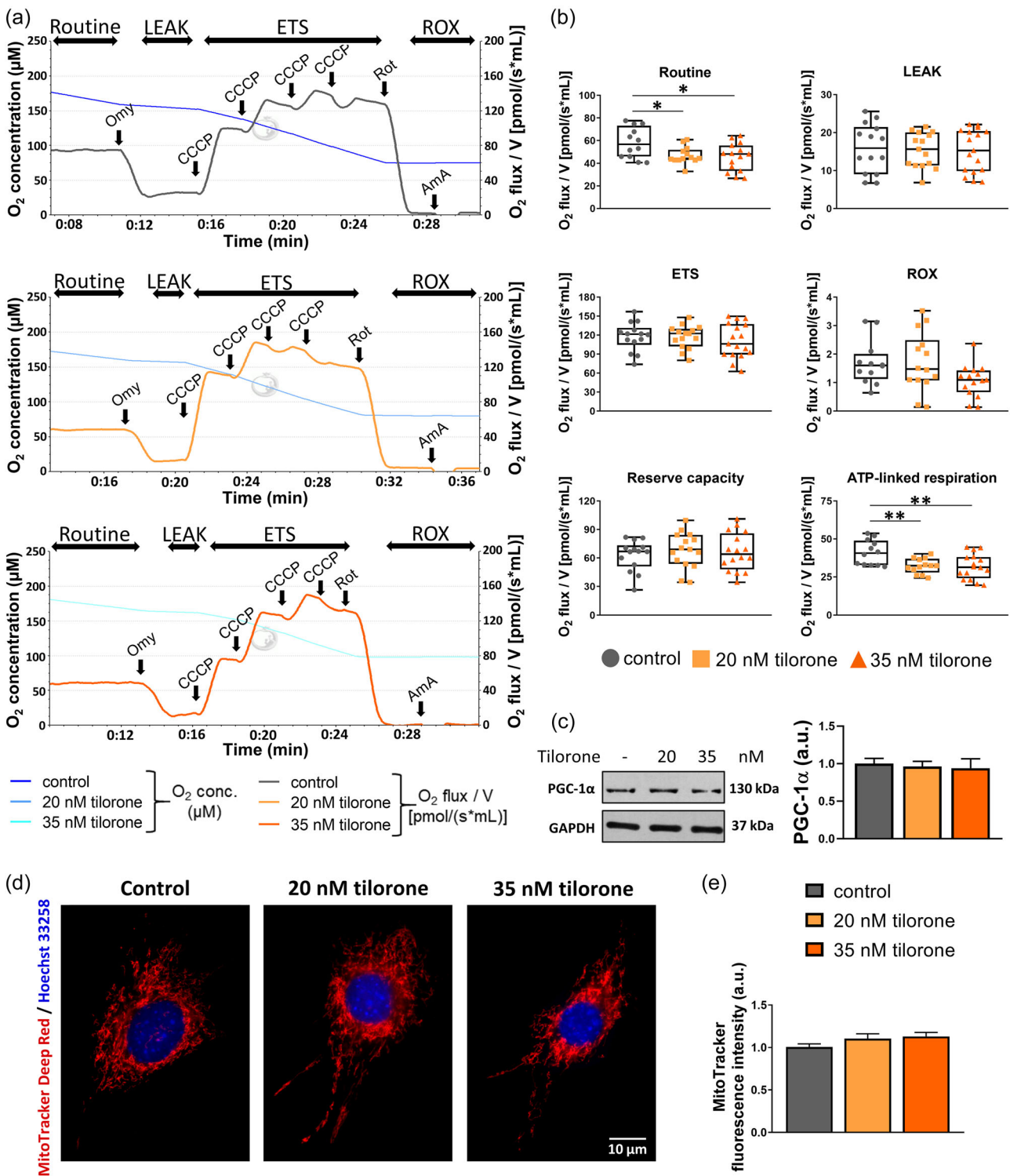


FIGURE 6 Changes in mitochondrial respiration in C2C12 myoblasts after tilorone treatment. (a) On the representative experimental figures of the mitochondrial respiration measurements, the lines illustrate chamber O_2 concentrations in control and tilorone-treated cells. Maximal electron transport system (ETS) capacity was achieved via stepwise titration of an uncoupler (carbonyl cyanide m-chlorophenylhydrazone [CCCP]). (b) Measured routine respiration, leak state, maximal ETS capacity, residual oxygen consumption (ROX), reserve capacity, and ATP-linked respiration are presented as O_2 flux/V ($\text{pmol}/[\text{s} \times \text{mL}]$). The box plots demonstrate the median (horizontal line in the box) and the 25th (lower whisker) and 75th (upper whisker) percentiles ($n = 12-17$ independent experiments). (c) Illustrative western blot image of PGC-1 α expression and GAPDH as a loading control. To quantify the results, the data were normalized to the control and then the mean + SEM was plotted ($n = 5$ independent experiments). (d) Representative images depict mitochondria labeled with MitoTracker Deep Red FM (red). Nuclei were stained by Hoechst 33258 (blue). (e) The fluorescence signal intensity of MitoTracker Deep Red FM staining was measured in the individual cells, and the total intensity values of the cells were compared. The results were normalized to control and reported as the mean + SEM ($n = 3-4$ independent experiments, 49-65 cells/treatment). * $p < 0.05$, ** $p < 0.01$. AmA, antimycin A; au, arbitrary unit; Omy, oligomycin; Rot, rotenone.

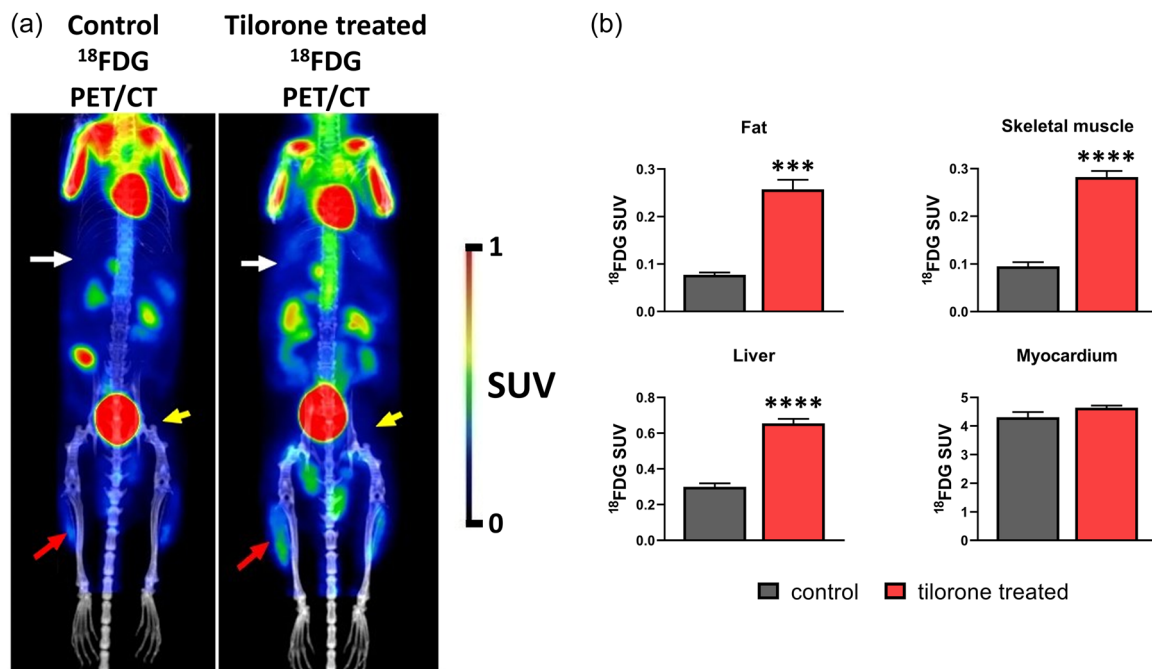


FIGURE 7 In vivo ^{18}F -fluoro-2-deoxyglucose (^{18}FDG) uptake in C57BL/6 mice after tilorone treatment. (a) Representative decay-corrected ^{18}FDG -PET/CT MIP (maximum intensity projection) images of the same C57BL/6 mouse before (left panel) and after (right panel) tilorone treatment (25 mg/kg). White arrows: liver, yellow arrows: fat, red arrows: muscle. (b) Quantitative analysis of ^{18}FDG uptake of selected tissues (fat, liver, skeletal muscle, myocardium). Results are reported as the mean of standardized uptake value (SUV) + SEM ($n = 4$ in each group); *** $p < 0.001$, **** $p < 0.0001$.

In our experiments, tilorone increased PPAR γ level. In considering the transcription-regulatory effects of Smad1/5/8 and Smad4, it is important to mention their ability to control PPAR γ (Schreiber et al., 2017). PPAR γ can regulate cell differentiation, glucose and lipid metabolism, lipid storage and mobilization (Janani & Ranjitha Kumari, 2015), and mitochondrial biogenesis with PGC-1 α (Jamwal et al., 2020). Via another pathway, BMP14 can activate Sirt1, which deacetylates and thus activates PPAR γ (D. Wang, Jiang et al., 2018). All of the BMPs we examined (i.e., BMP2, BMP4, BMP7, and BMP14) can positively regulate PPAR γ . Several targets of active PPAR γ include the Slc2a4 (GLUT4) gene (Armoni et al., 2007; Wu et al., 1998). Importantly, PPAR γ agonists have emerged as effective insulin sensitizers in the treatment of type 2 diabetes. Here we observed, that tilorone exhibits an insulin-sensitizer effect increasing insulin-mediated Akt2 phosphorylation and ^{18}FDG uptake of myotubes.

Importantly, we observed that tilorone treatment affects both insulin-dependent (via GLUT4 translocation) and insulin-independent (via GLUT1) glucose uptake of myoblasts. Both the increased GLUT4 levels and activated Akt2/AS160 signaling can lead to increased GLUT4-mediated glucose uptake after tilorone treatment (summarized in Figure 8). The specific inhibition of GLUT1 markedly decreased (more than 50% inhibition) the ^{18}FDG uptake of tilorone treated cells indicating the involvement of GLUT1 in glucose uptake. The increased GLUT1 levels might participate in this effect. GLUT1 is an insulin-independent transporter, and thus, it is essentially released into the plasma membrane of cells. The presence of GLUT1 in skeletal muscle was previously reported as the predominant GLUT

isoform in myoblasts (Zhao & Keating, 2007). It was reported earlier that BMP7 augmented glucose uptake in adipose tissue and muscle by increasing GLUT4 translocation to the plasma membrane via the PI3K/PDK1/Akt pathway (Chattopadhyay et al., 2017). Consistent with the aforementioned effect, the tilorone-mediated increase of BMP transcription was associated with increased GLUT4 levels and increased activity of the signaling pathway responsible for GLUT4 translocation in our experiments. However, it is important to note, that we do not conducted the evaluation of GLUT4 specifically at the plasma membrane. Since C2C12 cells are weak models for studying GLUT4 translocation, this is a limitation of the model system.

Akt2/AS160 signaling is a central regulator of GLUT4 translocation. The pAS160/AS160 ratio increased in both myoblasts and myotubes following tilorone treatment. However, the total AS160 level was decreased in myoblasts after tilorone administration but not in myotubes. Importantly, in myoblasts we applied tilorone for 40 h; therefore, the decreased level of total AS160 protein can be the consequence of a negative feedback effect following increased glucose uptake. The 40 h tilorone treatment of myoblasts already allowed a sufficiently long period for quantitative protein changes; however, few hours (2 or 5 h) treatment on myotubes only gave the opportunity for faster phosphorylation changes.

Skeletal muscle is one of the most energy-intensive tissues in the human body. The transcription factor PGC-1 α plays a central role in the regulation of cellular energy metabolism by maintaining mitochondrial biogenesis and oxidative metabolism (Liang & Ward, 2006). According to our results, the number of active

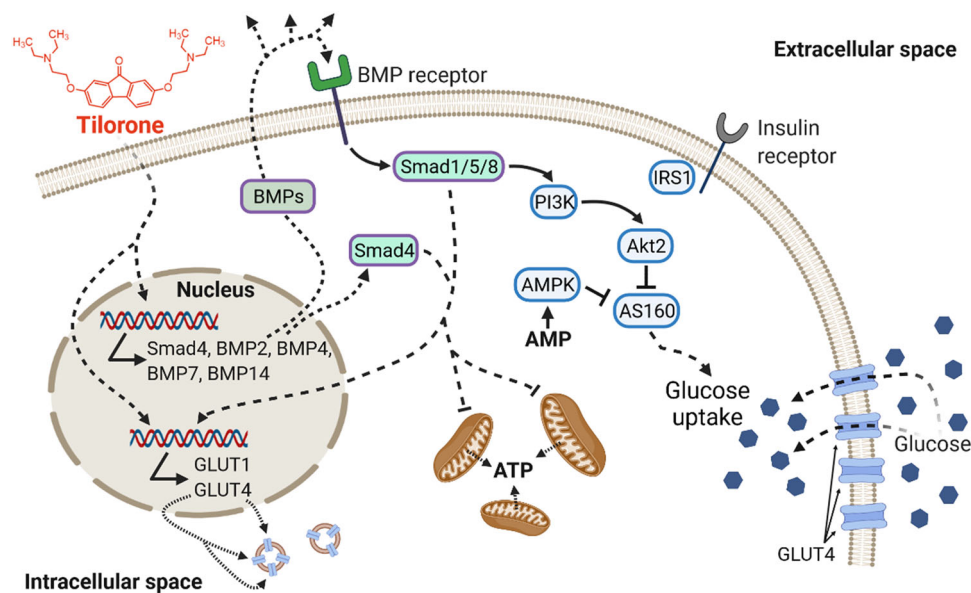


FIGURE 8 Schematic summary of the effects of tilorone on signaling pathways and glucose uptake. Tilorone induces the transcription of BMP2, BMP4, BMP7, and BMP14, and enhances the activity of the BMP pathway by increasing the phosphorylation of Smad1/5/8 and expression of Smad4. The increased glucose transporter (GLUT1 and GLUT4) levels and activation of the Akt2/AS160 pathway can participate in increased glucose uptake. The decreased mitochondrial routine and ATP-linked respiration also favors increased glucose uptake. The figure was created using [BioRender.com](#). Akt, protein kinase B; AMP, adenosine monophosphate; AMPK, AMP-activated protein kinase; AS160, Akt substrate of 160 kDa; ATP, adenosine triphosphate; BMP, bone morphogenetic proteins; GLUT, glucose transporter; IRS1, insulin receptor substrate 1; PI3K, phosphoinositide-3-kinase.

mitochondria did not change after tilorone treatment; however, the routine and ATP-linked respiration values were decreased despite the increased glucose uptake of the cells. Therefore, decreased mitochondrial function might explain the increased glucose uptake. It cannot be ignored that tilorone has other cellular effects in addition to inducing BMPs. Together, these effects might decrease ATP-linked respiration in mitochondria, and this presumably results in an increased intracellular AMP/ATP ratio. High levels of AMP inhibit AS160 through AMPK and thereby activate GLUT4 translocation (Huang & Czech, 2007).

Several studies investigated the role of BMPs in mitochondrial function and their effect on mitochondrial number in different tissues. In brown preadipocytes, BMP4 treatment decreased PGC-1 α mRNA levels, whereas increased PPAR γ 1 transcription (Modica et al., 2016). Consistent with this, the transcription of PGC-1 α was decreased in the brown adipose tissue of BMP-4 overexpressing transgenic mice without a change in the number of mitochondria, but the transcription of these genes was increased in white adipose tissue (Qian et al., 2013). Based on these findings, BMP4 plays a role in mitochondrial functions, albeit in a strongly tissue-specific manner. According to a study of brown adipose tissue, BMP7 can increase mitochondrial activity without increasing the number of mitochondria (Townsend et al., 2013). Increased mitochondrial oxygen consumption was also detected after BMP2 treatment in human chondrocytes (C. Wang, Silverman et al., 2018). Our results are partly consistent with these data; however, it is important to remember that we examined the effect of tilorone treatment.

In summary, this study demonstrated the complex mechanism of tilorone action as follows (Figure 8): (i) upregulation of BMPs expression and increasing BMP signaling, (ii) increasing the levels of GLUT1 and GLUT4, (iii) activating major signaling mechanisms regulating GLUT4 translocation, (iv) decreasing basal and ATP-linked respiration in mitochondria, and (v) sensitizing to insulin in myotubes. All of these changes can contribute to elevated glucose uptake, as demonstrated in the present study by the detection of an increased uptake of the glucose analog ^{18}F FDG in myoblasts and myotubes, and also the increased ^{18}F FDG uptake of skeletal muscle, liver, and adipose tissue. Further studies are necessary to elucidate the precise molecular mechanism of tilorone action and identify novel target genes besides BMPs. Since the BMP pathway is a promising drug target for the treatment of insulin resistance and DM it would also be required to test the potential therapeutic effect of tilorone in case of these diseases, as well as in skeletal muscle diseases in which BMP signaling is disturbed. Our study may expand the use of tilorone, which is already in the market.

ACKNOWLEDGMENTS

The authors thank Erzsebet Radi and Zita Makrane Felho (University of Szeged) for their excellent technical assistance. Authors wish to thank to Scanomed Ltd. (Scanomed Translational Centre, Debrecen, Hungary) for the in vivo imaging. This research was supported by the National Research, Development and Innovation Office of Hungary [grant numbers: GINOP-2.3.2-15-2016-00040 (MYOTeam), EFOP-

3.6.2-16-2017-00006, NKFI FK 134684, and NKFI K 132446]. Project no. TKP2021-EGA-28 has been implemented with the support provided by the Ministry of Innovation and Technology of Hungary from the National Research, Development and Innovation Fund, financed under the TKP2021-EGA funding scheme. The work was further supported by the János Bolyai Research Scholarship of the Hungarian Academy of Sciences (to A. K.-P.), UNKP-21-5-SZTE-571 New National Excellence Program of the Ministry for Innovation and Technology Sciences (to A. K.-P.), and University of Szeged Open Access Fund (grant number: 6150).

CONFLICT OF INTEREST STATEMENT

The authors declare no conflict of interest.

ORCID

Zoltan M. Kohler  <http://orcid.org/0000-0002-8299-105X>

Aniko Keller-Pinter  <http://orcid.org/0000-0002-4105-8458>

REFERENCES

- Armoni, M., Harel, C., & Karnieli, E. (2007). Transcriptional regulation of the GLUT4 gene: From PPAR-gamma and FOXO1 to FFA and inflammation. *Trends in Endocrinology and Metabolism: TEM*, 18(3), 100–107. <https://doi.org/10.1016/j.TEM.2007.02.001>
- Chattopadhyay, T., Singh, R. R., Gupta, S., & Surolia, A. (2017). Bone morphogenetic protein-7 (BMP-7) augments insulin sensitivity in mice with type II diabetes mellitus by potentiating PI3K/AKT pathway: BMP-7 potentiates insulin signaling, enhances glucose uptake. *Biofactors*, 43(2), 195–209. <https://doi.org/10.1002/biof.1334>
- DeFronzo, R. A., & Tripathy, D. (2009). Skeletal muscle insulin resistance is the primary defect in type 2 diabetes. *Diabetes Care*, 32(Suppl. 2), S157–S163. <https://doi.org/10.2337/dc09-S302>
- Doerrier, C., Garcia-Souza, L. F., Krumschnabel, G., Wohlfarter, Y., Mészáros, A. T., & Gnaiger, E. (2018). High-resolution Fluorescence Respirometry and OXPHOS protocols for human cells, permeabilized fibers from small biopsies of muscle, and isolated mitochondria. *Mitochondrial Bioenergetics* (pp. 31–70). Springer. https://doi.org/10.1007/978-1-4939-7831-1_3
- Dranka, B. P., Hill, B. G., & Darley-Usmar, V. M. (2010). Mitochondrial reserve capacity in endothelial cells: The impact of nitric oxide and reactive oxygen species. *Free Radical Biology and Medicine*, 48(7), 905–914. <https://doi.org/10.1016/j.freeradbiomed.2010.01.015>
- Duan, Y., Li, F., Wang, W., Guo, Q., Wen, C., & Yin, Y. (2017). Alteration of muscle fiber characteristics and the AMPK-SIRT1-PGC-1 α axis in skeletal muscle of growing pigs fed low-protein diets with varying branched-chain amino acid ratios. *Oncotarget*, 8(63), 107011–107021. <https://doi.org/10.18632/oncotarget.22205>
- Ekins, S., Lingerfelt, M. A., Comer, J. E., Freiberg, A. N., Mirsalis, J. C., O'Loughlin, K., Harutyunyan, A., McFarlane, C., Green, C. E., & Madrid, P. B. (2018). Efficacy of tilorone dihydrochloride against Ebola virus infection. *Antimicrobial Agents and Chemotherapy*, 62(2), e01711–17. <https://doi.org/10.1128/AAC.01711-17>
- Hardie, D. G., Ross, F. A., & Hawley, S. A. (2012). AMPK: A nutrient and energy sensor that maintains energy homeostasis. *Nature Reviews Molecular Cell Biology*, 13(4), 251–262. <https://doi.org/10.1038/nrm3311>
- Holman, N., Young, B., & Gadsby, R. (2015). Current prevalence of Type 1 and Type 2 diabetes in adults and children in the UK. *Diabetic Medicine*, 32(9), 1119–1120. <https://doi.org/10.1111/dme.12791>
- Horlock, D., Kaye, D. M., Winbanks, C. E., Gao, X. M., Kiriazis, H., Donner, D. G., Gregorevic, P., McMullen, J. R., & Bernardo, B. C. (2021). Old drug, new trick: Tilorone, a broad-spectrum antiviral drug as a potential anti-fibrotic therapeutic for the diseased heart. *Pharmaceuticals*, 14(3), 263. <https://doi.org/10.3390/PH14030263>
- Huang, S., & Czech, M. P. (2007). The GLUT4 glucose transporter, 5 *cell metabolism* §. Cell Press. <https://doi.org/10.1016/j.cmet.2007.03.006>
- Ishikura, S., Bilan, P. J., & Klip, A. (2007). Rabs 8A and 14 are targets of the insulin-regulated Rab-GAP AS160 regulating GLUT4 traffic in muscle cells. *Biochemical and Biophysical Research Communications*, 353(4), 1074–1079. <https://doi.org/10.1016/j.bbrc.2006.12.140>
- Jaldin-Fincati, J. R., Pavarotti, M., Frendo-Cumbo, S., Bilan, P. J., & Klip, A. (2017). Update on GLUT4 vesicle traffic: A cornerstone of insulin action. *Trends in Endocrinology and Metabolism: TEM*, 28(8), 597–611. <https://doi.org/10.1016/j.tem.2017.05.002>
- Jamwal, S., Blackburn, J., & Elsworth, J. D. (2020). PPAR γ /PGC1 α signaling as a potential therapeutic target for mitochondrial biogenesis in neurodegenerative disorders. *Pharmacology & Therapeutics*, 219, 107705. <https://doi.org/10.1016/j.pharmthera.2020.107705>
- Janani, C., & Ranjitha Kumari, B. D. (2015). PPAR gamma gene—A review. *Diabetes & Metabolic Syndrome*, 9(1), 46–50. <https://doi.org/10.1016/j.dsx.2014.09.015>
- Joost, H.-G., Bell, G. I., Best, J. D., Birnbaum, M. J., Charron, M. J., Chen, Y. T., Doege, H., James, D. E., Lodish, H. F., Moley, K. H., Moley, J. F., Mueckler, M., Rogers, S., Schürmann, A., Seino, S., & Thorens, B. (2002). Nomenclature of the GLUT/SLC2A family of sugar/polyol transport facilitators. *American Journal of Physiology-Endocrinology And Metabolism*, 282(4), E974–E976. <https://doi.org/10.1152/ajpendo.00407.2001>
- Kahn, B. B., & Mcgraw, T. E. (2010). Rosiglitazone, PPAR γ , and Type 2 diabetes. *New England Journal of Medicine*, 363, 2667–2669. <https://doi.org/10.1056/NEJMcibr1012075>
- Katz, E., Margalith, E., & Winer, B. (1976). Inhibition of herpesvirus deoxyribonucleic acid and protein synthesis by tilorone hydrochloride. *Antimicrobial Agents and Chemotherapy*, 9(1), 189–195. <https://doi.org/10.1128/AAC.9.1.189>
- Kocsis, T., Baán, J., Müller, G., Mandler, L., Dux, L., & Keller-Pintér, A. (2014). Skeletal muscle cellularity and glycogen distribution in the hypermuscular compact mice. *European Journal of Histochemistry*, 58(3), 169–175. <https://doi.org/10.4081/ejh.2014.2353>
- Krueger, R. F., & Mayer, G. D. (1970). Tilorone hydrochloride: An orally active antiviral agent. *Science*, 169(3951), 1213–1214. <https://doi.org/10.1126/science.169.3951.1213>
- Lane, T. R., & Ekins, S. (2020). Toward the target: Tilorone, quinacrine, and pyronaridine bind to ebola virus glycoprotein. *ACS Medicinal Chemistry Letters*, 11(8), 1653–1658. <https://doi.org/10.1021/acsmchemlett.0c00298>
- Leppäranta, O., Tikkanen, J. M., Bespalov, M. M., Koli, K., & Myllärniemi, M. (2013). Bone morphogenetic protein-inducer tilorone identified by high-throughput screening is antifibrotic in vivo. *American Journal of Respiratory Cell and Molecular Biology*, 48(4), 448–455. <https://doi.org/10.1165/rcmb.2012-0201OC>
- Leto, D., & Saltiel, A. R. (2012). Regulation of glucose transport by insulin: Traffic control of GLUT4. *Nature Reviews Molecular Cell Biology*, 13(6), 383–396. <https://doi.org/10.1038/nrm3351>
- Liang, H., & Ward, W. F. (2006). PGC-1 α : A key regulator of energy metabolism. *Advances in Physiology Education*, 30, 145–151. <https://doi.org/10.1152/advan.00052.2006>
- Loginova, S., Koval'chuk, A. V., Borisevich, S. V., Syromiatnikova, S. I., Borisevich, G. V., Pashchenko, I., Khamitov, R. A., Maksimov, V. A., & Shuster, A. M. (2004). Antiviral activity of an interferon inducer amixin in experimental West Nile Fever. *Voprosy Virusologii*, 49(2), 8–11.

- Mangnall, D., Bruce, C., & Fraser, R. B. (1993). Insulin-stimulated glucose uptake in C2C12 myoblasts. *Biochemical Society Transactions*, 21(4):438S. <https://doi.org/10.1042/BST021438S>
- Massagué, J., Seoane, J., & Wotton, D. (2005). Smad transcription factors. *Genes & Development*, 19(23), 2783–2810. <https://doi.org/10.1101/gad.1350705>
- Modica, S., Straub, L. G., Balaz, M., Sun, W., Varga, L., Stefanicka, P., Profant, M., Simon, E., Neubauer, H., Ukropcova, B., Ukropec, J., & Wolftrum, C. (2016). Bmp4 promotes a brown to white-like adipocyte shift. *Cell Reports*, 16(8), 2243–2258. <https://doi.org/10.1016/j.celrep.2016.07.048>
- Nászai, A., Terhes, E., Kaszaki, J., Boros, M., & Juhász, L. (2019). Ca²⁺ N it be measured? Detection of extramitochondrial calcium movement with high-resolution FluoRespirometry. *Scientific Reports*, 9(1), 19229. <https://doi.org/10.1038/s41598-019-55618-5>
- Nishimura, T., Okobira, T., Kelly, A. M., Shimada, N., Takeda, Y., & Sakurai, K. (2007). DNA binding of tilorone: 1H NMR and calorimetric studies of the intercalation. *Biochemistry*, 46(27), 8156–8163. <https://doi.org/10.1021/bi602402m>
- Pauk, M., Bordukalo-Niksic, T., Brkljacic, J., Paralkar, V. M., Brault, A. L., Dumic-Cule, I., Borovecki, F., Grgurevic, L., & Vukicevic, S. (2019). A novel role of bone morphogenetic protein 6 (BMP6) in glucose homeostasis. *Acta Diabetologica*, 56(3), 365–371. <https://doi.org/10.1007/s00592-018-1265-1>
- Puhl, A. C., Fritch, E. J., Lane, T. R., Tse, L. V., Yount, B. L., Sacramento, C. Q., Fintelman-Rodrigues, N., Tavella, T. A., Maranhão Costa, F. T., Weston, S., Logue, J., Frieman, M., Premkumar, L., Pearce, K. H., Hurst, B. L., Andrade, C. H., Levi, J. A., Johnson, N. J., Kisthardt, S. C., ... Ekins, S. (2021). Repurposing the ebola and marburg virus inhibitors tilorone, quinacrine, and pyronaridine: In vitro activity against SARS-CoV-2 and potential mechanisms. *ACS Omega*, 6(11), 7454–7468. <https://doi.org/10.1021/acsomega.0c05996>
- Qian, S.-W., Tang, Y., Li, X., Liu, Y., Zhang, Y.-Y., Huang, H.-Y., Xue, R. D., Yu, H. Y., Guo, L., Gao, H. D., Liu, Y., Sun, X., Li, Y. M., Jia, W. P., & Tang, Q. Q. (2013). BMP4-mediated brown fat-like changes in white adipose tissue alter glucose and energy homeostasis. *Proceedings of the National Academy of Sciences*, 110(9), E798–E807. <https://doi.org/10.1073/pnas.1215236110>
- Ratan, R. R., Siddiq, A., Aminova, L., Langley, B., McConoughey, S., Karpisheva, K., Lee, H. H., Carmichael, T., Kornblum, H., Coppola, G., Geschwind, D. H., Hoke, A., Smirnova, N., Rink, C., Roy, S., Sen, C., Beattie, M. S., Hart, R. P., Grumet, M., ... Gazaryan, I. (2008). Small molecule activation of adaptive gene expression: Tilorone or its analogs are novel potent activators of hypoxia inducible factor-1 that provide prophylaxis against stroke and spinal cord injury. *Annals of the New York Academy of Sciences*, 1147(1), 383–394. <https://doi.org/10.1196/annals.1427.033>
- Rauch, C., & Loughna, P. (2005). C2C12 skeletal muscle cells exposure to phosphatidylcholine triggers IGF-1 like-responses. *Cellular Physiology and Biochemistry*, 15(5), 211–224. <https://doi.org/10.1159/000086408>
- Reaven, G. M. (1988). Role of insulin resistance in human disease. *Diabetes*, 37(12), 1595–1607. <https://doi.org/10.2337/diab.37.12.1595>
- Saeedi, P., Petersohn, I., Salpea, P., Malanda, B., Karuranga, S., Unwin, N., Colagiuri, S., Guariguata, L., Motala, A. A., Ogurtsova, K., Shaw, J. E., Bright, D., & Williams, R. (2019). Global and regional diabetes prevalence estimates for 2019 and projections for 2030 and 2045: Results from the International Diabetes Federation Diabetes Atlas, 9th edition. *Diabetes Research and Clinical Practice*, 157, 107843. <https://doi.org/10.1016/j.diabres.2019.107843>
- Sartori, R., Hagg, A., Zampieri, S., Armani, A., Winbanks, C. E., Viana, L. R., Haidar, M., Watt, K. I., Qian, H., Pezzini, C., Zanganeh, P., Turner, B. J., Larsson, A., Zanchettin, G., Pierobon, E. S., Moletta, L., Valmasoni, M., Ponzoni, A., Attar, S., ... Sandri, M. (2021). Perturbed BMP signaling and denervation promote muscle wasting in cancer cachexia. *Science Translational Medicine*, 13(605), eaay9592. <https://doi.org/10.1126/scitranslmed.aay9592>
- Sartori, R., Schirwis, E., Blauw, B., Bortolanza, S., Zhao, J., Enzo, E., Stantzou, A., Mouisel, E., Toniolo, L., Ferry, A., Stricker, S., Goldberg, A. L., Dupont, S., Piccolo, S., Amthor, H., & Sandri, M. (2013). BMP signaling controls muscle mass. *Nature Genetics*, 45(11), 1309–1318. <https://doi.org/10.1038/ng.2772>
- Schreiber, I., Dörpholz, G., Ott, C. E., Kragestein, B., Schanze, N., Lee, C. T., Köhrle, J., Mundlos, S., Ruschke, K., & Knaus, P. (2017). BMPs as new insulin sensitizers: Enhanced glucose uptake in mature 3T3-L1 adipocytes via PPAR γ and GLUT4 upregulation. *Scientific Reports*, 7(1), 17192. <https://doi.org/10.1038/s41598-017-17595-5>
- Shen, L., Niu, J., Wang, C., Huang, B., Wang, W., Zhu, N., Deng, Y., Wang, H., Ye, F., Cen, S., & Tan, W. (2019). High-throughput screening and identification of potent broad-spectrum inhibitors of coronaviruses. *Journal of Virology*, 93(12), e00023-19. <https://doi.org/10.1128/JVI.00023-19>
- Sun, Y., Bilan, P. J., Liu, Z., & Klip, A. (2010). Rab8A and Rab13 are activated by insulin and regulate GLUT4 translocation in muscle cells. *Proceedings of the National Academy of Sciences*, 107(46), 19909–19914. <https://doi.org/10.1073/pnas.1009523107>
- Townsend, K. L., An, D., Lynes, M. D., Huang, T. L., Zhang, H., Goodyear, L. J., & Tseng, Y.-H. (2013). Increased mitochondrial activity in BMP7-treated brown adipocytes, due to increased CPT1-and CD36-mediated fatty acid uptake. *Antioxidants & Redox Signaling*, 19(3), 243–257. <https://doi.org/10.1089/ars.2012.4536>
- Tulipano, G., Spano, P., & Cocchi, D. (2008). Effects of olanzapine on glucose transport, proliferation and survival in C2C12 myoblasts. *Molecular and Cellular Endocrinology*, 292(1–2), 42–49. <https://doi.org/10.1016/j.mce.2008.04.010>
- Wang, C., Silverman, R. M., Shen, J., & O'Keefe, R. J. (2018). Distinct metabolic programs induced by TGF- β 1 and BMP2 in human articular chondrocytes with osteoarthritis. *Journal of Orthopaedic Translation*, 12, 66–73. <https://doi.org/10.1016/j.jot.2017.12.004>
- Wang, D., Jiang, X., Lu, A., Tu, M., Huang, W., & Huang, P. (2018). BMP14 induces tenogenic differentiation of bone marrow mesenchymal stem cells in vitro. *Experimental and Therapeutic Medicine*, 16(2), 1165–1174. <https://doi.org/10.3892/etm.2018.6293>
- Wong, C. Y., Al-Salami, H., & Dass, C. R. (2020). C2C12 cell model: Its role in understanding of insulin resistance at the molecular level and pharmaceutical development at the preclinical stage. *Journal of Pharmacy and Pharmacology*, 72(12), 1667–1693. <https://doi.org/10.1111/jphp.13359>
- Won, J. C. (2021). Thiazolidinediones (TZDs), In S. H. Lee & D. W. Kang (Eds.), *Stroke revisited: Diabetes in stroke*. Springer. https://doi.org/10.1007/978-981-16-5123-6_11
- Wu, Z., Xie, Y., Morrison, R. F., Bucher, N. L., & Farmer, S. R. (1998). PPARgamma induces the insulin-dependent glucose transporter GLUT4 in the absence of C/EBPalpha during the conversion of 3T3 fibroblasts into adipocytes. *Journal of Clinical Investigation*, 101(1), 22–32. <https://doi.org/10.1172/JCI1244>
- Yu, Y., Mutlu, A. S., Liu, H., & Wang, M. C. (2017). High-throughput screens using photo-highlighting discover BMP signaling in mitochondrial lipid oxidation. *Nature Communications*, 8(1), 865. <https://doi.org/10.1038/s41467-017-00944-3>
- Zhao, F.-Q., & Keating, A. (2007). Functional properties and genomics of glucose transporters. *Current Genomics*, 8(2), 113–128. <https://doi.org/10.2174/138920207780368187>
- Zhou, G., Myers, R., Li, Y., Chen, Y., Shen, X., Fenyk-Melody, J., Wu, M., Ventre, J., Doebber, T., Fujii, N., Musi, N., Hirshman, M. F., Goodyear, L. J., & Moller, D. E. (2001). Role

- of AMP-activated protein kinase in mechanism of metformin action. *Journal of Clinical Investigation*, 108(8), 1167–1174. <https://doi.org/10.1172/JCI13505>
- Zimmet, P., Alberti, K. G. M. M., & Shaw, J. (2001). Global and societal implications of the diabetes epidemic. *Nature*, 414(6865), 782–787. <https://doi.org/10.1038/414782a>
- Zorzano, A., Fandos, C., & Palacin, M. (2000). Role of plasma membrane transporters in muscle metabolism. *Biochemical Journal*, 349(3), 667–688. <https://doi.org/10.1042/BJ3490667>

How to cite this article: Kohler, Z. M., Trencsenyi, G., Juhasz, L., Zvara, A., Szabo, J. P., Dux, L., Puskas, L. G., Rovo, L., & Keller-Pinter, A. (2023). Tilorone increases glucose uptake in vivo and in skeletal muscle cells by enhancing Akt2/AS160 signaling and glucose transporter levels. *Journal of Cellular Physiology*, 1–15. <https://doi.org/10.1002/jcp.30998>

ANNEX

II.



Article

Astaxanthin Exerts Anabolic Effects via Pleiotropic Modulation of the Excitable Tissue

Mónika Gönczi, Andrea Csemer, László Szabó, Mónika Sztretye, János Fodor, Krisztina Pocsai, Kálmán Szenthe, Anikó Keller-Pintér, Zoltán Márton Köhler, Péter Nánási et al.

Special Issue

Advances in Skeletal Muscle Function and Metabolism

Edited by

Dr. Rasmus Kjøbsted





Article

Astaxanthin Exerts Anabolic Effects via Pleiotropic Modulation of the Excitable Tissue

Mónika Gönczi ^{1,†}, Andrea Csemer ^{1,2,†}, László Szabó ^{1,2}, Mónika Sztretye ¹, János Fodor ¹, Krisztina Pocsai ¹, Kálmán Szenthe ³, Anikó Keller-Pintér ⁴, Zoltán Márton Köhler ⁴, Péter Nánási ^{1,5}, Norbert Szentandrassy ^{1,6}, Balázs Pál ^{1,*} and László Csernoch ¹

- ¹ Department of Physiology, Faculty of Medicine, University of Debrecen, 4012 Debrecen, Hungary; gonczi.monika@med.unideb.hu (M.G.); csemer.andrea@med.unideb.hu (A.C.); szabo.laszlo@med.unideb.hu (L.S.); sztretye.monika@med.unideb.hu (M.S.); fodor.janos@med.unideb.hu (J.F.); deak-pocsai.krisztina@med.unideb.hu (K.P.); nanasi.peter@med.unideb.hu (P.N.); szentandrassy.norbert@med.unideb.hu (N.S.); csl@edu.unideb.hu (L.C.)
- ² Doctoral School of Molecular Medicine, University of Debrecen, 4012 Debrecen, Hungary
- ³ Carlsbad Research Organization Ltd., 9244 Újrónafő, Hungary; kszenthe@rt-europe.org
- ⁴ Department of Biochemistry, Albert Szent-Györgyi Medical School, University of Szeged, 6720 Szeged, Hungary; keller.aniko@med.u-szeged.hu (A.K.-P.); kohler.zoltan@med.u-szeged.hu (Z.M.K.)
- ⁵ Department of Dental Physiology and Pharmacology, Faculty of Dentistry, University of Debrecen, 4012 Debrecen, Hungary
- ⁶ Department of Basic Medical Sciences, Faculty of Dentistry, University of Debrecen, 4012 Debrecen, Hungary
- * Correspondence: pal.balazs@med.unideb.hu; Tel.: +36-52-255-575; Fax: +36-52-255-116
- † These authors contributed equally to this work.



Citation: Gönczi, M.; Csemer, A.; Szabó, L.; Sztretye, M.; Fodor, J.; Pocsai, K.; Szenthe, K.; Keller-Pintér, A.; Köhler, Z.M.; Nánási, P.; et al. Astaxanthin Exerts Anabolic Effects via Pleiotropic Modulation of the Excitable Tissue. *Int. J. Mol. Sci.* **2022**, *23*, 917. <https://doi.org/10.3390/ijms23020917>

Academic Editor: Rasmus Kjøbsted

Received: 17 November 2021

Accepted: 11 January 2022

Published: 14 January 2022

Publisher's Note: MDPI stays neutral with regard to jurisdictional claims in published maps and institutional affiliations.



Copyright: © 2022 by the authors. Licensee MDPI, Basel, Switzerland. This article is an open access article distributed under the terms and conditions of the Creative Commons Attribution (CC BY) license (<https://creativecommons.org/licenses/by/4.0/>).

Abstract: Astaxanthin is a lipid-soluble carotenoid influencing lipid metabolism, body weight, and insulin sensitivity. We provide a systematic analysis of acute and chronic effects of astaxanthin on different organs. Changes by chronic astaxanthin feeding were analyzed on general metabolism, expression of regulatory proteins in the skeletal muscle, as well as changes of excitation and synaptic activity in the hypothalamic arcuate nucleus of mice. Acute responses were also tested on canine cardiac muscle and different neuronal populations of the hypothalamic arcuate nucleus in mice. Dietary astaxanthin significantly increased food intake. It also increased protein levels affecting glucose metabolism and fatty acid biosynthesis in skeletal muscle. Inhibitory inputs innervating neurons of the arcuate nucleus regulating metabolism and food intake were strengthened by both acute and chronic astaxanthin treatment. Astaxanthin moderately shortened cardiac action potentials, depressed their plateau potential, and reduced the maximal rate of depolarization. Based on its complex actions on metabolism and food intake, our data support the previous findings that astaxanthin is suitable for supplementing the diet of patients with disturbances in energy homeostasis.

Keywords: astaxanthin; metabolism; food intake; gene expression; skeletal muscle; cardiac action potential; arcuate nucleus; excitability; inhibitory postsynaptic current

1. Introduction

Astaxanthin (AX) is a safe, lipid-soluble, bioavailable natural carotenoid compound present in several microorganisms and various aquatic and nonaquatic species including crustaceans, fish or the flamingo. A major source of AX is *Haematococcus pluvialis*, a green microalga with high AX content [1–4]. AX is a potent nutraceutical widely used as a nutritional supplement with antioxidant and anticancer actions. AX was shown to prevent diabetes, cardiovascular diseases, neurodegenerative disorders, and stimulate immunization [5,6]. As an antioxidant, AX reduces oxidative stress, increases the bioavailability of nitric oxide (NO) and the activity of antioxidant enzymes, and maintains the rheological properties of the blood [7]. It ameliorates skeletal muscle atrophy, and it exerts neuroprotective actions [8,9]. AX's anti-inflammatory properties involve modulating the

NF- κ B and MAPK signaling pathways, reducing the release of pro-inflammatory cytokines and increasing reverse cholesterol transport by HDL [10].

Furthermore, AX is believed to have an important role in the whole-body metabolism and helps to keep the body weight in the normal range [11,12]. Nevertheless, studies have shown that AX accelerates lipid breakdown during physical exercise, decreases body fat, and promotes muscle work during exercise [13–15].

The molecular mechanisms underlying adequate skeletal muscle maintenance involve an interplay between multiple signaling pathways. Under physiological conditions, a network of interconnected signals serve to control the precise balance between muscle protein synthesis and proteolysis. It includes changes in mTOR signaling stimulating protein synthesis [16,17], improvement of insulin sensitivity, and increased glucose uptake and breakdown with the consequential reduction of hyperglycemia [18–20]. Fatty acid metabolism is also affected by de novo synthesis of essential lipids for the formation of cell membrane, the production of extra energy via beta-oxidation, and lipid modification of proteins [21–25].

It is well established that the hypothalamus has a great impact on regulation of energy homeostasis. Neurons of the hypothalamic arcuate nucleus are influenced by peripheral signals and levels of nutrient molecules and affect food intake differently. The proopiomelanocortin (POMC) neurons inhibit while the neuropeptide Y (NPY) and agouti-related peptide (AgRP) positive ones increase food intake [26–28]. The latter ones also provide GABAergic inhibition on POMC neurons [29].

In the present work, we aimed to analyze the effects of AX on food intake and body weight changes. Chronic AX dietary supplementation increased food intake and led to increased body weight. This increased food intake is at least partially due to the enhanced inhibition of POMC neurons inhibiting this process. Our data support the hypothesis that glucose metabolism is affected by AX in a way which exerts anti-diabetic actions but partially challenges the view on findings with altered food intake.

2. Results

2.1. Actions of Astaxanthin Feeding on Metabolism and Food Intake

At first, the basic metabolic changes of control and AX fed mice were determined. Cumulative O₂ usage was similar before and after the four weeks of special feeding both in control and AX group (Figure 1A); however, when these parameters were normalized to the actual body weight, a significant decrease was observed following the treatment in both groups (Figure 1B). There was no significant difference between O₂ usage of control and AX groups. Similar observation was done regarding cumulative CO₂ production (Figure 1C), and its normalized values (Figure 1D). More specifically, average cumulative food intake revealed to be significantly higher in AX group compared to its control counterpart following 4 weeks of special feeding. Furthermore, food intake increased significantly after the treatment within the AX group (Figure 1E), while this parameter was similar in control animals before and after 4 weeks of feeding. Altogether, the average body weight changes in the AX group were significantly higher as compared to the control group (Figure 1F).

Activity (X_{amb} and X_{total}) was significantly reduced in both control and AX groups after 4 weeks of feeding. Other parameters involved in the overall metabolism measured in vivo were either lower (VO₂ and VCO₂), higher (cumulative water intake), or similar (RER, heat production, sleeping time) when comparing the data of control and AX animals before and after the 4 weeks of feeding. However, one must note that overall significant alterations were not observed as a consequence of the effect of AX administration (Table S1). Time-dependent changes of all the aforementioned parameters are plotted and presented in Figure S1A–F. Data from four individual measured points (equal with 72 min) were averaged in all animals within the same groups and were plotted as a function of time.

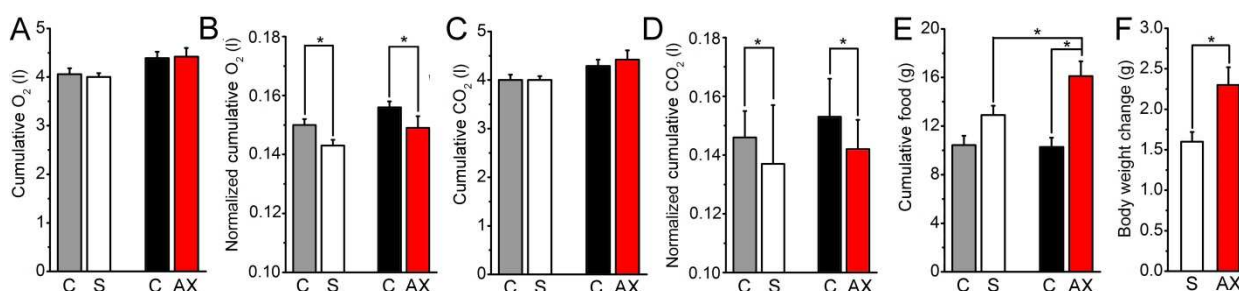


Figure 1. Metabolic effects of chronic astaxanthin feeding. (A,B) Actions on O_2 consumption without (A) and with normalization on body weight (B). Gray column: control group before sham feeding (C); hollow column: control group after sham feeding (S); black column: AX fed group before feeding of astaxanthin-containing chow (C); red column: AX fed group after feeding of astaxanthin-containing chow (AX). All panels have the same arrangement as above; (C,D) Effects on CO_2 consumption without (C) and with normalization on body weight (D); (E) Normalized actions on food intake; (F) Changes in body weight gain. * denotes significant differences at $p < 0.05$.

Using the respiratory ratio (VCO_2/VO_2), we calculated the calorific value (CV) using the equation ($CV = 3.815 \times 1.232 \times RER$), then total energy expenditure (TEE) was determined by multiplying CV and VO_2 . Subtracting resting/basal metabolic rate (RMR) from TEE we got the activity related energy expenditure ($TEE_{activity}$). Both versions of energy expenditure are plotted as a function of time (Figure S1G,H, respectively).

In summary, mice kept on AX supplemented diet had increased food intake compared to the control group. In line with this, parameters related to in vivo metabolic activity did not change following the four weeks of special AX feeding.

2.2. Astaxanthin Feeding Influences the Activation of Signaling Molecules Affecting Skeletal Muscle Metabolism

Skeletal muscles are responsible for a significant proportion of metabolism of the whole organism; therefore, we aimed to investigate whether proteins regulating skeletal muscle metabolism are affected by the AX diet. AX was shown to accumulate in skeletal muscle [30]; therefore, the effects of long-term AX administration on representative muscles known to be involved in force production such as the hindlimb (biceps femoris muscle) or forelimb (pectoral muscle; Figures 2 and S2) muscles of the mice were studied. The levels and phosphorylation of proteins involved in glucose uptake, regulation of cellular energy level, protein synthesis, and cell survival were also analyzed.

Nanostring nSolver analysis revealed significant differences in fatty acid synthase (Fasn) and stearoyl-CoA desaturase (Scd1) gene expression (2.47- and 2.06-fold change following AX-treatment, respectively, Figure S3), while pyruvate dehydrogenase kinase 4 (Pdk4) and xanthine dehydrogenase (Xdh) gene expression levels were lower (0.54-fold change and 0.66-fold change, respectively) in AX samples compared to control. Quantile normalization and class comparison generated a heatmap (Figure S3A) showing changes in gene expression between the two groups, but significant changes were also obvious following normalization of data for housekeeping genes (Figure S3B).

To evaluate the aforementioned changes at protein expression level, additional experiments were conducted using protein samples from biceps femoris, pectoral, and EDL muscles from control and AX fed animals. Similar alterations of Pdk4 protein expression as seen on RNA level were observed in all investigated muscle types, which is significantly lower in AX-treated biceps femoris and EDL samples as compared to control (Figures 2A,B and S2C,D), respectively, while the Pdk4 protein expression showed only a slight decrease in the pectoral muscle of AX mice as compared with its control counterpart (Figures 2B and S2B). Fasn protein expression was found to be significantly higher in AX-treated biceps femoris (Figures 2A and S2A); however, it was significantly lower in AX-treated EDL samples (Figure S1C), while in pectoral muscles there was no significant

difference between values from control and AX fed mice (Figures 2B and S2B). We could not detect significant alteration of Scd1 protein level in muscle samples.

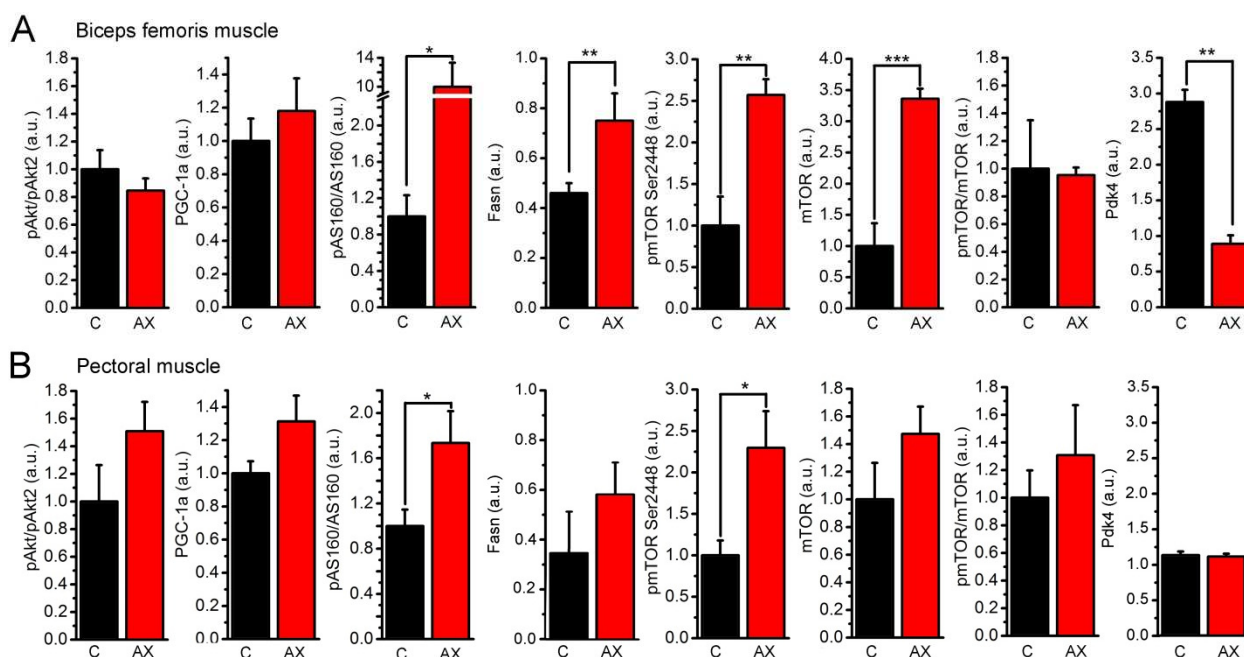


Figure 2. Effects of astaxanthin feeding on the levels of signaling proteins in biceps femoris and pectoral muscles. (A) Statistical analysis of changes in signaling protein expression of the biceps femoris muscle; (B) statistical analysis of changes in signaling protein expression of the pectoral muscles. Black columns (C): control, red columns (AX): astaxanthin feeding. Quantification of the results is reported as average \pm SEM ($n = 3-5$); * $p < 0.05$, ** $p < 0.01$, *** $p < 0.001$.

The levels and phosphorylation of proteins involved in glucose uptake, regulation of cellular energy level, protein synthesis, and cell survival were also analyzed. AX feeding increased mTOR phosphorylation (Ser2448) in biceps femoris and pectoral muscles (Figures 2A,B and S2A,B). Since the total amount of mTOR also increased, the mTOR(pSer2448)/mTOR ratio did not change significantly following AX treatment. AX feeding significantly increased pAS160/AS160 levels in both biceps femoris and pectoral muscle samples (Figures 2A,B and S2A,B). The expression of PGC-1 α was slightly increased in biceps femoris and pectoral muscle samples following AX administration (Figures 2A,B and S2A,B). Akt2 is the skeletal muscle specific isoform of Akt, and the p(Ser474)Akt2/Akt2 ratio did not change significantly in the studied samples, as only a mild elevation could be observed in pectoral muscles (Figures 2A,B and S2A,B).

In summary, our findings regarding certain changes in enzymes of the skeletal muscles point towards higher levels of metabolism as well as anti-diabetic effects exerted by AX administration.

2.3. Hypothalamic Actions of Chronic Astaxanthin Feeding

AX fed animals had an increased food intake which raised the possibility that brain structures regulating food intake might be affected. As the hypothalamic arcuate nucleus has a key role in food intake, this nucleus became the subject of the next sets of experiments. Hypothalamic slices containing the arcuate nucleus were prepared and 17 neurons were patched from control and 15 from the AX fed mice.

At first, the general changes of the excitability were checked (Figure 3A–E). There was no significant alteration of the input resistance (1065 ± 200 M Ω for control and 1163 ± 87 M Ω for fed mice, $p = 0.36$; Figure 3C). The maximal action potential firing frequency (measured as the frequency of the first two action potentials of the train elicited with 120 pA depolarization) was significantly greater (46 ± 8 Hz in control and 106 ± 18 Hz after

feeding; $p = 0.003$; Figure 3D). The average firing rate elicited by increasing depolarizing steps also showed a tendency of increase with AX feeding (11.6 ± 2.5 vs. 24.3 ± 4.4 Hz at 50 pA depolarizing step, $p = 0.01$; 13.4 ± 4 vs. 32 ± 13 Hz at 100 pA depolarizing step, $p = 0.0037$; Figure 3E).

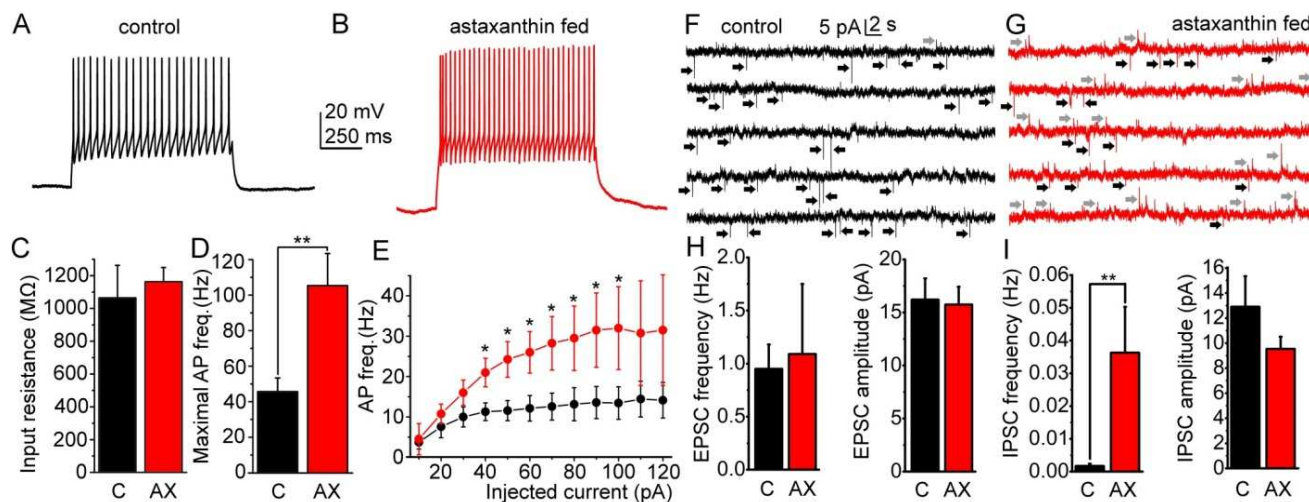


Figure 3. Effects of astaxanthin feeding on the excitability and synaptic currents of neurons in the hypothalamic arcuate nucleus. (A,B) Representative voltage traces of randomly chosen neurons of the arcuate nucleus in the control group (A, black) and in the AX fed population (B, red) elicited with 120 pA depolarizing current injection. (C–E) Statistical analysis of changes in input resistance (C), maximal action potential firing rate (D) and average action potential firing rate at different levels of depolarization (E). Black columns and graphs: control group (C), red columns, and graphs: astaxanthin fed population (AX). (F,G) Excitatory (black arrows) and inhibitory (gray arrows) postsynaptic currents (EPSCs and IPSCs, respectively) recorded from the control group (F, black) and from the AX fed group (G, red). (H,I) Statistical analysis of the EPSC frequency and amplitude (H) and the IPSC frequency and amplitude (I). Black columns: control group (C), red columns: astaxanthin fed population (AX). * $p < 0.05$, ** $p < 0.01$.

Secondly, changes of spontaneous excitatory and inhibitory postsynaptic potentials (EPSCs and IPSCs) were evaluated (Figure 3F–I). We found that AX feeding did not alter the EPSC frequency and amplitude (the frequency was 0.95 ± 0.23 Hz in control and 1.09 ± 0.66 Hz after feeding, $p = 0.41$; the amplitude was 16.24 ± 2.02 pA in control and 15.74 ± 1.67 pA after feeding, $p = 0.42$; Figure 3H). On the contrary, the IPSC frequency was very low in the control group (0.0017 ± 0.0007 Hz) which became much greater in the AX fed population (0.036 ± 0.014 ; $p = 0.003$). The IPSC amplitude did not change significantly (12.9 ± 2.4 pA in control and 9.53 ± 0.98 with AX feeding; $p = 0.099$; Figure 3I).

In summary, AX feeding led to increased excitability in neurons of the arcuate nucleus, together with an increased weight of inhibitory inputs.

2.4. Hypothalamic Effects of Acute Astaxanthin Application

In the next experiments, the acute responses to AX on different neuronal groups of the arcuate nucleus were evaluated. First, excitability and postsynaptic events of the POMC neurons ($n = 8$) were checked (Figure 4A). The input resistance, the maximal and average firing rates did not show significant differences with AX application compared to control (input resistance: 515.5 ± 59.74 MΩ in control and 667.33 ± 112.2 MΩ with AX, $p = 0.12$; maximal firing rate: 42.68 ± 9.63 Hz in control and 42.85 ± 10.69 Hz with AX, $p = 0.45$; firing rate at 50 pA depolarizing step: 9.8 ± 2.25 Hz in control and 11.5 ± 2.46 Hz with AX, $p = 0.31$; firing rate at 100 pA depolarizing step: 11.8 ± 5.18 Hz in control and 10.25 ± 4.07 Hz with AX, $p = 0.41$; Figure 4B,C). Tonic currents developed during AX application were also investigated. At -60 mV holding potential, the spontaneous fluctuation of

the holding current was -0.6 ± 1.35 pA, whereas AX application elicited -0.8 ± 1.19 pA tonic currents. Altogether the tonic current elicited by AX was not significantly different from the spontaneous fluctuation ($p = 0.46$; Figure 4D–F).

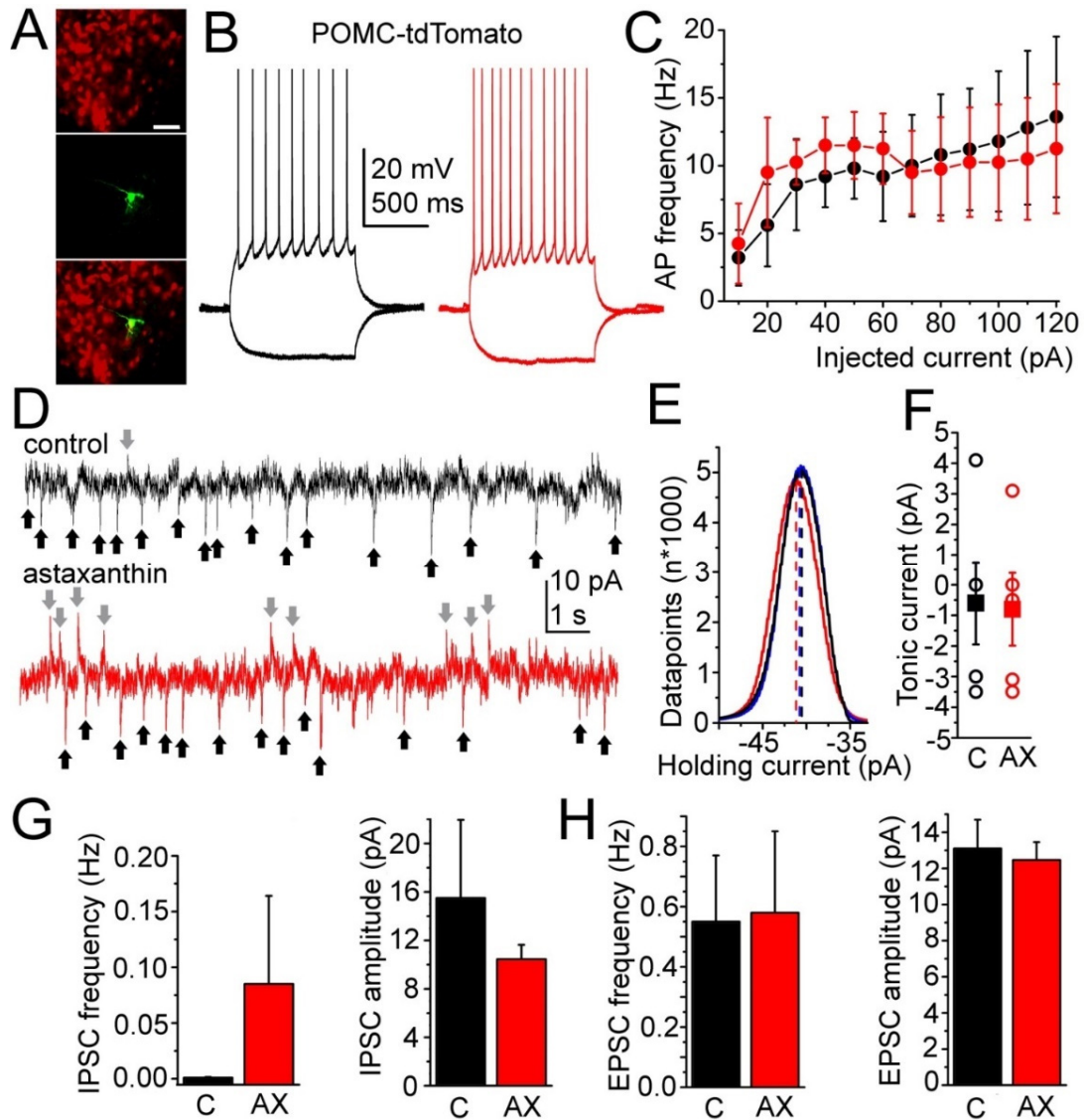


Figure 4. Changes by acute astaxanthin feeding on POMC-positive neurons of the arcuate nucleus. (A) Evaluation of the neuronal type. Upper panel: POMC-driven tdTomato expression in red. Middle panel: biocytin labeling (green). Lower panel: merged image. Images represent a single confocal z-stack with 1- μ m thickness. Scale bar: 50 μ m; (B) voltage traces from a POMC-positive neuron under control conditions (black) and with acute 2.5 μ M AX treatment (red) elicited with -30 and $+120$ pA current injections; (C) comparison of the average firing rate with different depolarizing steps under control conditions and during AX application (red); (D) synaptic currents of a POMC-positive neuron under control conditions (above) and during AX treatment (below). Black arrows: EPSCs, gray arrows: IPSCs; (E) a representative trace of histogram analysis of the holding current under control (black) and in the presence of astaxanthin (red); (F) statistical comparison of the spontaneous fluctuation of the holding current (C, black) and the effect of astaxanthin on the holding current (AX, red; hollow circles: individual data, filled squares: average \pm SEM); (G,H) statistical analysis of the IPSC (G) and EPSC (H) frequency and amplitude. Black columns: control conditions (C), red columns: astaxanthin treatment (AX).

Similar to the feeding experiments, there was no change in EPSC frequency and amplitude following acute AX application (the frequency was 0.55 ± 0.21 Hz in control and 0.58 ± 0.27 with AX, $p = 0.46$; the amplitude was 13.07 ± 1.57 pA in control and 12.46 ± 1.05 pA with AX, $p = 0.37$, Figure 4H). The IPSC frequency was increased with AX application (from 0.001 ± 0.0006 to 0.086 ± 0.079 Hz, Figure 4G). In a single case, when no IPSCs were seen in control, IPSCs occurred in AX with a frequency of 0.402 Hz; whereas a milder increase was seen in 4 other cases. The rest of the neurons ($n = 3$) lacked IPSCs in all experimental conditions. Because of this fluctuation in the strength of this effect, the difference between the two datasets was not significant ($p = 0.158$). The IPSC amplitude did not change significantly (15.55 ± 6.45 pA in control and 10.45 ± 1.19 pA with AX, $p = 0.19$; Figure 4G).

In summary, acute application of AX causes a tendency of increase in the frequency of inhibitory event on POMC neurons. In a subset of neurons, this effect might be stronger.

Following these, the acute effects of AX on the local GABAergic neurons and synapses were investigated. For this, samples expressing GCaMP6f genetically encoded calcium indicator in GABAergic neurons (see Methods) were used. In total, 22 greater regions of interest (neuronal somata) produced calcium transients. Acute application of AX increased the calcium transient frequency or elicited calcium transients in 77.3% of the regions, it did not affect the activity in 9.1% and it decreased or blocked the calcium transient activity in the rest (13.6%; Figure 5A–C). Similar to this, smaller regions of interest (likely GABAergic axon terminals) produced similar response following AX administration. From 8 regions of interest, 3 decreased or ceased calcium transient activity, whereas 5 of them had increased calcium transient activity. The average calcium transient frequency was 2.42 ± 0.78 Hz which increased to 3.73 ± 0.75 Hz with AX; showing overall a 3.27 ± 1.57 -fold increase. However, due to the decrease of calcium transient frequency in a smaller population, the calcium transient frequency was not significantly greater following acute AX treatment ($p = 0.11$; Figure 5C). Spontaneous action potential firing rate of GABAergic neurons increased from 0.57 ± 0.13 to 1.12 ± 0.24 Hz (2.55 ± 0.67 -fold increase, $p = 0.036$, $n = 10$, Figure 5D–F). Potential changes of excitatory inputs were also checked and no statistical difference was found in EPSC frequency and amplitude of GABAergic neurons (frequency in control: 0.19 ± 0.06 Hz, frequency in AX: 0.18 ± 0.05 Hz, $p = 0.44$; amplitude in control: 12.54 ± 1.45 pA, amplitude in AX: 13.12 ± 1.55 pA, $p = 0.38$, $n = 8$, Figure 5G,H). In 3 cases, the EPSC frequency had 1.62–3-fold increase, but the change in the EPSC amplitude was only 1.21– ± 0.28 -fold (Figure 5H).

Based on the data above, we hypothesize that AX directly increases the excitability of a GABAergic neuronal subpopulation in the arcuate nucleus; however, the increase in excitatory drive on certain GABAergic neurons cannot be excluded.

In conclusion, suppression on POMC neuronal population and the stimulation on GABAergic neurons are in accordance with the findings on increased food intake.

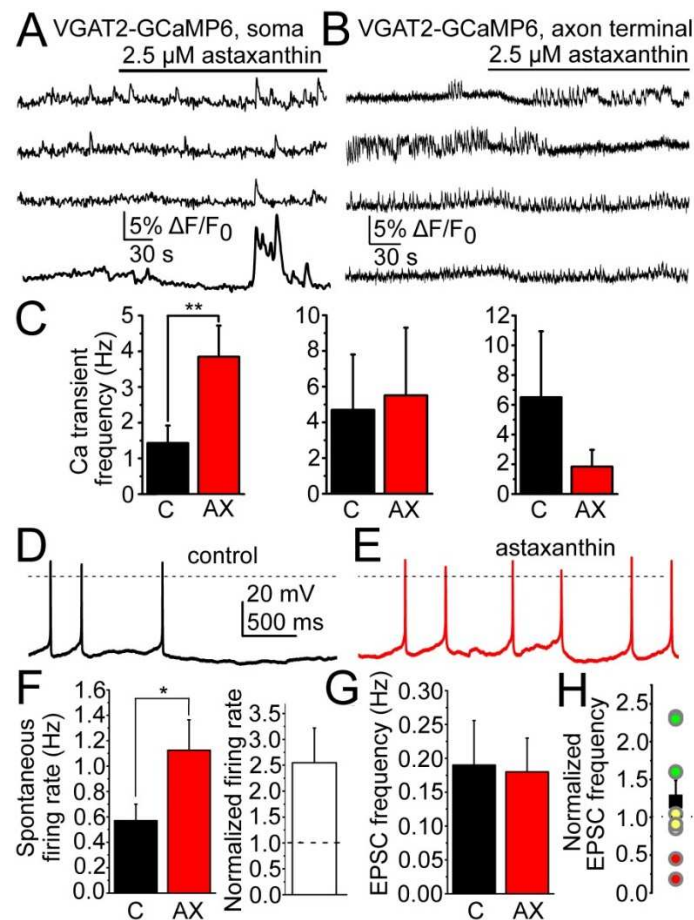


Figure 5. Changes in the excitability of the synaptic currents of the GABAergic inhibitory neurons of the arcuate nucleus. (A,B) Representative average calcium imaging traces from four GABAergic somata under control conditions and with application of 2.5 μM AX. (C) Statistical comparison of the calcium transient frequency of the GABAergic somata in control and with AX (black, C: control, red, AX) in the neuronal groups where increase, no change or decrease was seen (from left to right, respectively). Increase was seen in 77.3%, no change was observed in 9.1% and decrease was detected in 13.6% of the neuronal somata; (D,E) spontaneous activity of GABAergic neurons in control (black) and with AX (red); (F) statistical comparison of the spontaneous and normalized firing rate under control conditions and with AX (black, C: control, red, AX); (G) statistical representation of EPSC frequency in control (black, C) and with astaxanthin (red, AX); (H) average frequency change (black square) and frequency changes of the individual cases (green: increase, red: decrease, yellow: no change). * $p < 0.05$, ** $p < 0.01$.

2.5. Effects of Astaxanthin on Action Potential Configuration in Canine Left Ventricular Myocytes

We were also interested to investigate whether AX diet could potentially exert arrhythmogenic actions thus we evaluated if cardiac excitability is affected in any way by AX supplementation.

Action potentials were recorded under steady-state conditions at 700 ms cycle length. After stabilization of action potential parameters in control (containing also 0.1% ethanol) the cells were exposed to 2.5 μM AX for 4–6 min. As presented in Figure 6, the duration of action potentials was significantly reduced by AX both at 50% and 90% levels of repolarization (APD₅₀ and APD₉₀, respectively, Figure 6A,D,F). AX also significantly decreased the maximal rate of depolarization (V^{+max}) and the mid-plateau potential (measured at the time of 50% repolarization, Figure 6H,I). Other parameters, such as the resting membrane potential (-84.3 ± 0.9 vs. -83.1 ± 2.1 mV, Figure 6C), action potential

amplitude (118.8 ± 2.4 vs. 113.5 ± 4.5 mV, Figure 6E), and maximal rate of repolarization (-1.4 ± 0.1 vs. -1.4 ± 0.1 V/s, Figure 6J) were not altered significantly by AX.

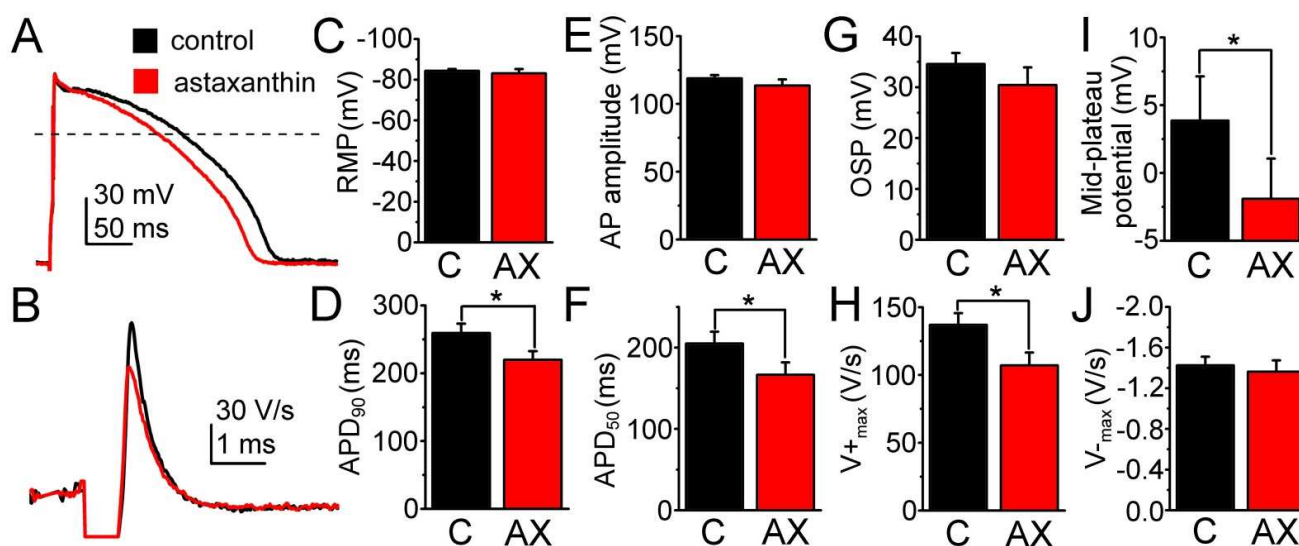


Figure 6. Effects of astaxanthin on the parameters of action potentials in canine left ventricular myocytes. (A) Representative superimposed action potentials recorded in control (black) and in the presence of 2.5 μ M astaxanthin (red). (B) First time derivative of the action potential upstroke with the same color code. (C–J) Average results obtained from 7 cells in control and in the presence of astaxanthin (black, C: control; red, AX: astaxanthin; columns and bars: mean \pm SEM; asterisks: significant differences are noted by * with $p < 0.05$).

In conclusion, acute AX administration does not seem to alter significantly cardiac excitability thus no serious risk of arrhythmias can be predicted.

3. Discussion and Conclusions

In this work, AX supplementation did not change markedly the metabolic parameters measured *in vivo*, however it facilitated food intake. As a possible reason for changes in food intake, inhibitory inputs of hypothalamic POMC neurons were strengthened. In parallel with these, carbohydrate signaling of skeletal muscle was altered which potentially increased metabolism in muscle and caused anti-diabetic effects. Kinetics of the cardiac action potentials were slightly altered but this change did not predict a greater risk for arrhythmias.

3.1. *In Vivo* Effects of Astaxanthin

We propose that AX supplemented feeding could affect the glucose metabolism and fatty acid biosynthesis in mouse skeletal muscles. The cumulative food intake increased significantly during 4 weeks of treatment in the AX group (Figure 1E). The cumulative O₂-usage and cumulative CO₂-production were not altered significantly following 4 weeks of AX supplementation (Figure 1A,C). On the other hand, the XY-movements and total activity were significantly lower in each group following 4 weeks of normal or special AX feeding. These findings could explain why AX administration would not be enough to counteract the effects of weight gain by itself (Figure 1G) due to increased food consumption. We thus propose that AX administration should be combined with adequate diet regimen and exercise to maintain a healthy body mass index.

3.2. Effects of Astaxanthin on Skeletal Muscle Metabolism

Our data suggest that AX exerts new signaling effects which can greatly influence skeletal muscle metabolism.

We detected significantly altered mRNA, and in some cases (see below) protein expression levels of Fasn, Pdk4, Scd1, and Xdh in AX supplemented muscle samples compared to the control group. Studies have shown that the increase in muscle Pdk4 activity in starvation and streptozotocin-induced diabetes were due to a selective upregulation of Pdk4 expression [31], which may largely be due to insulin deficiency rather than to increases in circulating free fatty acids (FFA) [32–34]. Data also suggest that increased Pdk4 activity in skeletal muscle might contribute to the development of insulin resistance by suppressing glucose oxidation [31]. Insulin stimulation of PI3K and/or Akt is often impaired in insulin resistant states [35,36], and this would decrease insulin's ability to regulate FOXO1 activity [37] and Pdk4 expression. Thus, increased Pdk4 expression, which would inhibit glucose oxidation, may be an important adaptive mechanism for glucose conservation [38]. Pdk4 phosphorylates and inhibits the PDH complex that catalyzes the conversion of pyruvate to acetyl-CoA. In our case, lower Pdk4 level and thereby increased PDH activity likely increased the generation of acetyl-CoA. This further elevated the synthesis of malonyl-CoA, the first molecule of fatty acid synthesis, causing increased Fasn4 production. Activation of PDH by downregulation of Pdk4 supports glucose catabolism instead of fatty acid utilization. Intracellular malonyl-CoA is an important factor in the regulation of fatty acids (FA); in healthy muscle, malonyl-CoA levels are associated with reciprocal changes in FA oxidation. Altogether, our results suggest increased glucose uptake which provides the possibility of elevated protein synthesis in skeletal muscles. Nevertheless, we recorded cumulative O₂ usage, CO₂ production, VO₂, and VCO₂ that were higher in AX animals, possibly because of their increased body weight. This explains why the normalized parameters were found to be significantly lower following AX supplemented feeding.

AS160 is a Rab GAP that regulates glucose uptake of skeletal muscle by controlling the activity of Rab GTPases. As a consequence, vesicular transport of GLUT4 from the cytosol to the plasma membrane increases which leads to increased glucose uptake. The increased phosphorylation of AS160 (pAS160) is an essential signal for the glucose uptake of skeletal muscle and adipose tissue. Earlier studies described that AX treatment increases glucose uptake in L6 myoblasts [19] or in high fat and high fructose diet-fed mice [20]. In our work, AX feeding significantly increased pAS160/AS160 levels in both biceps femoris and pectoralis muscle samples (Figures 2A,B and S2). The increased phosphorylation of AS160 can explain the beneficial effects of AX to improve insulin sensitivity. In the case of insulin resistance and type-2 diabetes mellitus the cellular amount of GLUT4 is decreased [39] and its translocation is impaired [40]; therefore, the improvement of GLUT4 translocation decreases blood glucose level. The increased pAS160/AS160 ratio following AX feeding presumably increases intracellular glucose levels and, consequently energy levels, allowing cells to improve protein synthesis and muscle mass gain. This idea is further supported by an increase in mTOR phosphorylation in the AX-fed group, since mTOR stimulates protein synthesis and inhibits autophagy [41,42]. Here, we found that AX feeding increased mTOR phosphorylation (Ser2448) in biceps femoris and pectoralis muscles (Figures 2A,B and S2). Since the total amount of mTOR also increased, the mTOR(pSer2448)/mTOR ratio did not change significantly following AX treatment.

PGC-1 α is a transcriptional coactivator important in energy metabolism and a master regulator of mitochondrial biogenesis. Moreover, PGC-1 α also increases GLUT4 levels and has multiple roles in the pathogenesis of type-2 diabetes mellitus [43,44]. In our experiments, the expression of PGC-1 α slightly increased in biceps femoris and pectoralis muscle samples following AX administration (Figures 2A,B and S2) which is in accordance with a previous work [12] where PGC-1 α was significantly elevated in skeletal muscle samples following AX intake in mice.

Although increased phosphorylation of Akt was earlier described in L6 muscle cells following AX administration [19], the p(Ser474)Akt2/Akt2 ratio did not change in our study (Figures 2A,B and S2).

3.3. Effects of Astaxanthin on Hypothalamic Neuronal Activity

The hypothalamic arcuate nucleus has a central role in food intake. Its two major neuronal types have distinct roles in appetite regulation: the anorexigenic POMC neurons decrease, whereas the orexigenic NPY- and AgRP-expressing neurons stimulate food intake [26–28]. Decreased activity of POMC cells is associated with obesity [26,29], whereas selective stimulation of them leads to weight loss [45].

GABAergic inputs to POMC neurons are capable of modulating them according to the actual energetic status of the organism [46]. POMC cells receive GABAergic inhibitory inputs from the dorsomedial hypothalamus (DMH) and the orexigenic hypothalamic AgRP neurons [26,29,47,48]. The frequency of spontaneous IPSCs onto POMC neurons increases during caloric deficits [26].

Glucose and fatty acid metabolism can affect cells of the arcuate nucleus by defining functional subgroups. There are glucose-excited and glucose-inhibited neurons reflecting changes of extracellular glucose levels in the normal range. Direct interaction was shown between glucose metabolism and fatty acid detection in regulation of neuronal activity in the arcuate nucleus. There are both oleic acid (OA) excited and oleic acid inhibited neurons, which are sensing glucose as well [49–52].

Mendoza et al. [53] investigated the effect of krill oil on restraint stress (RS) causing depressive-like behavior, memory deficiency and anxiety. Krill oil with high AX content has been shown to decrease depressive-like behavior and oxidative stress. Applying krill oil prevented appearance of depressive-like behavior and cognitive impairment by RS.

In the present work, we surprisingly found that, in contrast with oleic acid, AX did not elicit tonic changes of excitability. However, resembling conditions in hunger, an increase of sIPSC frequency on POMC neurons was seen. This increase was due to pleiotropic actions on GABAergic neurons, as the spontaneous firing rate was increased, probably partially caused by the strengthening of excitatory inputs in some cases. As inhibition of POMC neurons increases feeding, the increase of GABAergic activity might contribute to the increased food consumption seen with chronic AX supplementation. Although coronal slices contained the main sources of GABAergic inputs of the POMC neurons, the arcuate nucleus and the DMH, actions on the IPSCs were probably underestimated, as certain synaptic connections were lost in brain slices.

3.4. Effects of Astaxanthin on Cardiac Excitability

According to our knowledge cellular electrophysiological effects of AX in mammalian cardiac tissues were not reported yet. In present study, we used canine ventricular myocytes as their electrical properties greatly resemble those of the human myocardium [54,55]. Furthermore, canine heart is believed to be a good model to study the cardioprotective effects of AX [56]. Acute AX treatment shortened the action potential, depressed the plateau potential and reduced depolarization velocity (Figure 6A,I,H). These changes are congruent with a mild inhibition of inward currents (such as the L-type Ca^{2+} and Na^{+} currents) by AX. A reduction in Ca^{2+} entry may also contribute to the well documented cardioprotective effect of AX [57], presently attributed to decreasing the consequences of oxidative stress by supporting the function of the mitochondria [15,58,59]. Since the resting potential and the maximal rate of repolarization remained unchanged, AX seems to leave the inward rectifier K^{+} current unaffected (Figure 6C,J). However, further detailed studies are required to elucidate the exact molecular mechanisms of the cardiac electrophysiological effects of AX.

In conclusion, we propose that AX exerts complex effects on whole body metabolism (Figure 7). It affects food intake via hypothalamic regulatory centers of energy homeostasis, as well as via increased metabolism and anti-diabetic actions by direct effects on the target organs of mice; without presenting serious risks for cardiac arrhythmias on a canine model. Our results support the idea that AX, this widely used nutraceutical, is a potent candidate for treatment of diseases of energy homeostasis; however, one must acknowledge that

solely its administration will not replace a healthy diet and lifestyle but rather will be best achieved in conjunction with them.

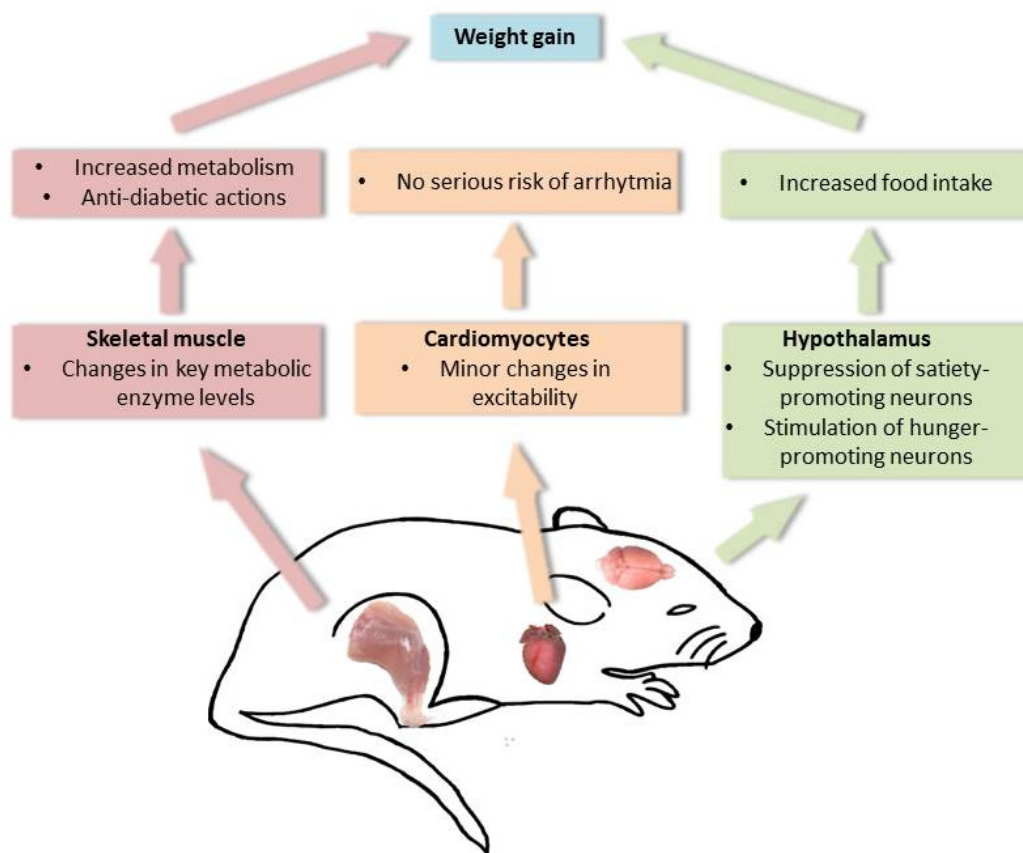


Figure 7. Proposed mode of action of AX in mice. Summary of our findings on the responses by AX on skeletal muscle metabolism, cardiac excitability and hypothalamic neuronal activity that could lead potentially to weight gain. AX facilitates the increase in metabolism and exerts anti-diabetic actions on skeletal muscle, promotes food intake via actions on the hypothalamus, and exerts minor changes on cardiac excitability.

4. Materials and Methods

4.1. Animals

Animal experiments were conducted in accordance with the appropriate national and international (EU Directive 2010/63/EU for animal experiments) institutional guidelines and laws on the care of research animals. Experimental protocols were approved by the Committee of Animal Research of the University of Debrecen (3-1/2019/DEMÁB).

Young adult (3-months-old) wild-type mice C57BL6 ($n = 16$) were used for chronic, 4-week-long AX feeding experiments (8 were fed with AX supplemented chow and 8 were fed normal rodent chow). The special chow was prepared with the addition of 4 g/kg of AstaReal A1010 (dissolved in 100% ethanol) to the standard rodent pellet (protein 20%, carbohydrates 70%, fats 4%, fibers 5%, vitamins, micro- and macronutrients) for a final concentration of 0.02% AX. This concentration was chosen according to the literature [13,15]. The mice had ad libitum access to water and food intake. Room illumination was set automatically to cycles of 12-h dark and 12-h light.

For acute experiments, mice expressing the tdTomato fluorescent protein in a pro-opiomelanocortin (POMC)- or glutamate decarboxylase type 2 (GAD2)-dependent way ($n = 8$ for both groups), as well as mice expressing GCaMP6f genetically encoded calcium indicator in a type 2 vesicular gamma-aminobutyric acid transporter (VGAT2) dependent way were used ($n = 3$) from both sexes. Homozygous floxed-stop tdTomato

(B6;129S6-Gt(ROSA)26Sortm9(CAG-tdTomato)Hze/J; JAX mice accession number 007905) and GAD2-cre lines (STOCK Gad2tm2(cre)Zjh/J; JAX number: 010802), as well as the heterozygous POMC-cre line (STOCK Tg(Pomc1-cre)16Low1/J; JAX number: 005965M) were purchased from Jackson Laboratories (Bar Harbor, ME, USA) and were crossed in the animal house of the Department of Physiology. Homozygous floxed-stop GCaMP6f (B6;129S-Gt(ROSA)26Sortm95.1(CAG-GCaMP6f)Hze/J; JAX number: 024105) and VGAT2-cre mice (STOCK Slc32a1tm2(cre)Low1/J; JAX number: 016962) were also purchased from Jackson Laboratories and crossed in the animal house of the Department of Anatomy. VGAT2-GCaMP6 mice were generously provided by Dr. Péter Szücs (Department of Anatomy, University of Debrecen).

Adult mongrel dogs of either sex were anaesthetized with intramuscular injections of 10 mg/kg ketamine hydrochloride (Calypsol, Richter Gedeon, Budapest, Hungary) and 1 mg/kg xylazine hydrochloride (Sedaxylan, Eurovet Animal Health BV, Bladel, The Netherlands) according to protocols approved by the local ethical committee (9/2015/DEMÁB) in line with the ethical standards laid down in the Declaration of Helsinki.

4.2. Metabolic Cage Experiments

A Comprehensive Lab Animal Monitoring System (CLAMS) was used to monitor the metabolism of 8 control and 8 AX-treated mice. Three-month-old animals were selected for the experiments and were divided into 4 groups. As the monitoring system could measure 8 animals at the same time, 4–4 mice were measured for control and AX group, then the remaining 4–4 animals were put into the special cages. During 48 h of continuous monitoring, several parameters (food and water intake, calorimetry data, activity of the animals, and sleeping time) were followed where total or accelerated (cumulative) data were given for the whole measuring period or for 12 h of dark and light daily periods.

Animal activity was recorded with an array of infrared photo beams that surround the cage. When the animal moved, the beams were interrupted, generating one count. Since the beams were arranged in a grid pattern, the XY position of the animal could be continuously recorded (X_{amb}). When equipped with the Z axis sensor, total movements could be determined (X_{total}). Bouts of inactivity of certain duration were scored in an event file as sleeping events.

The system collected calorimetry parameters: VO_2 , VCO_2 , RER, and heat production. The calculation of oxygen consumption (VO_2) and carbon dioxide production (VCO_2) values required the use of both the input (V_i) and output (V_o) flows to the chamber. The respiratory exchange ratio (RER) can be calculated from either set of consumption and production rates ($RER = VCO_2 / VO_2$). Calorific value (CV) was calculated from RER using the following equation: $CV = 3.815 \times 1.232 \times RER$. Total energy expenditure (TEE) was calculated by multiplying CV and VO_2 . As this parameter contains resting/basal metabolic rate and activity related energy expenditure, resting metabolic rate was determined by averaging the ten minima values of energy expenditure within the 48-h measurement. RMR was subtracted from TEE giving the TEE activity values.

4.3. Metabolic Pathways Panel

Functional annotations for different pathways and processes were assigned to the genes in the nCounter Metabolic Pathways Panel (Nanostring, Fairview, WA, USA). The pathways and processes that are included in this panel provide a comprehensive view of cell metabolism. Exact genes regarding the different metabolic pathways can be found at the website of Nanostring company.

Total RNA samples were prepared from m. extensor digitorum longus (EDL) of 6 control and 6 AX-treated mice following 4 weeks of special feeding. The samples were subjected to RNA isolation using Trizol reagent (Sigma–Aldrich, St. Louis, MO, USA). The concentration of the samples was determined by the Nanodrop2000 spectrophotometer (ThermoFisher Scientific, Waltham, MA, USA). Samples were loaded into the specific metabolic panel and the appropriate reaction was carried out. Data were first analyzed

using the nSolver program, where all data from the metabolic program measurement were normalized to 12 different housekeeping genes and the threshold suggested by Nanostring was determined from these results. Significant differences between control and AX-treated samples were determined by giving the fold change ratio of the appropriate genes. BRB array tool analysis was used to further improve the quality of the measurement and to ensure the assessment of significant changes of certain genes.

4.4. Protein Isolation and Western Blotting

EDL, biceps femoris, and pectoralis muscles of control and AX-fed mice were homogenized in buffer containing 50 mM of Tris-HCl pH 7.6, 100 mM of NaCl, 10 mM of EDTA, 1 mM of NaF, 1 mM of Na_3VO_4 , and protease inhibitor cocktail (Sigma–Aldrich, St. Louis, MO, USA). After centrifugation of the samples at $16,000\times g$ for 10 min at 4 °C to eliminate cellular debris, the protein concentration of the supernatants was measured using BCA Protein Assay Kit (Thermo Fisher Scientific, Waltham, MA, USA). The samples (25 μg /lane) were separated by SDS/PAGE, and blotted to Protran nitrocellulose membrane (Amersham, GE Healthcare, Little Chalfont, UK). After blocking, membranes were overnight incubated with rabbit anti-phospho(Ser2448)-mTOR (#5536), mTOR (#2983), phospho(Thr642)-AS160 (#8881), AS160 (#2670), PGC-1 α (#2178), phospho(Ser474)-Akt2 (#8599), Akt2 (#3063), or mouse anti-GAPDH (#2118) primary antibodies, all from Cell Signaling Technology (Danvers, MA, USA). This was followed by incubation with the appropriate horse-radish peroxidase-conjugated anti-IgG secondary antibodies from DAKO (Glostrup, Denmark). In other experiments membranes were incubated with mouse anti-FASN, mouse anti-SCD1, and rabbit anti-PDK4 primary antibodies (all from Novus Biologicals, Abingdon, UK), followed by incubation with appropriate HRP-conjugated secondary antibodies (Bio-Rad, Hercules, CA, USA). Peroxidase activity was visualized by the enhanced chemiluminescent procedure (Advansta, San Jose, CA, USA; and Thermo Fisher, Waltham, MA, USA). Quantification of signal intensity was performed by Quantity One software (Bio-Rad, Hercules, CA, USA) and ImageJ (NIH, Bethesda, MD, USA).

4.5. Acute Hypothalamic Slice Preparation

The recording solution for experiments on the hypothalamus was an artificial cerebrospinal fluid (aCSF) with the following composition (in mM): NaCl, 120; KCl, 2.5; NaHCO_3 , 26; glucose, 10; NaH_2PO_4 , 1.25; CaCl_2 , 2; MgCl_2 , 1; myo-inositol, 3; ascorbic acid, 0.5; and sodium-pyruvate, 2; pH 7.2. In the solution used for preparation (low Na aCSF), 95 mM of NaCl was replaced by glycerol (60 mM) and sucrose (130 mM). All chemicals were purchased from Sigma (St. Louis, MO, USA) unless stated otherwise.

After decapitation of the animal and removal of the brain, 200- μm -thick coronal slices were prepared from the area including the hypothalamus in ice-cold low Na aCSF with a Microm HM 650V vibratome (Microm International GmbH, Walldorf, Germany). Prior to recording, the slices were incubated in normal aCSF for 60 min at 37 °C.

4.6. Isolation of Canine Ventricular Myocytes

Single myocytes were obtained by enzymatic dispersion using the segment perfusion technique. Briefly, the heart was quickly removed and washed in a cold Tyrode's solution. Left anterior descending coronary artery was cannulated, then a wedge-shaped section of the ventricular wall supplied by the artery was dissected and perfused with a nominally Ca^{2+} -free Joklik solution (Minimum Essential Medium Eagle, Joklik Modification, Sigma–Aldrich Co., St. Louis, MO, USA, product no. M0518) for 5 min. This was followed by perfusion with Joklik solution supplemented with 1 mg/mL collagenase (Type II, Worthington Biochemical Co., Lakewood, NJ, USA) and 0.2% bovine serum albumin (Fraction V., Sigma) containing 50 μM Ca^{2+} for 30 min. After this, normal external Ca^{2+} concentration was gradually restored, and cells were kept in Minimum Essential Medium Eagle (Sigma–Aldrich Co., product no. M0643) until use.

4.7. Electrophysiology

Hypothalamic coronal slices were visualized with a Zeiss Axioscope microscope (Carl Zeiss AG, Oberkochen, Germany). Patch pipettes with 6–7-M Ω pipette resistance were pulled, and filled with internal solution composed of (in mM): K-gluconate, 120; NaCl, 5; 4-(2-hydroxyethyl)-1-piperazineethanesulfonic acid (HEPES), 10; EGTA, 2; CaCl₂, 0.1; Mg-ATP, 5; Na₃-GTP, 0.3; Na₂-phosphocreatine, 10; biocytin, 8; pH 7.3. Whole-cell patch-clamp recordings were performed using an Axopatch 200A amplifier (Molecular Devices, Union City, CA, USA). Data acquisition was achieved by Clampex 10.0 software (Molecular Devices, Union City, CA, USA), while data analysis was performed using Clampfit 10.0 (Molecular Devices) and MiniAnalysis (Synaptosoft, Decatur, GA, USA) software. During recording, slices were kept in oxygenated nACSF at room temperature. For testing acute effects of AX, 2.5 μ M AX was dissolved in nACSF with 0.1% ethanol. In preliminary experiments on spontaneous EPSCs and IPSCs, the action of aCSF with 0.1% ethanol was compared with ethanol-free nACSF and no significant changes were found.

For recording action potential trains, a current clamp protocol with 1-s-long depolarizing steps was employed from -30 to $+120$ pA with 10 pA increments. The resting membrane potential was set to -60 mV. Recordings of spontaneous firing rates was done in current clamp mode. The neurons were kept on their own resting membrane potential and no current injection was administered. Fifty-second-long traces were evaluated with each neuron and condition.

For tonic currents and spontaneous EPSCs and IPSCs, gap-free voltage-clamp traces were recorded at a holding potential of -60 mV before and after drug application (10 min in each condition). Tonic currents were assessed by making histograms of the recorded current values from the last minute of the trace; and the current values at the histogram peaks were considered as the amplitude of the tonic current. Spontaneous changes of the holding current were calculated as the difference between the first and the last minute of the control recording. At the end of the experiment, slices were continuously perfused with 10 μ M of 2,3-dihydroxy-6-nitro-7-sulfamoyl-benzo[f]quinoxaline-2,3-dione (NBQX), 50 μ M of D-2-amino-5-phosphonopentanoate (D-AP5), 1 μ M of strychnine, and 10 μ M of bicuculline (Tocris Cookson Ltd., Bristol, UK).

Cardiac action potentials were recorded at 37 °C, maintained by an electronic temperature controller (Cell MicroControls, Norfolk, VA, USA). The rod-shaped viable cells showing clear striation were sedimented in a plexiglass chamber of 1-mL volume allowing continuous superfusion (at a rate of 2 mL/min) with Tyrode's solution. The Tyrode solution contained (in mM): NaCl, 121; KCl, 4; MgCl₂, 1; CaCl₂, 1.3; HEPES, 10; glucose, 10; NaHCO₃, 25; at pH = 7.3. Membrane voltage was recorded using 3 M of KCl filled sharp glass microelectrodes having tip resistance between 20 and 40 M Ω . These electrodes were connected to the input of an Axoclamp 2B, Multiclamp 700A or 700B amplifiers (Molecular Devices, Sunnyvale, CA, USA). The cells were paced through the recording electrode at steady cycle length of 0.7 s using 1–2 ms wide rectangular current pulses having amplitudes of 120% diastolic threshold. Action potentials were digitized (at 50 kHz using Digidata 1322A or 1440A A/D card, Molecular Devices, Sunnyvale, CA, USA) and stored for later analysis. Cells were exposed to 2.5 μ M of AX for 4–6 min (dissolved in ethanol yielding a final ethanol concentration of 0.1%). Control solution also contained this concentration of ethanol.

4.8. Calcium Imaging

Calcium imaging experiments were performed on slices from VGAT2-GCaMP6 mice. Slices were prepared similarly as for electrophysiology experiments. A Zeiss Axioscope microscope (Carl Zeiss AG) equipped with a fluorescent imaging system (Till Photonics GmbH, Gräfeling, Germany) containing a xenon bulb-based Polychrome V light source, a CCD camera (SensiCam, PCO AG, Kelheim, Germany), an imaging control unit (ICU), and the Till Vision software (version 4.0.1.3) were used. The fluorescent filter set contained an emission filter (LP 515, Till Photonics) and a dichroic mirror (Omega XF2031 505DRLPXR;

Omega Drive, Brattleboro, VT, USA). Frames with 344×260 -pixel resolution were taken with a frame rate of 10 Hz.

4.9. Post Hoc Identification of the Labeled Neurons

During recording, neurons were labelled with biocytin. Slices with the filled neurons were fixed overnight (4% paraformaldehyde in 0.1 M of phosphate buffer; pH = 7.4; 4 °C). For permeabilization, Tris buffered saline (in mM, Tris base, 8; Trisma HCl, 42; NaCl, 150; pH = 7.4) with 0.1% Triton X-100 and 10% bovine serum was used for 60 min. Incubation was performed in phosphate buffer supplemented with streptavidin-conjugated Alexa488 (1:300; Molecular Probes Inc., Eugene, OR, USA) for 90 min. The cells were visualized with a Zeiss LSM 510 confocal microscope (Carl Zeiss AG).

4.10. Statistics

Results are expressed as mean \pm SEM values. GraphPad Prism 7.0 (GraphPad Software Inc., San Diego, CA, USA) was used for graphing and statistical analyses. Statistical significance of differences was evaluated using Student's *t*-test. Differences were considered significant when *p* was less than 0.05.

Supplementary Materials: The following supporting information can be downloaded at: <https://www.mdpi.com/article/10.3390/ijms23020917/s1>.

Author Contributions: Research on metabolism and body weight was performed by L.S., J.F., M.G. and M.S. Research on signaling molecules of the skeletal muscle was performed by L.S., M.G., K.S., A.K.-P. and Z.M.K. Experiments with AX on hypothalamus were done by A.C., K.P. and B.P.; whereas research on cardiomyocytes was performed by N.S., P.N., L.S., J.F., Z.M.K., A.C., K.P., M.G., M.S. and N.S. performed the experiments and analysed the results, whereas M.G., M.S., B.P., A.K.-P., N.S., P.N. and L.C. designed the experiments and wrote the manuscript. All authors have read and agreed to the published version of the manuscript.

Funding: This research was supported by the National Research, Development and Innovation Office of Hungary (grant numbers: GINOP-2.3.2-15-2016-00040 (MYOTeam), GINOP-2.3.3.15-2016-00020, NKFI FK 134684 (A.K.-P), NKFIH PD-128370 (M.S.), NKFIH-K115397 (P.N.), NKFIH-K138090 (N.S.)) and the János Bolyai Research Scholarship of the Hungarian Academy of Sciences (to A.K.-P.). This work was also supported by the project EFOP-3.6.3-VEKOP-16-2017-00009 (M.S.) and EFOP-3.6.2-16-2017-00006 (P.N.). Project no. TKP2020-IKA-04 was implemented with the support provided from the National Research, Development and Innovation Fund of Hungary, financed under the 2020-4.1.1-TKP2020 funding scheme. Support was also obtained from the Thematic Excellence Program of the Ministry for Innovation and Technology in Hungary (TKP-2020-NKA-04), within the framework of the Space Sciences thematic program of the University of Debrecen.

Institutional Review Board Statement: Animal experiments were conducted in accordance with the appropriate national and international (EU Directive 2010/63/EU for animal experiments) institutional guidelines and laws on the care of research animals. Experimental protocols were approved by the Committee of Animal Research of the University of Debrecen (3-1/2019/DEMÁB and 9/2015/DEMÁB).

Informed Consent Statement: Not applicable.

Data Availability Statement: Data will be made available on reasonable request.

Acknowledgments: The authors are indebted to Éva Sági and Tamara Lövei for their excellent technical assistance. We are grateful to AstaReal Co., Ltd., (Nacka, Sweden) for providing astaxanthin (AstaReal A1010) for research purposes.

Conflicts of Interest: The authors declare no conflict of interest.

References

1. Nakao, R.; Nelson, O.L.; Park, J.S.; Mathison, B.D.; Thompson, P.A.; Chew, B.P. Effect of astaxanthin supplementation on inflammation and cardiac function in BALB/c mice. *Anticancer Res.* **2010**, *30*, 2721–2725.
2. Ambati, R.R.; Phang, S.M.; Ravi, S.; Aswathanarayana, R.G. Astaxanthin: Sources, extraction, stability, biological activities and its commercial applications—A review. *Mar. Drugs* **2014**, *12*, 128–152. [[CrossRef](#)] [[PubMed](#)]
3. Baralic Andjelkovic, M.; Djordjevic, B.; Dikic, N.; Radivojevic, N.; Suzin-Zivkovic, V.; Radojevic-Skodric, S.; Pejic, S. Effect of astaxanthin supplementation on salivary IgA, oxidative stress, and inflammation in young soccer players. *Evid. -Based Complement. Altern. Med.* **2015**, *2015*, 783761. [[CrossRef](#)]
4. Hu, J.; Nagarajan, D.; Zhang, Q.; Chang, J.S.; Lee, D.J. Heterotrophic cultivation of microalgae for pigment production: A review. *Biotechnol. Adv.* **2017**, *36*, 54–67. [[CrossRef](#)] [[PubMed](#)]
5. Sztretye, M.; Dienes, B.; Gönczi, M.; Czirják, T.; Csernoch, L.; Dux, L.; Szentesi, P.; Keller-Pintér, A. Astaxanthin: A potential mitochondrial-targeted antioxidant treatment in diseases and with aging. *Oxid. Med. Cell. Longev.* **2019**, *2019*, 3849692. [[CrossRef](#)]
6. Pereira, C.P.M.; Souza, A.C.R.; Vasconcelos, A.R.; Prado, P.S.; Name, J.J. Antioxidant and anti-inflammatory mechanisms of action of astaxanthin in cardiovascular diseases. *Int. J. Mol. Med.* **2021**, *47*, 37–48. [[CrossRef](#)]
7. Miyawaki, H.; Takahashi, J.; Tsukahara, H.; Takehara, I. Effects of astaxanthin on human blood rheology. *J. Clin. Biochem. Nutr.* **2008**, *43*, 69–74. [[CrossRef](#)] [[PubMed](#)]
8. Galasso, C.; Orefice, I.; Pellone, P.; Cirino, P.; Miele, R.; Ianora, A.; Brunet, C.; Sansone, C. On the neuroprotective role of astaxanthin: New perspectives? *Mar. Drugs* **2018**, *16*, 247. [[CrossRef](#)] [[PubMed](#)]
9. Al-Amin, M.M.; Akhter, S.; Hasan, A.T.; Alam, T.; Hasan, S.N.; Saifullah, A.; Shohel, M. The antioxidant effect of astaxanthin is higher in young mice than aged: A region specific study on brain. *Metab. Brain Dis.* **2015**, *30*, 1237–1246. [[CrossRef](#)] [[PubMed](#)]
10. Chang, M.X.; Xiong, F. Astaxanthin and its effects in inflammatory responses and inflammation-associated diseases: Recent advances and future directions. *Molecules* **2020**, *25*, 5342. [[CrossRef](#)] [[PubMed](#)]
11. Bhuvanewari, S.; Arunkumar, E.; Viswanathan, P.; Anuradha, C.V. Astaxanthin restricts weight gain, promotes insulin sensitivity and curtails fatty liver disease in mice fed a obesity-promoting diet. *Process. Biochem.* **2010**, *45*, 1406–1414. [[CrossRef](#)]
12. Liu, P.H.; Aoi, W.; Takami, M.; Terajima, H.; Tanimura, Y.; Naito, Y.; Itoh, Y.; Yoshikawa, T. The astaxanthin-induced improvement in lipid metabolism during exercise is mediated by a PGC-1 α increase in skeletal muscle. *J. Clin. Biochem. Nutr.* **2014**, *54*, 86–89. [[CrossRef](#)] [[PubMed](#)]
13. Aoi, W.; Naito, Y.; Takanami, Y.; Ishii, T.; Kawai, Y.; Akagiri, S.; Kato, Y.; Osawa, T.; Yoshikawa, T. Astaxanthin improves muscle lipid metabolism in exercise via inhibitory effect of oxidative CPT I modification. *Biochem. Biophys. Res. Commun.* **2008**, *366*, 892–897. [[CrossRef](#)] [[PubMed](#)]
14. Aoi, W.; Naito, Y.; Yoshikawa, T. Potential role of oxidative protein modification in energy metabolism in exercise. In *Lipid Hydroperoxide-Derived Modification of Biomolecules. Subcellular Biochemistry*; Springer: Dordrecht, The Netherlands, 2014; Volume 77, pp. 175–187. [[CrossRef](#)]
15. Sztretye, M.; Singlár, Z.; Szabó, L.; Angyal, Á.; Balogh, N.; Vakilzadeh, F.; Szentesi, P.; Dienes, B.; Csernoch, L. Improved tetanic force and mitochondrial calcium homeostasis by astaxanthin treatment in mouse skeletal muscle. *Antioxidants* **2020**, *9*, 98. [[CrossRef](#)]
16. Acosta-Jaquez, H.A.; Keller, J.A.; Foster, K.G.; Ekim, B.; Soliman, G.A.; Feener, E.P.; Ballif, B.A.; Fingar, D.C. Site-specific mTOR phosphorylation promotes mTORC1-mediated signaling and cell growth. *Mol. Cell Biol.* **2009**, *29*, 4308–4324. [[CrossRef](#)] [[PubMed](#)]
17. Melick, C.H.; Jewell, J.L. Regulation of mTORC1 by upstream stimuli. *Genes* **2020**, *11*, 989. [[CrossRef](#)] [[PubMed](#)]
18. Ishikura, S.; Bilan, P.J.; Klip, A. Rabs 8A and 14 are targets of the insulin-regulated Rab-GAP AS160 regulating GLUT4 traffic in muscle cells. *Biochem. Biophys. Res. Commun.* **2007**, *353*, 1074–1079. [[CrossRef](#)]
19. Ishiki, M.; Nishida, Y.; Ishibashi, H.; Wada, T.; Fujisaka, S.; Takikawa, A.; Urakaze, M.; Sasaoka, T.; Usui, I.; Tobe, K. Impact of divergent effects of astaxanthin on insulin signaling in L6 cells. *Endocrinology* **2013**, *154*, 2600–2612. [[CrossRef](#)] [[PubMed](#)]
20. Arunkumar, E.; Bhuvanewari, S.; Anuradha, C.V. An intervention study in obese mice with astaxanthin, a marine carotenoid—effects on insulin signaling and pro-inflammatory cytokines. *Food Funct.* **2012**, *3*, 120–126. [[CrossRef](#)]
21. Gudi, R.; Bowker-Kinley, M.M.; Kedishvili, N.Y.; Zhao, Y.; Popov, K.M. Diversity of the pyruvate dehydrogenase kinase gene family in humans. *J. Biol. Chem.* **1995**, *270*, 28989–28994. [[CrossRef](#)]
22. Rowles, J.; Scherer, S.W.; Xi, T.; Majer, M.; Nickle, D.C.; Rommens, J.M.; Popov, K.M.; Harris, R.A.; Riebow, N.L.; Xia, J.; et al. Cloning and characterization of PDK4 on 7q21.3 encoding a fourth pyruvate dehydrogenase kinase isoenzyme in human. *J. Biol. Chem.* **1996**, *271*, 22376–22382. [[CrossRef](#)]
23. Pender, C.; Trentadue, A.R.; Pories, W.J.; Dohm, G.L.; Houmard, J.A.; Youngren, J.F. Expression of genes regulating malonyl-CoA in human skeletal muscle. *J. Cell Biochem.* **2006**, *99*, 860–867. [[CrossRef](#)] [[PubMed](#)]
24. Lodhi, I.J.; Wei, X.; Semenkovich, C.F. Lipoexpediency: De novo lipogenesis as a metabolic signal transmitter. *Trends Endocrinol. Metab.* **2011**, *22*, 1–8. [[CrossRef](#)]
25. Chakravarthy, M.V.; Lodhi, I.J.; Yin, L.; Malapaka, R.R.; Xu, H.E.; Turk, J.; Semenkovich, C.F. Identification of a physiologically relevant endogenous ligand for PPAR α in liver. *Cell* **2009**, *138*, 476–488. [[CrossRef](#)]
26. Rau, A.R.; Hentges, S.T. GABAergic inputs to POMC neurons originating from the dorsomedial hypothalamus are regulated by energy state. *J. Neurosci.* **2019**, *39*, 6449–6459. [[CrossRef](#)] [[PubMed](#)]

27. Jeong, J.H.; Lee, D.K.; Jo, Y.H. Cholinergic neurons in the dorsomedial hypothalamus regulate food intake. *Mol. Metab.* **2017**, *6*, 306–312. [[CrossRef](#)]
28. Joly-Amado, A.; Cansell, C.; Denis, R.G.P.; Delbes, A.S.; Castel, J.; Martinez, S.; Luquet, S. The hypothalamic arcuate nucleus and the control of peripheral substrates. *Best Pract. Res. Clin. Endocrinol. Metab.* **2014**, *28*, 725–737. [[CrossRef](#)] [[PubMed](#)]
29. Atasoy, D.; Betley, J.N.; Su, H.H.; Sternson, S.M. Deconstruction of a neural circuit for hunger. *Nature* **2012**, *488*, 172–177. [[CrossRef](#)]
30. Aoi, W.; Naito, Y.; Sakuma, K.; Kuchide, M.; Tokuda, H.; Maoka, T.; Toyokuni, S.; Oka, S.; Yasuhara, M.; Yoshikawa, T. Astaxanthin limits exercise-induced skeletal and cardiac muscle damage in mice. *Antioxid. Redox Signal.* **2003**, *5*, 139–144. [[CrossRef](#)] [[PubMed](#)]
31. Wu, P.; Sato, J.; Zhao, Y.; Jaskiewicz, J.; Popov, K.M.; Harris, R.A. Starvation and diabetes increase the amount of pyruvate dehydrogenase kinase isoenzyme 4 in rat heart. *Biochem. J.* **1998**, *329*, 197–201. [[CrossRef](#)]
32. Randle, P.J.; Priestman, D.A.; Mistry, S.; Halsall, A. Mechanisms modifying glucose oxidation in diabetes mellitus. *Diabetologia* **1994**, *37* (Suppl. 2), S155–S161. [[CrossRef](#)] [[PubMed](#)]
33. Sugden, M.C.; Bulmer, K.; Holness, M.J. Fuel-sensing mechanisms integrating lipid and carbohydrate utilization. *Biochem. Soc. Trans.* **2001**, *29*, 272–278. [[CrossRef](#)] [[PubMed](#)]
34. Lee, F.N.; Zhang, L.; Zheng, D.; Choi, W.S.; Youn, J.H. Insulin suppresses PDK-4 expression in skeletal muscle independently of plasma FFA. *Am. J. Physiol. Endocrinol. Metab.* **2004**, *287*, E69–E74. [[CrossRef](#)] [[PubMed](#)]
35. Folli, F.; Saad, M.J.; Backer, J.M.; Kahn, C.R. Regulation of phosphatidylinositol 3-kinase activity in liver and muscle of animal models of insulin-resistant and insulin-deficient diabetes mellitus. *J. Clin. Investig.* **1993**, *92*, 1787–1794. [[CrossRef](#)] [[PubMed](#)]
36. Brozinick, J.T., Jr.; Roberts, B.R.; Dohm, G.L. Defective signaling through Akt-2 and -3 but not Akt-1 in insulin-resistant human skeletal muscle: Potential role in insulin resistance. *Diabetes* **2003**, *52*, 935–941. [[CrossRef](#)] [[PubMed](#)]
37. Brunet, A.; Bonni, A.; Zigmond, M.J.; Lin, M.Z.; Juo, P.; Hu, L.S.; Anderson, M.J.; Arden, K.C.; Blenis, J.; Greenberg, M.E. Akt promotes cell survival by phosphorylating and inhibiting a forkhead transcription factor. *Cell* **1999**, *96*, 857–868. [[CrossRef](#)]
38. Sugden, M.C.; Honess, M.J. Recent advances in mechanisms regulating glucose oxidation at the level of the pyruvate dehydrogenase complex by PDKs. *Am. J. Physiol. Endocrinol. Metab.* **2003**, *284*, E855–E862. [[CrossRef](#)]
39. Schreiber, I.; Dörpholz, G.; Ott, C.E.; Kragesteen, B.; Schanze, N.; Lee, C.T.; Köhrle, J.; Mundlos, S.; Ruschke, K.; Knaus, P. BMPs as new insulin sensitizers: Enhanced glucose uptake in mature 3T3-L1 adipocytes via PPAR γ and GLUT4 upregulation. *Sci. Rep.* **2017**, *7*, 17192. [[CrossRef](#)]
40. Jaldin-Fincati, R.; Pavarotti, M.; Frendo-Cumbo, S.; Bilan, P.J.; Klip, A. Update on GLUT4 vesicle traffic: A cornerstone of insulin action. *Trends Endocrinol. Metab.* **2017**, *28*, 597–611. [[CrossRef](#)]
41. Feng, Z.; Yao, D.; Klionsky, J. How to control self-digestion: Transcriptional, post-transcriptional, and post-translational regulation of autophagy. *Trends Cell Biol.* **2015**, *25*, 354–363. [[CrossRef](#)]
42. Ma, X.M.; Blenis, J. Molecular mechanisms of mTOR-mediated translational control. *Nat. Rev. Mol. Cell Biol.* **2009**, *10*, 307–318. [[CrossRef](#)] [[PubMed](#)]
43. Soyak, S.; Krempler, H.; Oberkofler, H.; Patsch, W. PGC-1 α : A potent transcriptional cofactor involved in the pathogenesis of type 2 diabetes. *Diabetologia* **2006**, *49*, 1477–1488. [[CrossRef](#)] [[PubMed](#)]
44. Ruegsegger, G.N.; Creo, A.L.; Cortes, T.M.; Dasari, S.; Nair, K.S. Altered mitochondrial function in insulin-deficient and insulin-resistant states. *J. Clin. Investig.* **2018**, *128*, 3671–3681. [[CrossRef](#)] [[PubMed](#)]
45. Aponte, Y.; Atasoy, D.; Sternson, S.M. AGRP neurons are sufficient to orchestrate feeding behavior rapidly and without training. *Nat. Neurosci.* **2011**, *14*, 351–355. [[CrossRef](#)] [[PubMed](#)]
46. Williams, K.W.; Elmquist, J.K. From neuroanatomy to behavior: Central integration of peripheral signals regulating feeding behavior. *Nat. Neurosci.* **2012**, *15*, 1350–1355. [[CrossRef](#)]
47. McIntire, S.L.; Reimer, R.J.; Schuske, K.; Edwards, R.H.; Jorgensen, E.M. Identification and characterization of the vesicular GABA transporter. *Nature* **1997**, *389*, 870–876. [[CrossRef](#)] [[PubMed](#)]
48. Vong, L.; Ye, C.; Yang, Z.; Choi, B.; Chua, S., Jr.; Lowell, B.B. Leptin action on GABAergic neurons prevents obesity and reduces inhibitory tone to POMC neurons. *Neuron* **2011**, *71*, 142–154. [[CrossRef](#)]
49. Silver, I.A.; Erecinska, M. Glucose-induced intracellular ion changes in sugar-sensitive hypothalamic neurons. *J. Neurophysiol.* **1998**, *79*, 1733–1745. [[CrossRef](#)] [[PubMed](#)]
50. Song, Z.; Routh, V.H. Differential effects of glucose and lactate on glucosensing neurons in the ventromedial hypothalamic nucleus (VMN). *Diabetes* **2005**, *54*, 15–22. [[CrossRef](#)]
51. Wang, R.; Liu, X.; Hentges, S.T.; Dunn-Meynell, A.A.; Levin, B.E.; Wang, W.; Routh, V.H. The regulation of glucose-excited neurons in the hypothalamic arcuate nucleus by glucose and feeding-relevant peptides. *Diabetes* **2004**, *53*, 1959–1965. [[CrossRef](#)]
52. Wang, R.; Cruciani-Guglielmacci, C.; Migrenne, S.; Magnan, C.; Coterio, V.E.; Routh, V.H. Effects of oleic acid on distinct populations of neurons in the hypothalamic arcuate nucleus are dependent on extracellular glucose levels. *J. Neurophysiol.* **2006**, *95*, 1491–1498. [[CrossRef](#)]
53. Mendoza, C.; Perez-Urrutia, N.; Alvarez-Ricartes, N.; Barreto, G.E.; Pérez-Ordás, R.; Iarkov, A.; Echeverria, V. Cotinine plus krill oil decreased depressive behavior, and increased astrocytes survival in the hippocampus of mice subjected to restraint stress. *Front. Neurosci.* **2018**, *12*, 952. [[CrossRef](#)]

54. Szentandrásy, N.; Banyasz, T.; Biro, T.; Szabo, G.; Toth, B.I.; Magyar, J.; Lazar, J.; Varro, A.; Kovacs, L.; Nanasi, P.P. Apico-basal inhomogeneity in distribution of ion channels in canine and human ventricular myocardium. *Cardiovasc. Res.* **2005**, *65*, 851–860. [[CrossRef](#)] [[PubMed](#)]
55. Szabó, G.; Szentandrásy, N.; Bíró, T.; Tóth, B.I.; Czifra, G.; Magyar, J.; Bányász, T.; Varró, A.; Kovács, L.; Nánási, P.P. Asymmetrical distribution of ion channels in canine and human left-ventricular wall: Epicardium versus midmyocardium. *Pflügers Arch.* **2005**, *450*, 307–316. [[CrossRef](#)] [[PubMed](#)]
56. Gross, G.J.; Lockwood, S.F. Acute and chronic administration of disodium disuccinate astaxanthin (Cardax™) produces marked cardioprotection in dog hearts. *Mol. Cell. Biochem.* **2005**, *272*, 221–227. [[CrossRef](#)] [[PubMed](#)]
57. Fassett, R.G.; Coombes, J.S. Astaxanthin in cardiovascular health and disease. *Molecules* **2012**, *17*, 2030–2048. [[CrossRef](#)] [[PubMed](#)]
58. Krestinina, O.; Baburina, Y.; Krestinin, R.; Odinkova, I.; Fadeeva, I.; Sotnikova, L. Astaxanthin prevents mitochondrial impairment induced by isoproterenol in isolated rat heart mitochondria. *Antioxidants* **2020**, *9*, 262. [[CrossRef](#)] [[PubMed](#)]
59. Kato, T.; Kasai, T.; Sato, A.; Ishiwata, S.; Yatsu, S.; Matsumoto, H.; Shitara, J.; Murata, A.; Shimizu, M.; Suda, S.; et al. Effects of 3-month astaxanthin supplementation on cardiac function in heart failure patients with left ventricular systolic dysfunction—A pilot study. *Nutrients* **2020**, *12*, 1896. [[CrossRef](#)] [[PubMed](#)]

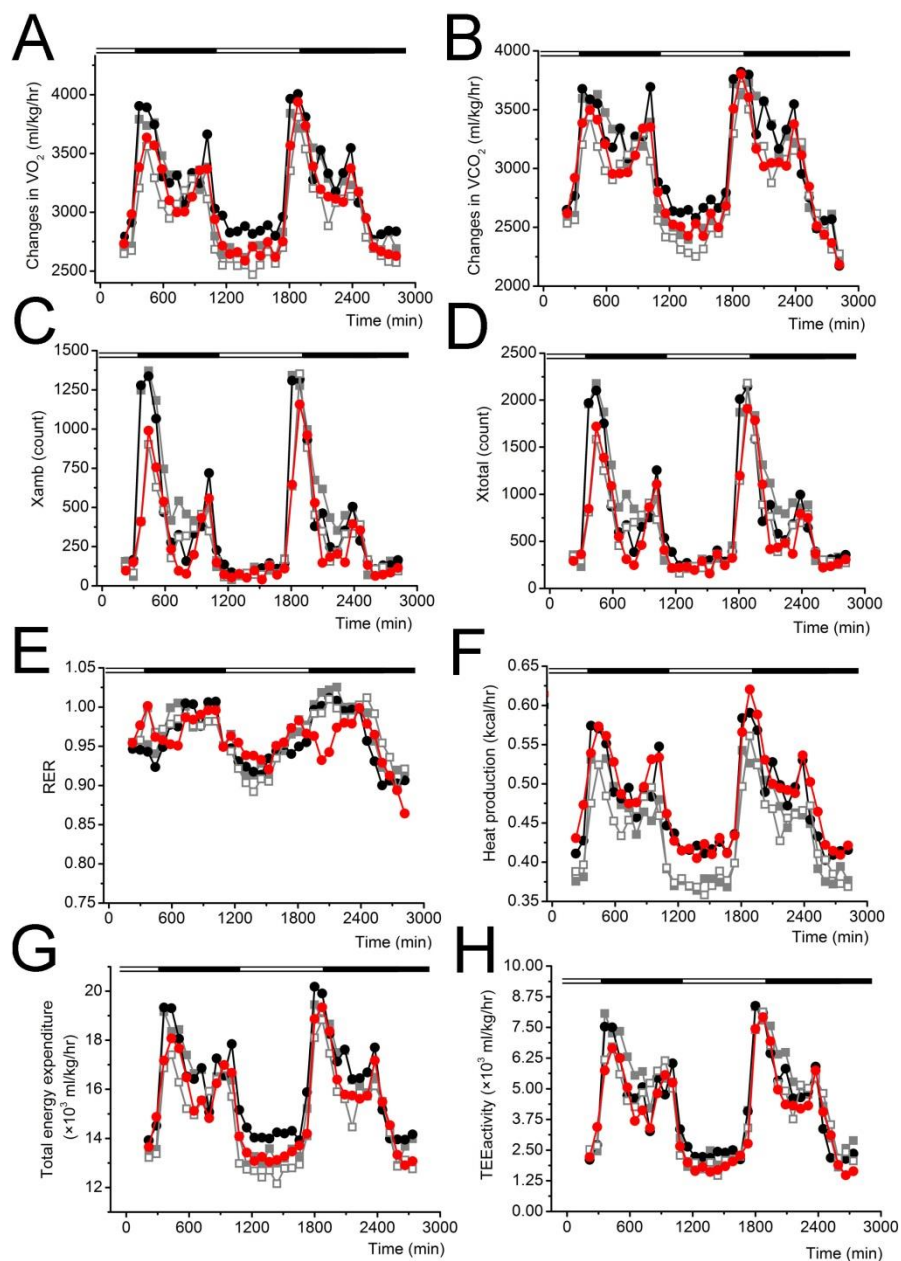


Figure S1. Changes of in vivo metabolic parameters before and following astaxanthin feeding. Continuous changes of VO_2 (A), VCO_2 (B), Xamb (C), Xtotal (D), RER (E), and heat production (F). Data from 4 measured points (equal with 4×18 minutes) were averaged for all animals and time course of the aforementioned parameters were plotted as a function of time. Total energy expenditure (TEE) was calculated by multiplying CV and VO_2 and plotted as a function of time (G). As this parameter contain resting/basal metabolic rate and activity related energy expenditure, we determined resting metabolic rate by averaging the ten minima values of energy expenditure within the 48-hour measurement. RMR was subtracted from TEE giving the TEE_{activity} values of the different animal groups (H). Black lines above the graphs indicate periods in darkness, whereas hollow lines represent periods of light.

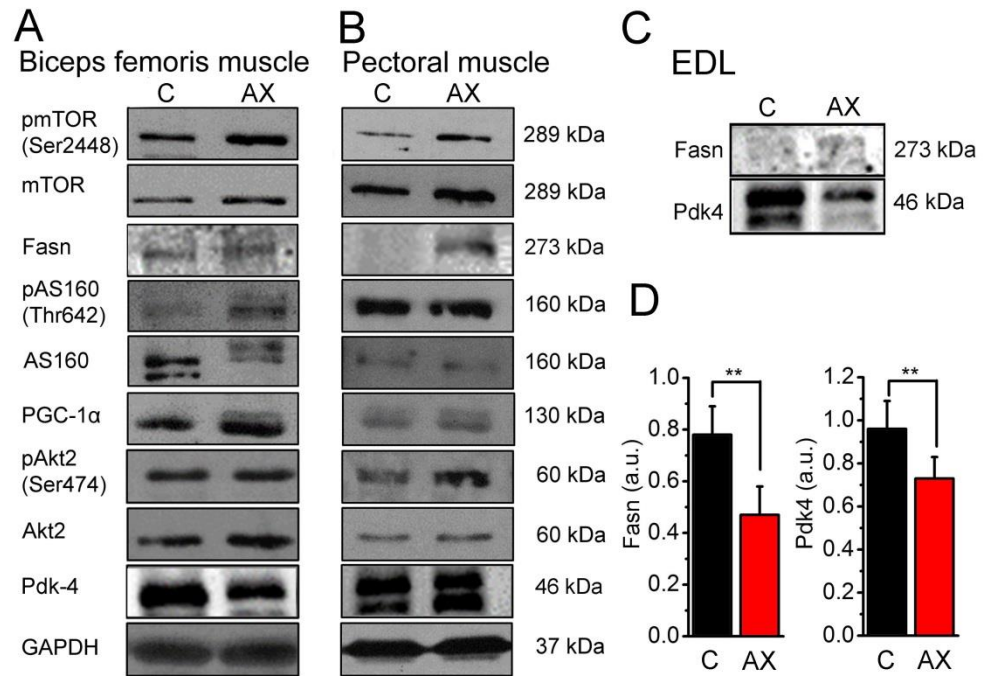


Figure S2. Effects of astaxanthin feeding on the levels of signaling proteins in biceps femoris, pectoral and extensor digitorum longus muscles. **(A)** Representative Western blot images show the levels of phospho(Ser2448)-mTOR, mTOR, Fasn, phospho(Thr642)-AS160, AS160, PGC-1 α , phospho(Ser474)-Akt2, Akt2 and Pdk-4 in control samples (C) and in astaxanthin-treated mice (AX). GAPDH was used as a loading control. **(B)** Representative Western blot images from samples obtained from pectoralis muscles show the levels of phospho(Ser2448)-mTOR, mTOR, Fasn, phospho(Thr642)-AS160, AS160, PGC-1 α , phospho(Ser474)-Akt2, Akt2 and Pdk4 in control samples (C) and AX treated mice, respectively. GAPDH was used as a loading control. **(C)** Representative Western blot experiments from extensor digitorum longus (EDL) muscle show significantly decreased Fasn and Pdk4 protein levels. **(D)** Statistical analysis of changes in Fasn and Pdk4 in EDL (black, C: control; red, AX: astaxanthin).

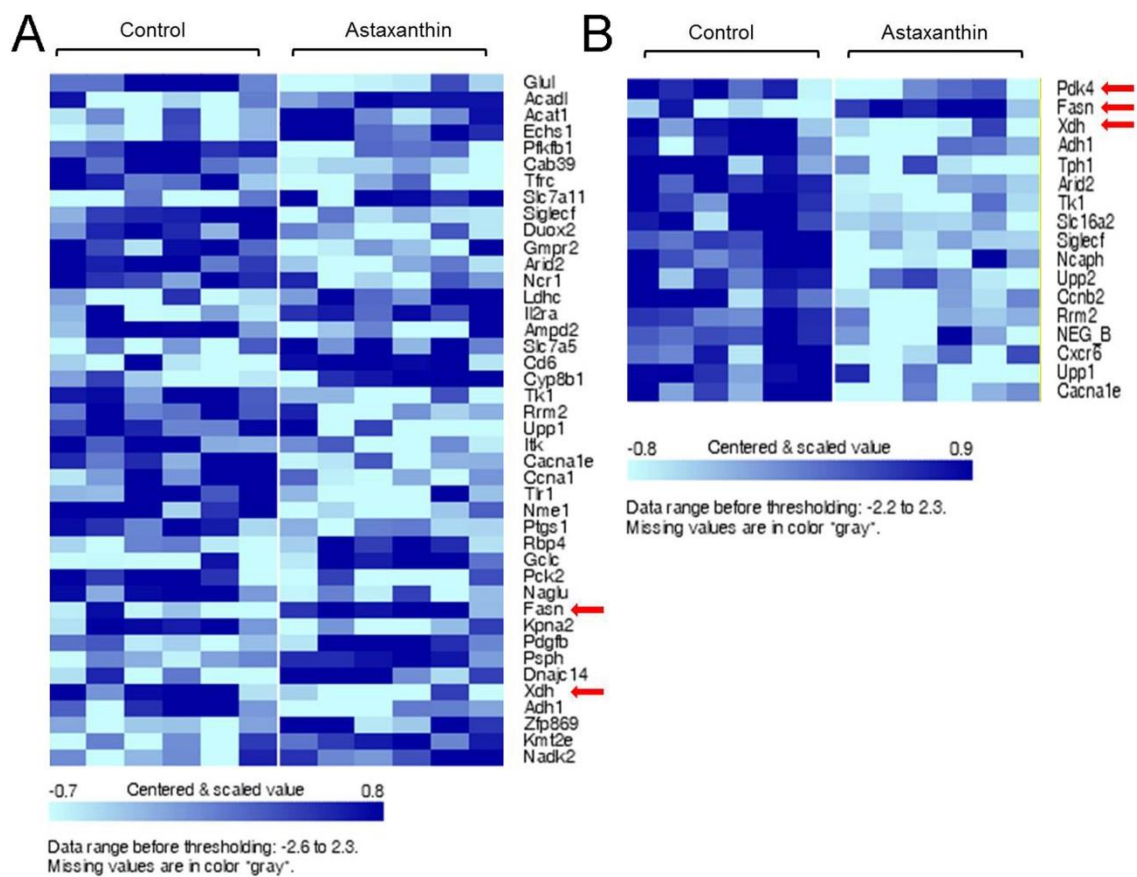


Figure S3. Clustered heatmap of significantly expressed genes in samples from EDL muscles. **(A)** Clustered heatmap following quantile normalization; arrays grouped by class. **(B)** Clustered heatmap of significantly expressed genes normalized to housekeeping genes; arrays grouped by class. Arrows indicate altered gene expression in AX treated samples compared to the controls.

Table S1. Metabolic parameters measured during 48 h before and after the 4 weeks of special feeding in control and astaxanthin-treated mice. Significance was calculated between control and astaxanthin-treated groups at different periods of the day and accepted to be significantly different, when $p < 0.05$.

		1 st Period (Dark)		2 nd Period (Light)		3 rd Period (Dark)		4 th Period (Light)	
		Ctrl	Astx	Ctrl	Astx	Ctrl	Astx	Ctrl	Astx
VO ₂ (ml/kg/hr)	Before	3395.9 ± 32.1	3430 ± 32.3	2747.8 ± 28.5	2927.9 ± 28.6	3383.5 ± 32.91	3466.5 ± 32.5	2735.2 ± 37.4	2816.3 ± 38.1
	After	3208.2 ± 28.9	3291.2 ± 29.9	2588.2 ± 24.5	2699.9 ± 23.5	3244.6 ± 31.3	3369.9 ± 30.9	2660.2 ± 34.7	2711.2 ± 33.9
VCO ₂ (ml/kg/hr)	Before	3333.4 ± 32.9	3350.6 ± 33.1	2584.9 ± 31.0	2746.6 ± 30.6	3386.9 ± 35.2	3422.3 ± 33.7	2468.2 ± 49.2	2463.9 ± 53.9
	After	3144.0 ± 30.2	3218.9 ± 31.3	2412.5 ± 27.7	2562.2 ± 24.9	3226.3 ± 32.7	3271.7 ± 32.9	2438.6 ± 45.6	2423.6 ± 44.3
X _{amb} (counts)	Before	692.1 ± 37.1	594.3 ± 35.5	133.9 ± 16.9	156.5 ± 18.2	656.9 ± 37.6	563.2 ± 33.9	116.6 ± 20.1	131.0 ± 18.5
	After	440.5 ± 26.2	428.3 ± 27.8	93.2 ± 9.3	84.4 ± 8.4	509.7 ± 32.9	472.3 ± 29.3	108.7 ± 13.8	88.5 ± 12.3
X _{total} (counts)	Before	1198.8 ± 53.2	1049.3 ± 50.9	326.5 ± 27.1	377.9 ± 29.3	1164.1 ± 54.4	1024.6 ± 46.9	292.6 ± 35.3	312.6 ± 33.6
	After	876.6 ± 40.7	858.4 ± 43.9	267.8 ± 17.9	264.8 ± 16.7	960.2 ± 49.0	924.7 ± 45.6	287.7 ± 26.0	263.6 ± 25.1
RER	Before	0.92 ± 0.003	0.97 ± 0.003	0.94 ± 0.004	0.93 ± 0.003	0.99 ± 0.002	0.98 ± 0.002	0.92 ± 0.005	0.9 ± 0.005
	After	0.98 ± 0.003	0.97 ± 0.003	0.93 ± 0.004	0.95 ± 0.003	0.99 ± 0.002	0.97 ± 0.003	0.93 ± 0.004	0.91 ± 0.004
Heat production (kcal/hr)	Before	0.48 ± 0.005	0.51 ± 0.005	0.38 ± 0.004	0.43 ± 0.005	0.48 ± 0.005	0.52 ± 0.005	0.38 ± 0.006	0.41 ± 0.006
	After	0.47 ± 0.004	0.52 ± 0.005	0.38 ± 0.004	0.42 ± 0.004	0.48 ± 0.005	0.53 ± 0.005	0.39 ± 0.005	0.42 ± 0.005
Total sleep time (min)	Before			156.0 ± 8.4	137.8 ± 15.4	51.6 ± 7.5	54.8 ± 9.8	207.4 ± 14.8	192.4 ± 21.1
	After			152.1 ± 15.1	137.5 ± 11.7	75.4 ± 10.7	55.1 ± 7.5	234.8 ± 25.3	192.4 ± 13.4

Co-author certification

I, myself as a corresponding author of the following publication declare that the authors have no conflict of interest, and Zoltán Márton Köhler Ph.D. candidate had significant contribution to the jointly published research(es). The results discussed in his thesis were not used and not intended to be used in any other qualification process for obtaining a PhD degree.

23/08/2023

.....
date

Balázs Pál

.....
Balázs Pál
corresponding author

The publication relevant to the applicant's thesis:

Gönczi, Mónika, Andrea Csemer, László Szabó, Mónika Sztretye, János Fodor, Krisztina Pocsai, Kálmán Szenthe, Anikó Keller-Pintér, **Zoltán Márton Köhler**, Péter Nánási, Norbert Szentandrassy, Balázs Pál, and László Csernoch (2022). Astaxanthin Exerts Anabolic Effects via Pleiotropic Modulation of the Excitable Tissue. *International Journal of Molecular Sciences* 23(2):917.

<https://doi.org/10.3390/ijms23020917>

Figure 2.; Supplementary figure 2.

Co-author certification

I, myself as a co-author of the following publication declare that the authors have no conflict of interest, and Zoltán Márton Köhler Ph.D. candidate had significant contribution to the jointly published research(es). The results discussed in his thesis were not used and not intended to be used in any other qualification process for obtaining a PhD degree.

2023.08.07.

.....
date



.....
Andrea Csemer
co-author

The publication relevant to the applicant's thesis:

Gönczi, Mónika, Andrea Csemer, László Szabó, Mónika Sztretye, János Fodor, Krisztina Pocsai, Kálmán Szenthe, Anikó Keller-Pintér, **Zoltán Márton Köhler**, Péter Nánási, Norbert Szentandrassy, Balázs Pál, and László Csernoch (2022). Astaxanthin Exerts Anabolic Effects via Pleiotropic Modulation of the Excitable Tissue. *International Journal of Molecular Sciences* 23(2):917.

<https://doi.org/10.3390/ijms23020917>

Figure 2.; Supplementary figure 2.